LINKS BETWEEN CARBON AND WATER CYCLES IN NORTHERN ECOSYSTEMS: CONSTRAINTS FROM STABLE ISOTOPES

Thesis by

Lisa R. Welp

In Partial Fulfillment of the Requirements for the

degree of

Doctor of Philosophy

CALIFORNIA INSTITUTE OF TECHNOLOGY

Pasadena, California

2006

(Defended May 17th 2006)

ACKNOWLEDGEMENTS

I would first like to sincerely thank my advisor Jim Randerson for his mentoring during my graduate career and making the Ph.D. process a rewarding educational experience. His genuine excitement for science has been an inspiration. I deeply appreciate the opportunities he gave me to do research in some very exciting and beautiful locations. I also thank Jim and Mike Hoffmann for allowing me to continue working at Caltech after Jim made the move to UCI. I would like to express my appreciation to my other thesis committee members, Jess Adkins, John Eiler and Paul Wennberg, for their advice and help keeping my degree on track.

I also thank everyone at the Earth System Science department at UCI for making me feel welcome in Croul Hall. I am deeply grateful to Sue Trumbore and Xiaomei Xu for allowing me to use their lab facilities and automated isotope ratio mass spectrometer which made this thesis possible. Coincidentally, it was also Xiaomei who got me started in the lab when I first arrived at Caltech. I am indebted to everyone who worked in the N. Mudd basement stable isotope lab and who were always willing to answer questions, including Xiaomei, Julianna Fessenden, Sally Newman, Nami Kitchen, Zhengrong Wang, Julie O'leary, Thom Rahn and Hagit Afek. They also made it a very pleasant working environment. A special thanks goes to the late Bob Becker for not only teaching me how to take apart a mass spectrometer and put it back together, but also for being so selfless with his time and kindness.

Julianna was a great friend and mentor to me during her postdoc at Caltech. She taught me how to make field measurements and really helped get me started on my thesis project. I also thank Jamie Lindfors for being an entertaining friend and a valuable group

member. They both made field trips to Alaska and Siberia productive and fun adventures. The scientists at the Northeast Siberia Research Station, Sergey and Galya Zimov and Sergey and Anna Davydov, were tremendous hosts and wonderful collaborators. I can't wait to go back to Cherskii someday. Without their help and that of VECO Polar Resources, Terry Chapin, and others in the RAISE collaboration group, my Arctic research would have been impossible. I thank Dave Noone, Bill Riley, and Chris Still for contributing many useful brainstorming discussions on biosphere-atmosphere isotope exchange and for help with global modeling efforts currently underway. Heping Liu has been a great coauthor; contributing all the eddy covariance tower data. Financial support was provided by the NCER STAR EPA Graduate Fellowship program, and I benefited from several student travel grants provided by the BASIN network.

I am fortunate to have found wonderful friends here at Caltech that have made my time in Pasadena memorable, especially those in the ESE department, Jennie, Fok, and my chemistry friends for making my first few days less scary. Thank you, Megan and Rebecca, for the many hiking, canyoneering and biking adventures we've had, and Asha, for the late nights and weekend conventions dancing west coast swing. I also want to thank Greg for being a wonderful surprise in my life these last few months. Finally, I thank my family for all their support, encouragement and love. You taught me common sense and gave me curiosity to figure out how things work; the character traits that made me a scientist. Thank you for understanding my move far away from home to follow my own path.

ABSTRACT

High-latitude climate change will have an impact on the carbon and water cycles in northern ecosystems. Stable isotopes in these systems can serve as indicators of changes and feedbacks. Monitoring the stable isotopic composition of Arctic river discharge provides a means to investigate integrated basin-scale hydrologic changes in remote northern regions. I measured water $\delta^{18}O$ and δD from the Kolyma River in Siberia and local precipitation to partition the river flow into 60% snow and 40% rain inputs. Comparing this estimate with seasonal precipitation across the watershed showed a significant portion of snowmelt is retained in the soils of this permafrost dominated region, and contributes to ~40% of the growing season transpiration. The seasonal cycles of atmospheric CO_2 and $\delta^{18}O$-CO_2 at high northern latitudes have the potential to serve as indicators of ecological change. Effective interpretation of atmospheric observations requires an understanding of how different species and ecosystems contribute to biosphere-atmosphere exchange. By combining isotopic signatures of ecosystem water pools with measured CO_2 fluxes in three stands of an Alaskan boreal fire chronosequence (recent burn, intermediate-aged deciduous and mature evergreen forests), I compared the relative effects of stand age on the phase and amplitude of the seasonal cycles of CO_2 and $\delta^{18}O$-CO_2. Higher rates of mid-summer net carbon exchange and a shorter growing season at the deciduous stand resulted in the largest seasonal CO_2 amplitude and also delayed the drawdown of atmospheric CO_2 compared to the evergreen stand. Reduced levels of photosynthesis at the deciduous stand early in the growing season caused atmospheric $\delta^{18}O$-CO_2 to increase more slowly compared to fluxes from the evergreen stand. The

distribution of stand ages in northern boreal forests is likely to determine the response of net ecosystem exchange (NEE) to future climate changes. I used three years of NEE measurements from the Alaskan fire chronosequence to determine that the sensitivity of growing season NEE to spring air temperatures and summer drought was greater at the deciduous forest than the evergreen forest. As forest fire disturbance increases due to climate warming, the shift to younger forests should increase interannual variability in atmospheric CO_2 concentrations.

TABLE OF CONTENTS

Acknowledgements ..... iii-iv
Abstract ..... v-vi
Table of Contents ..... vii-viii
List of Figures ..... ix-xii
List of Tables xiii
Nomenclature xiv
Chapter 1 Introduction 1-1
1.1 The boreal forest 1-1
1.2 Climate change in high-northern latitudes 1-2
1.3 Consequences for terrestrial ecosystems 1-4
1.4 Consequences for the Arctic hydrologic cycle 1-5
1.5 Stable isotopes as tools to detect climate change 1-6
1.5.1 Oxygen and hydrogen in water 1-7
1.5.2 Oxygen in CO_2 1-8
1.6 Eddy covariance technique 1-9
1.7 Major thesis results and conclusions 1-10
1.8 References 1-12
Chapter 2 A high-resolution time series of oxygen isotopes from the Kolyma River: Implications for the seasonal dynamics of discharge and basin-scale water use 2-1
2.1 Abstract 2-1
2.2 Introduction 2-2
2.3 Methods 2-3
2.3.1 Study area 2-3
2.3.2 Water sampling and isotopic analysis 2-4
2.3.3 Partitioning approach 2-5
2.3.4 Data sources 2-7
2.4 Results and Discussion 2-8
2.4.1 Stable oxygen isotope observations 2-8
2.4.2 Partitioning river flow into snow and rain components 2-10
2.4.3 Annual water balance 2-11
2.4.4 Evaporation influence estimated from δD and $\delta^{18}O$ 2-13
2.4.5 Partitioning error and sensitivity analysis 2-14
2.5 Conclusions 2-14
2.6 Appendix to section 2.3.3 2-15
2.7 References 2-17
2.8 Data appendix 2-19

Chapter 3 Seasonal exchange of CO_2 and $\delta^{18}O$-CO_2 varies with post-fire succession in boreal forest ecosystems 3-1
3.1 Abstract 3-1
3.2 Introduction 3-2
3.3 Site description 3-7
3.4 Methods 3-9
3.4.1 Eddy covariance and micrometeorological measurements 3-9
3.4.2 Isotopic measurements 3-10
3.4.3 Isotopic modeling of water pools 3-12
3.4.4 Partitioning CO_2 fluxes 3-17
3.4.5 Atmospheric modeling 3-20
3.5 Results 3-25
3.5.1 CO_2 fluxes 3-25
3.5.2 Observations and modeling of the $\delta^{18}O$ of water pools 3-30
3.5.3 Atmospheric modeling 3-32
3.5.4. Sensitivity of the $\delta^{18}O$-CO_2 seasonal cycle to C_c/C_a 3-37
3.6 Discussion 3-39
3.6.1 Disturbance induced changes in CO_2 seasonal amplitude and phase 3-39
3.6.2 Factors controlling the seasonal cycle of $\delta^{18}O$-CO_2 3-42
3.6.3 Future work 3-44
3.7 Conclusions 3-45
3.8 References 3-48
Chapter 4 Ecosystem carbon flux response to spring warming and summer drought depends on plant functional type in boreal forest ecosystems 4-1
4.1 Abstract 4-1
4.2 Introduction 4-2
4.3 Methods 4-5
4.4 NEE measurements and partitioning results 4-6
4.5 Early season warming 4-10
4.6 Late-summer drought 4-13
4.7 Net growing season 4-15
4.8 Conclusions 4-15
4.9 Acknowledgements 4-16
4.10 References 4-17
Chapter 5 Predictions for future changes in $\delta^{18}O$ of atmospheric CO_2 5-1
5.1 New hypothesis 5-1
5.2 Warmer air temperatures are correlated with increased $\delta^{18}O$ of precipitation 5-2
5.3 Sensitivity of the $\delta^{18}O$-CO_2 seasonal cycle to the mean $\delta^{18}O$ of precipitation 5-3
5.4 Advantages of $\delta^{18}O$-CO_2 5-6
5.5 References 5-9

LIST OF FIGURES

Figure 1.1 The circumpolar boreal forest (green) and tundra (blue). Ecosystem complex classifications from *Olsen et al.* [1985]. 1-2

Figure 1.2 Surface air temperature annual anomalies in the Arctic (land and ocean between 64°N–90°N) from the Global Historical Climatology Network [*GHCN*, 2006] dataset (bars), at the Big Delta, Alaska climate station of the Western Regional Climate Center [*WRCC*, 2006] and across the Kolyma River basin in Siberia from the NCEP reanalysis [*Oelke*, 2003]. All anomalies are relative to the 1961–1980 mean..... 1-3

Figure 1.3 Diagram of oxygen isotope transfer between CO_2 and H_2O. Source: ISOLSM model [*Riley et al.*, 2002]..... 1-9

Figure 2.1 Water sampling was conducted at Cherskii, near the mouth of the Kolyma River, and the discharge gauging station was located at Kolymskoye. (Map source: *Cornell University Interactive Mapping Tool*) 2-4

Figure 2.2 $\delta^{18}O$ of the Kolyma River sampled at Cherskii, from September 2002 through April 2004. Error bars represent the analytical standard deviation. The *Q*-weighted mean for the one-year period from October 2002 to September 2003 was -22.2‰, marked by the dashed line..... 2-9

Figure 2.3 (a) Kolyma *Q* ($m^3\ s^{-1}$) measured at Kolymskoye, (b) fraction of snow component calculated from $\delta^{18}O$ partitioning, and (c) the discharge ($m^3\ s^{-1}$) associated with snow (solid line) and rain components (dotted line). The fraction of snow peaked in early June at 82%, and the rain component peak was delayed until early July. 2-10

Figure 2.4 (a) Rescaled NCEP monthly mean *P* (mm mon^{-1}) [*Serreze et al.*, 2003] for the Kolyma watershed (circles) and measured at the Cherskii airport (squares). (b) Monthly mean surface air temperature from the elevation corrected NCEP reanalysis for the Kolyma watershed (circles) [*Oelke*, 2003] and measured at the Cherskii airport (squares). (c) ET estimated from *Serreze et al*. [2003]. 2-12

Figure 2.5 $\delta^{18}O$ versus δD relationships for precipitation (rain and snow) with d-excess values greater than zero (grey diamonds) and d-excess values less than zero (pluses), the Kolyma River (blue circles), and the local stream (green squares). A least-squares fit line for precipitation using all data (diamonds and pulses) is $\delta D = 6.6 \bullet \delta^{18}O - 23.7$ and when using only d-excess values greater than zero, the regression is $\delta D = 7.0 \bullet \delta^{18}O - 11.7$. The Kolyma River regression is $\delta D = 6.8 \bullet \delta^{18}O - 19.1$. The local stream regression is $\delta D = 5.2 \bullet \delta^{18}O - 55.1$. The global meteoric water line (GMWL) is plotted for reference, $\delta D = 8 \bullet \delta^{18}O + 10$ (dashed line). Error bars are smaller than the symbols..... 2-13

Figure 3.1 Daily micrometeorological data from Delta Junction during 2002. (a) Daily maximum photosynthetic photon flux density (*PPFD*), (b) daily mean above canopy air temperature averaged across all stands, (c) daily mean above canopy relative humidity averaged across all stands, and (d) daily mean soil temperature measured 10 cm below the surface at each stand. 3-8

Figure 3.2 (a) $\delta^{18}O$ of precipitation collected at Delta Junction during 2001–2003 as a function of mean surface air temperature for the week preceding collection. Monthly precipitation data from the GNIP IAEA network stations Fort Smith, Mayo, Whitehorse and Yellowknife are plotted as a function of monthly mean air temperature. GNIP station time series are intermittent and span from 1961 to 1993. Regressions are shown for 2002 Delta Junction measurements (solid line) and GNIP measurements (dashed line). The temperature regression for 2002 Delta Junction precipitation yielded a slope of 0.25‰/°C and an intercept of -20.22‰, r^2=0.62, n=75, p<0.001. This was similar to the regression for the combined GNIP stations which had a slope of 0.25‰/°C and an intercept of -20.96‰, r^2=0.47, n=236, p<0.001. (b) Monthly mean $\delta^{18}O$ of precipitation for each GNIP station and the estimate for Delta Junction (derived from the temperature regression shown in the upper panel). Standard deviations about the GNIP monthly means are ~3‰ at all locations, but were excluded from the figure for clarity..... 3-14

Figure 3.3 Measured (symbols) and modeled (lines) $\delta^{18}O$ of leaf water, precipitation, soil and xylem water and water vapor for the year 2002..... 3-15

Figure 3.4 Measured (black filled circles) and modeled (solid grey line) weekly mean NEE for the three stands in 2002. This plot shows mean diurnal cycles constructed from 7-day intervals of 30-minute NEE data. The mean diurnal cycles are plotted sequentially to allow examination of the seasonality in GPP (indicated partly by the daytime minima) and R_e (indicated partly by the nighttime maxima). The growing season at the 15-year stand is shorter and more intense (with a larger diurnal cycle in mid-summer). Linear regression slopes between modeled and measured (weekly mean) NEE are 0.18 at the 3-year stand (r^2=0.35), 0.75 at the 15-year stand (r^2=0.76) and 0.59 at the 80-year stand (r^2=0.72). CO_2 fluxes at the 3-year stand are small making them difficult to measure and model and resulting in poor correlation statistics. 3-27

Figure 3.5 (a) A comparison between modeled NEE and measured NEE at each stand during the growing season, DOY 100–300. The solid lines are cumulative modeled NEE estimates and the dotted lines are measured NEE values that were gap filled with modeled estimates during periods of missing data. Modeled NEE has a bias towards decreased net carbon uptake at each stand. (b) Cumulative modeled NEE for the entire year (DOY 1–365) for each stand. The sign convention is such that positive values are fluxes to the atmosphere and negative values are uptake by the ecosystem. The 3-year stand was a source with a flux of approximately 3.4 mol CO_2 m^{-2} yr^{-1} (40.8 g C m^{-2} yr^{-1}) while the 15-year stand was a sink with a flux of approximately -9.5 mol CO_2 m^{-2} yr^{-1} (-114 g C m^{-2} yr^{-1}). The mature 80-year stand was a smaller sink of CO_2 with a flux of approximately -5.8 mol CO_2 m^{-2} yr^{-1} (-69.6 g C m^{-2} yr^{-1})..... 3-29

Figure 3.6 Measured $\delta^{18}O$ of leaf water and xylem water (symbols) are shown with model predictions (lines) during intensive field campaigns during (a) 16–22 June 2002 and (b) 10–16 August 2002. The leaf water model used in this study was a non-steady state model with a leaf water turnover time of 2 hours. Modeled xylem water was set equal to the $\delta^{18}O$ of precipitation. 3-31

Figure 3.7 Predicted seasonal cycles of (a) CO_2 and (b) $\delta^{18}O$-CO_2 for fluxes from each stand compared to the mean seasonal cycle of the NOAA CMDL flask network observations at Pt Barrow (1990–1997). Error bars on the Pt. Barrow observations represent the standard deviation about each mean monthly value for the entire data record. The phase of the 15-year CO_2 seasonal cycle was delayed relative to that at the 80-year stand and the amplitude is increased. In contrast, the phase of 15-year $\delta^{18}O$-CO_2 seasonal cycle was advanced relative to that predicted for the 80-year stand. 3-33

Figure 3.8 Cumulative (a) GPP and (b) R_e components of CO_2 forcing with the annual trend removed, (c) GPP and (d) R_e cumulative isoforcing, and (e) GPP and (f) R_e cumulative isoforcing with the annual trend removed. Note that the y-axis units in panels a,b,e, and f are relative units – they are not absolute values. At no time during the year was the cumulative GPP isoforcing negative (c) nor was the cumulative R_e isoforcing positive (d). 3-35

Figure 3.9 Cumulative net annual isoflux at each stand. All stands were predicted to deplete the atmosphere in $\delta^{18}O$-CO_2 because ecosystem water pools in the far north are extremely depleted in $\delta^{18}O$. The atmospheric $\delta^{18}O$-CO_2 was not in steady state with surface water pools at this latitude due to mixing with southern air masses with higher $\delta^{18}O$-CO_2. 3-36

Figure 3.10 (a) Daily GPP-weighted leaf $\delta^{18}O$-CO_2 and $\delta^{18}O$ of atmospheric CO_2 ($\delta_{a,i}^{CO_2}$) and (b) daily R_e-weighted respired soil $\delta^{18}O$-CO_2 (diffusion fractionation of -7.2‰ has been included, $\delta_{soil}^{CO_2} - \varepsilon_{diff}$) for the 15-year stand. High $\delta^{18}O$ values of leaf CO_2 (and leaf water) in the beginning of the growing season (around DOY 150) were due to low relative humidity levels during this period (Figure 3.1c). This resulted in more positive Δ_A values on average earlier in the growing season and decreasing Δ_A towards the end of the season. Differences in the magnitude and seasonal distribution of GPP at each stand resulted in variations in the isoforcing among stands, even though the modeled $\delta^{18}O$ of leaf water was similar across stands. Soil temperature differences resulted in different equilibrium fractionation factors between CO_2 and water, and therefore, $\delta^{18}O$ of soil respired CO_2 at each stand. 3-39

Figure 4.1 NEE measurements from 2002–2004. The recent burn (a) occurred in 1999, the deciduous forest (b) burned in 1987 and the evergreen (c) burned in approximately 1920. Positive values represent a release of CO_2 from the ecosystem into the atmosphere and negative values denote uptake of CO_2 by the ecosystem……..4-8

Figure 4.2 Weekly mean NEE, GPP and R_e. Positive values in panels (c) and (d) are R_e fluxes to the atmosphere and negative values are GPP uptake by the forests. Spring temperatures increased from 2002 through 2004 and a severe drought occurred during August of 2004 (shaded intervals)……4-9

Figure 4.3 Weekly mean climate conditions. (a) Air temperature measured above the canopy, (b) vapor pressure deficit calculated from temperature and relative humidity measurements above the canopy, (c) monthly mean precipitation, (d) volumetric water content (VWC) measured at 4 cm at the evergreen site and (e) VWC measured at 2 cm at the deciduous site. ……..4-11

Figure 5.1 The modeled seasonal cycle of $\delta^{18}O\text{-}CO_2$ at the 15-year forest in Chapter 3 (contemporary, solid black) and the sensitivity to a +1, +2, and +3‰ change in precipitation or plant source water (solid, dashed, and dotted blue). The contemporary seasonal cycle most closely resembles that of the R_e isoforcing (Figure 5.2b), however, as precipitation $\delta^{18}O$ increases, the seasonal cycle transitions to reflect stronger GPP isoforcing (Figure 5.2a). 5-4

Figure 5.2 The effects of (a) GPP and (b) R_e isoforcing on the seasonal cycle of monthly mean $\delta^{18}O\text{-}CO_2$ as predicted by the model in Chapter 3. The contemporary atmosphere resembles the R_e seasonal isoforcing. Also, the cumulative annual (c) GPP and (d) R_e isoforcing for a +1, +2, and +3‰ change in $\delta^{18}O$ of precipitation. The increase in GPP isoforcing was much larger than the decrease in R_e isoforcing. 5-4

Figure 5.3 (a) $\delta^{18}O\text{-}CO_2$ measured in the atmosphere at Pt. Barrow, Alaska (NOAA/CMDL) compared to modeled $\delta^{18}O$ of CO_2 diffusing out of leaves (proportional to GPP isoforcing) and (b) $\delta^{18}O$ of CO_2 diffusing out of the soil at the 15-year forest modeled in Chapter 3. 5-6

Figure 5.4 Time series of stem waters from Siberia during the 2003 growing season. *Betula* and *Larix* stem water were similar in June, but diverged as the growing season progressed. The shallower rooted *Betula* stem water $\delta^{18}O$ approached the mean summer rain water $\delta^{18}O$ towards the end of the growing season, and deeper rooted *Larix* stem water became very negative, indicating an increased contribution of snowmelt or permafrost melt. 5-8

LIST OF TABLES

Table 2.1 Annual water budget of the Kolyma River basin 2-11

Table 2.2 Kolyma River stable isotope data. 2-19

Table 2.3 Cherskii rain stable isotope data. 2-20

Table 2.4 Cherskii snow stable isotope data 2-21

Table 2.5 Cherskii local stream stable isotope data. 2-22

Table 3.1 Model parameters used to partition NEE into GPP and R_e components. 3-19

Table 3.2 Annual ecosystem fluxes, isofluxes, and other model parameters. 3-28

Table 3.3 Sensitivity analysis of the $\delta^{18}O\text{-}CO_2$ seasonal cycle 3-37

Table 4.1 Seasonal summary of climate and carbon fluxes for each year of the study.. 4-12

NOMENCLATURE

Autotrophic respiration. The combination of energy used for growth and maintenance of plant tissues. This is a positive value and source of CO_2 to the atmosphere.

Ecosystem respiration (R_e). Total ecosystem respiration includes autotrophic, heterotrophic and microbial CO_2 loss pathways from the ecosystem. This is a positive value and source of CO_2 to the atmosphere.

Eddy covariance. This is a technique that involves measuring the upward and downward fluxes of CO_2 and H_2O using high-frequency measurements of vertical component of the wind speed and scalars. It is a standard measurement of CO_2 (NEE), H_2O, momentum, sensible and latent heat fluxes over an ecosystem.

Gross primary production (GPP). The total amount of carbon taken up by plants during photosynthesis. The sign convention used in this thesis presents GPP as negative values because it is a sink of CO_2 from the atmosphere.

Heterotrophic respiration. The release of CO_2 during decomposition of organic matter in the soil by animals, fungi and other decomposers. This is a positive value or source of CO_2 to the atmosphere.

Leaf area index (LAI). The one sided green leaf area per unit ground area in broadleaf canopies, or as the projected needleleaf area per unit ground area in needle canopies.

Microbial respiration. The release of CO_2 during decomposition of organic matter in the soil by microbes. This is a positive value and source of CO_2 to the atmosphere.

Net carbon uptake. = -NEE

Net ecosystem exchange (NEE). The net carbon uptake or loss by an ecosystem as CO_2. Positive values indicate a source of CO_2 to the atmosphere and negative values indicate a sink of CO_2 from the atmosphere. $NEE = GPP + R_e$

Phenology. The study of the annual cycles of plants and animals and how they respond to seasonal changes in the environment.

Photosynthetic flux. = -GPP

Plant functional type. A grouping of species that shows close similarities in their response to environmental controls.

Chapter 1

INTRODUCTION

1.1 The boreal forest

The circumpolar region between 50°N and 70°N, covering the Canadian and Siberian landmasses, is home to the boreal forest (Figure 1.1). It is the second largest forest biome after the tropical evergreen forest [*Landsberg and Gower*, 1997]. It covers approximately 10% of the Earth's land surface area (13.7 million km^2) [*Chapin et al.*, 2002], but accounts for a disproportionately large percentage (up to 25%) of the carbon in the global terrestrial biosphere [*Dixon et al.*, 1994]. Most of the carbon is stored in soils with extremely low respiration rates due to poor drainage, cold temperatures, and permafrost [*Hobbie et al.*, 2000; *Harden et al.*, 2001]. This region experiences cold winters, warm summers, short growing seasons (approximately 4 months), and low annual precipitation (200–600 mm yr^{-1}). Recent glaciations and slow species migrations result in low species diversity [*McClone*, 1996] with forest types consisting of either pure broadleaf deciduous, pure conifer, mixed deciduous/conifer, pine/lichen or spruce/moss [*Baldocchi et al.*, 2000]. Evergreen conifer species, including *Picea mariana*, *Picea glauca* and *Pinus banksiana*, are widely distributed across Alaska and Canada, whereas, deciduous conifer species, including *Larix siberica*, are found primarily in Siberia. Broadleaf deciduous species such as *Populus tremuloides*, *Populus balsamifera*, *Betula papyrifera*, *Salix* spp. and *Alnus* spp. are typically present on both continents after fire disturbance.

The boreal forest has a large effect on the atmosphere through the carbon and water cycles and the Earth's energy budget [*Chapin et al.*, 2000]. Estimates of the net annual carbon budget of high-northern latitude ecosystems (boreal forests plus Arctic tundra) varies widely from a sink of 1 Pg C yr^{-1} to a source of 0.2 Pg C yr^{-1} [*Chapin et al.*, 2000; *Oechel et al.*, 2000]. To predict future climate feedbacks due to increasing atmospheric CO_2 concentrations and air temperatures, it is necessary to understand the current carbon budget of the boreal forest and the mechanisms that regulate carbon uptake and loss.

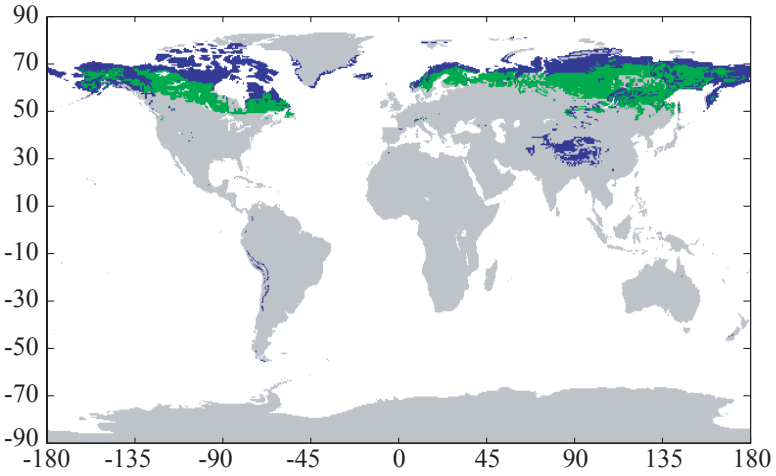

Figure 1.1 The circumpolar boreal forest (green) and tundra (blue). Ecosystem complex classifications from *Olsen et al.* [1985].

1.2 Climate change in high-northern latitudes

The Arctic is currently undergoing a system-wide response to an altered climate state [*Hinzman et al.*, 2005]. Throughout the twentieth century, measurable increases in air temperature, thinning of sea ice, melting of glaciers, thawing of permafrost and reduction in the amount of snow cover have been reported [*Chapman and Walsh*, 1993;

Serreze et al., 2000]. During the last century, the Arctic was the warmest it has been in 400 years [*Overpeck et al.*, 1997] and mean surface air temperature increased at a rate of 0.09°C per decade [*ACIA*, 2004] (Figure 1.2). The warming has been regional, confined to western North America and Siberia, with largest trends in spring air temperatures [*Hansen et al*., 1999; *Keyser et al.*, 2000], while eastern Canada has experienced some cooling [*Serreze et al.*, 2000]. Recent warming trends in the Arctic have been 50% larger than the global mean [*IPCC*, 2001], due in part to temperature-albedo feedbacks of snow and ice cover [*Cess et al.*, 1991]. Future acceleration of this trend is predicted as greenhouse gas concentrations continue to increase, the extent of reflective snow and ice cover is reduced [*ACIA*, 2004], and shrubs and trees encroach northward into the tundra and alter regional radiation budgets [*Chapin et al.*, 2005].

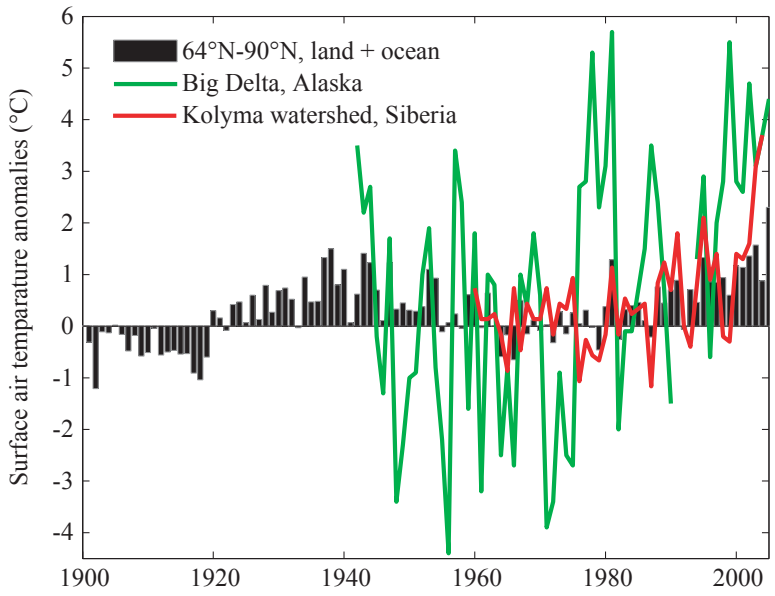

Figure 1.2 Surface air temperature annual anomalies in the Arctic (land and ocean between 64°N–90°N) from the Global Historical Climatology Network [*GHCN*, 2006] dataset (bars), at the Big Delta, Alaska climate station of the Western Regional Climate Center [*WRCC*, 2006] and across the Kolyma River basin in Siberia from the NCEP reanalysis [*Oelke*, 2003]. All anomalies are relative to the 1961–1980 mean.

1.3 Consequences for terrestrial ecosystems

Warmer spring air temperatures have impacted ecosystems by advancing soil thaw [*McDonald et al.*, 2004; *Smith et al.*, 2004] and bud-break by several days [*Keyser et al.*, 2000; *Walther et al.*, 2002; *Delbart et al.*, 2006]. High-latitude ecosystems are sensitive to subtle changes in climate and contribute to regional climate feedbacks through sensible heat, latent heat, and albedo changes. They also contribute to global climate feedbacks through the emission of CO_2 and CH_4 greenhouse gases [*Chapin et al.*, 2000]. Global effects are seen in early season uptake of atmospheric CO_2 caused by spring warming [*Keeling et al.*, 1996; *Myneni et al.*, 1997; *Randerson et al.*, 1999]. Earlier snowmelt allows plant growth to start sooner while moisture levels are high and solar radiation is at its annual peak. However, warm summers (that may increase ecosystem respiration rates and forest fire frequency) could cancel out the increased spring uptake of CO_2 and result in an annual zero balance or even a source of CO_2 to the atmosphere [*Zimov et al.*, 1999; *Angert et al.*, 2005]. Soil moisture dynamics may also play a role in determining the net carbon balance of boreal forests in the future [*Harden et al.*, 2001].

The annual burned area due to forest fires has doubled in North America in the last twenty years at the same time that the climate has warmed [*Kasischke and Stocks*, 2000]. Consequences of changes in fire disturbance rates not only involve direct carbon emissions but also a shift in mean stand age and species composition due to post-fire succession. Accurate climate predictions require understanding ecosystem and disturbance related feedbacks that affect greenhouse gas emissions and radiative forcing.

1.4 Consequences for the Arctic hydrologic cycle

Rivers that enter the Arctic Ocean originate largely in boreal watersheds, and are therefore sensitive to the precipitation and evapotranspiration in that biome [*Serreze et al.*, 2000]. Eurasian Arctic river discharge increased 7% from 1936–1999 following trends in surface air temperature and the North Atlantic oscillation [*Peterson et al.*, 2002]. The input of freshwater to the Arctic Ocean is of critical importance to the salinity and formation of North Atlantic deepwater which regulates the Earth's heat balance. If freshwater input continues to increase, deepwater formation may shut down [*Clark et al.*, 2002]. The likely cause of the increased discharge is suspected to be increased precipitation by the process of elimination. The effects of dams, permafrost thaw, and fires are not large enough to account for the observed increase in discharge [*McClelland et al.*, 2004]. Accurate measurements of precipitation over large Arctic watersheds have proved difficult due to a sparse observational network and collector biases during snow capture [*Serreze et al.*, 2003]. One recent analysis suggests that increased atmospheric CO_2 has led to increased plant water use efficiency (through reduced stomatal conductance) and contributed to increasing discharge by decreasing transpiration losses [*Gedney et al.*, 2006]. However, it is challenging to reconcile this result with observations of a longer growing season [*McDonald et al.*, 2004; *Smith et al.*, 2004], higher leaf area index (LAI) [*Lucht et al.*, 2002] and increases in normalized difference vegetation index (NDVI) [*Myneni et al.*, 1997] that all suggest the potential for summer transpiration has increased.

The largest effects on the Arctic hydrologic cycle in the future will be through melting permafrost. As permafrost degrades, water at the surface becomes more closely connected to subsurface groundwater. As a consequence, soil drainage improves, winter stream flow increases, and summer stream flow decreases [*Hinzman et al.*, 2005]. Despite slight increases in precipitation [*Frey and Smith*, 2003], widespread patterns in lake area changes suggest large regions of permafrost are already thawing [*Smith et al.*, 2005].

1.5 Stable isotopes as tools to detect climate change

Elements are defined by the number of protons in the nucleus of the atom, and isotopes are variations of a given element that contain differing numbers of neutrons which result in measurable differences in atomic mass. Stable isotopes are not radioactive and the most common elemental building blocks in nature are present in at least two stable isotope forms (^{1,2}H, ^{12,13}C, ^{14,15}N, ^{16,17,18}O and ^{32,33,34,36}S). The ratio of heavy to light isotopes (e.g., the $^{18}O/^{16}O$ ratio) may change due to chemical, physical or biological processes. This is known as isotopic fractionation. Isotopic measurements are performed using an isotope ratio mass spectrometer and are reported using delta notation (Equation 1.1) in units of per mil (‰).

$$\delta^{18}O(‰) = \frac{(^{18}O/^{16}O)_{sample} - (^{18}O/^{16}O)_{reference}}{(^{18}O/^{16}O)_{reference}} \cdot 1000 \qquad (1.1)$$

The reference standard for δ^{18}O of water is VSMOW (Vienna Standard Mean Ocean Water) and the most common standard for δ^{18}O of atmospheric CO_2 is VPDB-CO_2 (CO_2 extracted from Vienna Pee Dee Belemnite carbonate by acid digestion at 25°C).

Although the VSMOW scale will not be used for $\delta^{18}O\text{-}CO_2$ in this thesis, it is sometimes used in other reports. The conversion between VSMOW and VPDB-CO_2 is given by Equation 1.2.

$$\delta_{VSMOW} = 1.04143 \cdot \delta_{VPDB\text{-}CO2} + 41.43 \text{ ‰} \quad (1.2)$$

Measurements of isotope ratios and fractionations yield information about the spatial origin and processing history of water and CO_2 in addition to many other compounds.

1.5.1 Oxygen and hydrogen in water

Stable isotopes of precipitation are one indicator of future climate change because they are sensitive to temperature changes and weather patterns. Lighter water molecules ($H_2{}^{16}O$) evaporate more readily than heavier ones ($H_2{}^{18}O$ and $HD^{16}O$), leaving water vapor isotopically depleted in the heavy molecules, and the residual liquid water enriched. This fractionation associated with evaporation is controlled by a combination of temperature sensitive equilibrium and kinetic fractionation effects [*Craig and Gordon*, 1965; *Majoube*, 1971; *Cappa et al.*, 2003].

In general, water evaporates from tropical oceans, and is later removed in the form of rain or snow as the air mass travels towards the poles and across continents. Heavier molecules condense out preferentially and the remaining vapor becomes depleted in the heavy isotopes. The precipitation formed from the vapor of the traveling air mass becomes lighter (more negative δ values) toward the poles and in the interior of continents. This is known as Rayleigh distillation or the rain-out effect [*Dansgaard*, 1964]. Correlations are found in global measurements of $\delta^{18}O$ (and δD) with mean air temperature [*Yurtsever*, 1975]. As air temperature decreases, the water content of an air

mass decreases. In the north, a strong seasonal cycle in air temperature induces a seasonal cycle in δ values, with low δ values in the winter and high δ values in the summer [*Mazor*, 1991]. As global temperatures rise, there may be a measurable increase in the δ values of precipitation in the Arctic.

1.5.2 Oxygen in CO_2

The $\delta^{18}O$ of atmospheric CO_2 ($\delta^{18}O$-CO_2) has the potential to be a useful tracer of biosphere-atmosphere exchange because it is largely controlled by oxygen atom exchange with liquid water pools in the environment and gross biospheric CO_2 fluxes [*Francey and Tans*, 1987]. Figure 1.3 diagrams the processes controlling $\delta^{18}O$-CO_2. Precipitation initially sets the $\delta^{18}O$ of soil water, and then evaporation from the surface sets up an isotopic gradient in the surface soil water [*Riley et al.*, 2002]. CO_2 that is respired in the soil equilibrates isotopically with the surface soil water as it diffuses out of the soil column into the atmosphere [*Tans*, 1998; *Miller et al.*, 1999]. Water is taken up by the roots with no fractionation and is carried to the leaves [*Dawson and Ehleringer*, 1991]. Evaporation from the leaf surface leads to isotopic enrichment, the extent of which is controlled by atmospheric humidity, temperature and the $\delta^{18}O$ of water vapor [*Dongmann et al.*, 1974; *Flanagan et al.*, 1991; *Wang and Yakir*, 1995]. CO_2 diffuses into leaves through the leaf stomata and carbonic anhydrase catalyzes the hydration of CO_2 in leaf water. Approximately ⅔ of the CO_2 diffuses out of the leaf before it can be fixed as plant organic matter, and this CO_2 carries the enriched leaf water $\delta^{18}O$ signal [*Flanagan et al.*, 1997]. Photosynthesis and respiration leave distinct isotopic signatures

on $\delta^{18}O\text{-}CO_2$, as do changes in the $\delta^{18}O$ of precipitation, air temperature, and humidity. For this reason, $\delta^{18}O\text{-}CO_2$ may be a useful diagnostic of ecosystem function and changing environmental conditions.

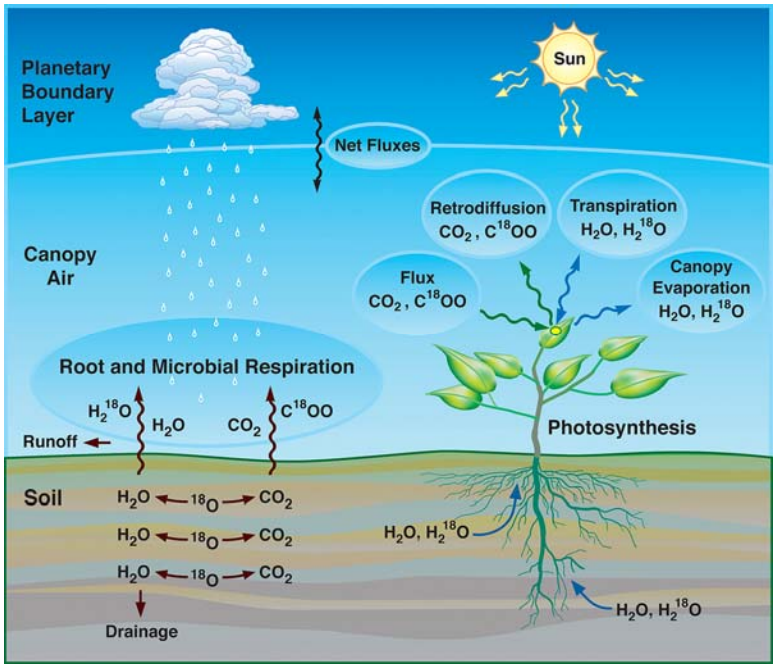

Figure 1.3 Diagram of oxygen isotope transfer between CO_2 and H_2O. Source: ISOLSM model [*Riley et al.*, 2002].

1.6 Eddy covariance technique

Eddy covariance is a micrometeorological technique that measures the net exchange of CO_2 between the atmosphere and several hectares of the local ecosystem [*Baldocchi et al.*, 1988; *Wofsy et al.*, 1993]. Measurements of CO_2 concentrations along with three-dimensional wind speed make it possible to calculate the amount of CO_2 leaving the ecosystem or taken up by the ecosystem averaged over 30-minute time periods. Long-term measurements of net ecosystem exchange (NEE) are improving our

understanding of the terrestrial biosphere's role in the global carbon cycle. However, interpretation of NEE measurements by eddy covariance should be made cautiously [*Goulden et al.*, 1996]. There are, for example, selective systematic errors that occur when the accuracy of the measurement changes as a function of the environmental conditions. Specifically, eddy covariance has been shown to underestimate nighttime respiration during periods of low turbulence [*Goulden et al.*, 1996]. In addition, gaps in the data due to instrument failure, maintenance or unsuitable weather conditions (including low turbulence) introduce sampling uncertainty in long-term datasets. Filling gaps in NEE time series using ecosystem CO_2 flux models parameterized by micrometeorological records and available NEE measurements reduces the uncertainty of sampling error in annual eddy covariance estimates of carbon sequestration.

1.7 Major thesis results and conclusions

Arctic hydrologic, biological, and climatatologic systems are fully coupled and the research presented here examines several interactions among these systems. In the hydrologic study of Chapter 2, I used stable isotope measurements of a major Siberian Arctic river and local precipitation to construct a two-member mixing model to partition snow and rain sources of river discharge and watershed evapotranspiration. I discovered that (1) there is strong seasonality in the $\delta^{18}O$ of river discharge, (2) transpiration was the dominant loss pathway from the watershed during summer and (3) that summer transpiration (plant water use) was fueled by a significant amount (~43%) of snowmelt water.

Measurements of ecosystem CO_2 fluxes and soil, stem, and leaf water $\delta^{18}O$ were used to parameterize a one-box atmosphere model of the seasonality of atmospheric CO_2 and $\delta^{18}O$-CO_2. The biological effects of forest stand-age, or plant functional type, on the atmospheric seasonal cycles are described in Chapter 3. The results showed that a shift to younger deciduous ecosystems in Alaska should delay the phase of the seasonal CO_2 cycle and increase the amplitude. An advance in the phase of $\delta^{18}O$-CO_2 was predicted as well as an increase in the $\delta^{18}O$-CO_2 background. Such predictions and observations are necessary to make sense of trends in the atmospheric CO_2 and $\delta^{18}O$-CO_2 records.

Finally, in Chapter 4, I investigated the response of NEE measured by eddy covariance, and model partitioned gross primary production and total ecosystem respiration, to climatologic variability during warm springs and summer drought in an Alaskan deciduous aspen forest and an evergreen black spruce forest, comparing the differences in response to plant functional type. The younger deciduous forest was more sensitive to climate variability than the older evergreen forest. This suggests that the interannual variability observed in Northern Hemisphere atmospheric CO_2 concentrations may be disproportionately controlled by broadleaf deciduous plant functional types.

1.8 References

ACIA (2004), *Impacts of a Warming Arctic: Arctic Climate Impact Assessment*, Cambridge University Press, http://www.acia.uaf.edu.

Angert, A., S. Biraud, A. Bonfils, C. C. Henning, W. Buermann, J. Pinzon, C. J. Tucker, and I. Fung (2005), Drier summer cancel out the CO_2 uptake enhancement induced by warmer springs, *Proc. Nat. Acad. Sci. U. S. A.*, *102*, 31, 10823-10827.

Baldocchi, D. D., B. B. Hicks, and T. P. Meyers (1988), Measuring biosphere-atmosphere exchanges of biologically related gases with micrometeorological methods, *Ecology*, *69*, 5, 1331-1340.

Baldocchi, D., F. M. Kelliher, T. A. Black, and P. Jarvis (2000), Climate and vegetation controls on boreal zone energy exchange, *Global Change Biol.*, *6*, 69-83.

Cappa, C. D., M. B. Hendricks, D. J. DePaolo, and R. C. Cohen (2003), Isotopic fractionation of water during evaporation, *J. Geophys. Res.*, *108*, D16, 4525, doi:4510.1029/2003JD003597.

Cess, R. D., et al. (1991), Interpretation of snow-climate feedback as produced by 17 general-circulation models, *Science*, *253*, 5022, 888-892.

Chapin, F. S., et al. (2000), Arctic and boreal ecosystems of western North America as components of the climate system, *Global Change Biol.*, *6*, 211-223.

Chapin, F. S., P. A. Matson, and H. A. Mooney (2002), *Principles of Terrestrial Ecosystem Ecology*, Springer-Verlag, New York.

Chapin, F. S., et al. (2005), Role of land-surface changes in Arctic summer warming, *Science*, *310*, 5748, 657-660.

Chapman, W. L., and J. E. Walsh (1993), Recent variations of sea ice and air-temperature in high-latitudes, *Bull. Am. Meteorol. Soc.*, *74*, 1, 33-47.

Clark, P. U., N. G. Pisias, T. F. Stocker, and A. J. Weaver (2002), The role of the thermohaline circulation in abrupt climate change, *Nature*, *415*, 6874, 863-869.

Craig, H., and L. I. Gordon (1965), Deuterium and oxygen-18 variations in the ocean and the marine atmosphere, paper presented at Proceedings of a Conference on Stable Isotopes in Oceanographic Studies and Paleotemperatures, Spoleto, Italy.

Dansgaard, W. (1964), Stable isotopes in precipitation, *Tellus*, *16*, 436-468.

Dawson, T. E., and J. R. Ehleringer (1991), Streamside trees that do not use stream water, *Nature*, *350*, 335-337.

Delbart, N., T. Le Toan, L. Kergoat, and V. Fedotova (2006), Remote sensing of spring phenology in boreal regions: A free of snow-effect method using NOAA-AVHRR and SPOT-VGT data (1982-2004), *Remote Sens. Environ.*, *101*, 1, 52-62.

Dixon, R. K., S. Brown, R. A. Houghton, A. M. Solomon, M. C. Trexler, and J. Wisniewski (1994), Carbon pools and flux of global forest ecosystems, *Science*, *263*, 5144, 185-190.

Dongmann, G., H. W. Nurnberg, H. Forstel, and K. Wagener (1974), Enrichment of $H_2{}^{18}O$ in leaves of transpiring plants, *Radiation and Environmental Biophysics*, *11*, 1, 41-52.

Flanagan, L. B., J. P. Comstock, and J. R. Ehleringer (1991), Comparison of modeled and observed environmental-influences on the stable oxygen and hydrogen isotope composition of leaf water in *Phaseolus vulgaris* L., *Plant Physiol.*, *96*, 2, 588-596.

Flanagan, L. B., J. R. Brooks, G. T. Varney, and J. R. Ehleringer (1997), Discrimination against (COO)-O-18-O-16 during photosynthesis and the oxygen isotope ratio of respired CO_2 in boreal forest ecosystems, *Glob. Biogeochem. Cycle*, *11*, 1, 83-98.

Francey, R. J., and P. P. Tans (1987), Latitudinal variation in O-18 of atmospheric CO_2, *Nature*, *327*, 6122, 495-497.

Frey, K. E., and L. C. Smith (2003), Recent temperature and precipitation increases in West Siberia and their association with the Arctic Oscillation, *Polar Research*, *22*, 2, 287-300.

Gedney, N., P. M. Cox, R. A. Betts, O. Boucher, C. Huntingford, and P. A. Stott (2006), Detection of a direct carbon dioxide effect in continental river runoff records, *Nature*, *439*, 7078, 835-838.

GHCN (2006), Global Historical Climatology Network, http://data.giss.nasa.gov/gistemp/graphs/, edited by NASA/GISS.

Goulden, M. L., J. W. Munger, S. M. Fan, B. C. Daube, and S. C. Wofsy (1996), Measurements of carbon sequestration by long-term eddy covariance: Methods and a critical evaluation of accuracy, *Global Change Biol.*, *2*, 3, 169-182.

Hansen, J., R. Ruedy, J. Glascoe, and M. Sato (1999), GISS analysis of surface temperature change, *J. Geophys. Res.*, 104, D24, 30,997-31,002.

Harden, J. W., R. Meier, C. Silapaswan, D. K. Swanson, and A. D. McGuire (2001), Soil drainage and its potential for influencing wildfires in Alaska, *Studies by the U.S. Geological Survey in Alaska*, U.S. Geological Survey Professional Paper 1678.

Hinzman, L. D., et al. (2005), Evidence and implications of recent climate change in northern Alaska and other arctic regions, *Clim. Change*, *72*, 3, 251-298.

Hobbie, S. E., J. P. Schimel, S. E. Trumbore, and J. R. Randerson (2000), Controls over carbon storage and turnover in high-latitude soils, *Global Change Biol.*, *6*, 196-210.

IPCC (2001), *Intergovernmental Panel on Climate Change, Climate change 2001*, Cambridge Univ. Press, New York.

Kasischke, E. S., and B. J. Stocks (2000), *Fire, Climate Change, and Carbon Cycling in the Boreal Forest.*, 461 pp., Springer, New York.

Keeling, C. D., J. F. S. Chin, and T. P. Whorf (1996), Increased activity of northern vegetation inferred from atmospheric CO_2 measurements, *Nature*, *382*, 6587, 146-149.

Keyser, A. R., J. S. Kimball, R. R. Nemani, and S. W. Running (2000), Simulating the effects of climate change on the carbon balance of North American high-latitude forests, *Global Change Biol.*, *6*, 185-195.

Landsberg, J. J., and S. T. Gower (1997), *Application of Physiological Ecology to Forest Management*, Academic Press, San Diego, CA.

Lucht, W., I. C. Prentice, R. B. Myneni, S. Sitch, P. Friedlingstein, W. Cramer, P. Bousquet, W. Buermann, and B. Smith (2002), Climatic control of the high-

latitude vegetation greening trend and Pinatubo effect, *Science*, *296*, 5573, 1687-1689.

Majoube, M. (1971), Oxygen-18 and deuterium fractionation between water and steam, *Journal de Chimie Physique et de Physico-Chimie Biologique*, *68*, 10, 1423-1436.

Mazor, E. (1991), Stable hydrogen and oxygen isotopes, in *Applied Chemical and Isotopic Groundwater Hydrology*, pp. 122-146, Halstead Press, New York.

McClelland, J. W., R. M. Holmes, B. J. Peterson, and M. Stieglitz (2004), Increasing river discharge in the Eurasian Arctic: Consideration of dams, permafrost thaw, and fires as potential agents of change, *J. Geophys. Res.*, *109*, D18102, doi:10.1029/2004JD004583.

McClone, M. S. (1996), When history matters: scale, time, climate and tree diversity, *Global Ecology and Biogeography Letters*, *5*, 309-314.

McDonald, K. C., J. S. Kimball, E. Njoku, R. Zimmermann, and Z. Maosheng (2004), Variability in springtime thaw in the terrestrial high latitudes: Monitoring a major control on the biospheric assimilation of atmospheric CO_2 with spaceborne microwave remote sensing, *Earth Interactions*, *8*, 20, 1-23.

Miller, J. B., D. Yakir, J. W. C. White, and P. P. Tans (1999), Measurement of O-18/O-16 in the soil-atmosphere CO_2 flux, *Glob. Biogeochem. Cycle*, *13*, 3, 761-774.

Myneni, R. B., C. D. Keeling, C. J. Tucker, G. Asrar, and R. R. Nemani (1997), Increased plant growth in the northern high latitudes from 1981 to 1991, *Nature*, *386*, 6626, 698-702.

Oechel, W. C., G. L. Vourlitis, S. J. Hastings, R. C. Zulueta, L. Hinzman, and D. Kane (2000), Acclimation of ecosystem CO_2 exchange in the Alaskan Arctic in response to decadal climate warming, *Nature*, *406*, 6799, 978-981.

Oelke, C. (2003), NCEP sigma 0.995 level temperature [K] with topography correction, new RIMS landmask with 39926 pixels, edited by NSIDC.

Olsen, J. S., J. A. Watts, and L. J. Allison (1985), Major world ecosystem complexes ranked by carbon in live vegetation: A database (ORNL/CDIAC-134, NDP-017), Carbon Dioxide Information Center, Oak Ridge National Laboratory, Oak Ridge, Tennessee, U.S.A. (Revised 2001) http://cdiac.ornl.gov/epubs/ndp/ndp017/ndp017.html.

Overpeck, J., et al. (1997), Arctic environmental change of the last four centuries, *Science*, *278*, 5341, 1251-1256.

Peterson, B. J., R. M. Holmes, J. W. McClelland, C. J. Vorosmarty, R. B. Lammers, A. I. Shiklomanov, I. A. Shiklomanov, and S. Rahmstorf (2002), Increasing river discharge to the Arctic Ocean, *Science*, *298*, 5601, 2171-2173.

Randerson, J. T., C. B. Field, I. Y. Fung, and P. P. Tans (1999), Increases in early season ecosystem uptake explain recent changes in the seasonal cycle of atmospheric CO_2 at high northern latitudes, *Geophys. Res. Lett.*, *26*, 17, 2765-2768.

Riley, W. J., C. J. Still, M. S. Torn, and J. A. Berry (2002), A mechanistic model of (H_2O)-O-18 and (COO)-O-18 fluxes between ecosystems and the atmosphere: Model description and sensitivity analyses, *Glob. Biogeochem. Cycle*, *16, 4*, 1095, doi:10.1029/2002GB001878.

Serreze, M. C., et al. (2000), Observational evidence of recent change in the northern high-latitude environment, *Clim. Change*, *46*, 1-2, 159-207.

Serreze, M. C., M. P. Clark, and D. H. Bromwich (2003), Monitoring precipitation over the Arctic terrestrial drainage system: Data requirements, shortcomings, and applications of atmospheric reanalysis, *J. Hydrometeorol.*, *4*, 2, 387-407.

Smith, L. C., Y. Sheng, G. M. MacDonald, and L. D. Hinzman (2005), Disappearing Arctic lakes, *Science*, *308*, 5727, 1429-1429.

Smith, N. V., S. S. Saatchi, and J. T. Randerson (2004), Trends in high northern latitude soil freeze and thaw cycles from 1988 to 2002, *J. Geophys. Res.*, *109*, D12101, doi:10.1029/2003JD004472.

Tans, P. P. (1998), Oxygen isotopic equilibrium between carbon dioxide and water in soils, *Tellus, Ser. B*, *50*, 2, 163-178.

Walther, G. R., E. Post, P. Convey, A. Menzel, C. Parmesan, T. J. C. Beebee, J. M. Fromentin, O. Hoegh-Guldberg, and F. Bairlein (2002), Ecological responses to recent climate change, *Nature*, *416*, 6879, 389-395.

Wang, X. F., and D. Yakir (1995), Temporal and spatial variations in the oxygen-18 content of leaf water in different plant species, *Plant Cell Envior.*, *18*, 12, 1377-1385.

Wofsy, S. C., M. L. Goulden, J. W. Munger, S. M. Fan, P. S. Bakwin, B. C. Daube, S. L. Bassow, and F. A. Bazzaz (1993), Net exchange of CO_2 in a midlatitude forest, *Science*, *260*, 5112, 1314-1317.

WRCC (2006), Western Regional Climate Center, http://www.wrcc.dri.edu/climsum.html.

Yurtsever, Y. (1975), *Worldwide survey of stable isotopes in precipitation. Report of the Isotope Hydrology Section*, 40 pp, International Atomic Energy Agency, Vienna.

Zimov, S. A., S. P. Davidov, G. M. Zimova, A. I. Davidova, F. S. Chapin, M. C. Chapin, and J. F. Reynolds (1999), Contribution of disturbance to increasing seasonal amplitude of atmospheric CO_2, *Science*, *284*, 5422, 1973-1976.

Chapter 2

A HIGH-RESOLUTION TIME SERIES OF OXYGEN ISOTOPES FROM THE KOLYMA RIVER: IMPLICATIONS FOR THE SEASONAL DYNAMICS OF DISCHARGE AND BASIN-SCALE WATER USE*

*Adapted from Welp, L. R., J. T. Randerson, J. C. Finlay, S. P. Davydov, G. M. Zimova, A. I. Davydova, and S. A. Zimov (2005), *Geophysical Research Letters*, 32, LI4401, doi:10.1029/2005GL022857.

2.1 Abstract

Intensification of the Arctic hydrologic cycle and permafrost melt are expected as concentrations of atmospheric greenhouse gases increase. Quantifying hydrologic cycle change is difficult in remote northern regions; however, monitoring the stable isotopic composition of water runoff from Arctic rivers provides a means to investigate integrated basin-scale changes. We measured river water and precipitation $\delta^{18}O$ and δD to partition the river flow into snow and rain components in the Kolyma River basin. On an annual basis, we found water leaving the basin through the river consisted of 60% snow and 40% rain. This is compared with annual precipitation inputs to the watershed of 47% snow and 53% rain. Despite the presence of continuous permafrost, and fully frozen soils in the spring, our analysis showed not all spring snowmelt runs off into the river immediately. Instead, a significant portion is retained and leaves the basin as growing season evapotranspiration.

2.2 Introduction

Total annual discharge from the six largest Eurasian rivers has increased significantly from 1936 to 1999 [2002]. If this trend in freshwater input continues, North Atlantic deepwater formation may be disrupted, with potentially serious consequences for climate [*Clark et al.*, 2002]. In addition, such hydrologic changes alter the delivery of carbon and nutrients from land to the Arctic Ocean [*Dittmar and Kattner*, 2003]. Increasing rates of permafrost melt and loss of forests to fire may contribute to a small part of the trend in river discharge, but cannot account for the entire magnitude of change. Increased precipitation is the most likely cause [*McClelland et al.*, 2004]. Unfortunately, measuring precipitation over large Arctic watersheds has been challenging [*Serreze et al.*, 2003]. Stable water isotope measurements of major Arctic rivers have potential to provide insights about mechanisms responsible for observed discharge trends.

The isotopic composition of precipitation is largely controlled by water vapor source, the formation temperature of precipitation, and relative fraction of water vapor removed from the atmosphere [*Gat*, 1996]. Most IAEA stations analyzed for stable isotopes exhibit seasonal cycles similar to air temperature variations [*Gat and Gonfiantini*, 1981], with enrichment of heavy isotopes during warm summer months and depletion in cold winter months. Previous work on Siberian water isotopes have exploited temperature dependence to reconstruct paleoclimate temperatures using stable water isotopes preserved in ice wedges [*Vasil'chuk*, 1992]. In Canada, modern lake stable isotopes have been used to partition regional evapotranspiration fluxes [*Gibson*

and Edwards, 2002] and river stable isotopes were used to estimate the basin-scale transpiration flux of the Mississippi basin [*Lee and Veizer*, 2003].

Here, we present a time series of $\delta^{18}O$ in the northeast Siberian Kolyma River. The Kolyma is the sixth largest Arctic river and the only river that showed no increase in discharge in the study by *Peterson et al.* [2002]. It is also the largest Arctic river completely underlain by continuous permafrost [*Brabets et al.*, 2000; *McClelland et al.*, 2004]. Permafrost influences watershed hydrology through shallow and seasonally varying active layer storage capacity [*McNamara et al.*, 1997]. Consequently, Arctic river transport of water, carbon, and nutrients is strongly seasonal [*Dittmar and Kattner*, 2003]. Our objectives were to (1) measure a baseline in the Kolyma against which to compare future effects of Arctic climate change and (2) use stable water isotopes and a two end-member mixing model to determine seasonal export of snow and rain from the basin.

2.3 Methods

2.3.1 Study area

The Kolyma drains an area of 650,000 km^2 with a mean annual discharge of 132 $km^3\ yr^{-1}$ [*McClelland et al.*, 2004]. Our sampling locations were near the town of Cherskii (69°N, 161°E), 150 km from the mouth of the Kolyma and ~50 km south of the northern tree line (Figure 2.1). Discharge was measured at the Kolymskoye gauge station, an additional 160 km upstream of Cherskii. The Anniui River confluence is located between the sampling and gauging stations and contributes ~ 4% of the river

flow. Cherskii has a strongly continental climate with warm summers (June-August average temperature of 12°C), cold winters (average January temperature is -35°C) and low annual precipitation (185 mm yr^{-1}). The Kolyma watershed is dominated by deciduous larch taiga and tundra vegetation, and ~10% of land area is covered by lakes.

Figure 2.1 Water sampling was conducted at Cherskii, near the mouth of the Kolyma River, and the discharge gauging station was located at Kolymskoye. (Map source: *Cornell University Interactive Mapping Tool*)

2.3.2 Water sampling and isotopic analysis

We sampled the Kolyma from August 2002 to April 2004, with monthly collections during winter and more frequent collections during the ice-free season. We collected samples just below the river surface during ice-free months (under the ice during winter) in 4–25 mL glass vials with inverted cones inside screw top caps. The vials were sealed with parafilm, and kept cool during storage. We sampled individual

rain events in Cherskii[1] using pan collectors (emptied immediately following the event to minimize evaporation). Volunteers surveyed snow on April 8–19, 2003, at 23 locations within 300 km of Cherskii. By sampling snow immediately prior to spring thaw, we attempted to include post-deposition isotopic effects within the snow pack. Surface and sub-surface samples were allowed to thaw in 125 mL plastic bottles and transferred to 25 mL glass vials.

We analyzed waters for $\delta^{18}O$ by CO_2 equilibration with a GasBenchII connected to a Thermo Finnigan Delta Plus isotope ratio mass spectrometer at UC Irvine. We sent a subset to the Center for Stable Isotope Biogeochemistry at UC Berkeley for δD analysis using a Thermo Finnigan MAT H/Device. All isotope results in this paper are presented on the VSMOW scale. Analytical uncertainty was 0.1‰ for $\delta^{18}O$ and 1.6‰ for δD.

2.3.3 Partitioning approach

We calculated contributions of snow and rain inputs to the river for each sampling period using a two end-member mixing model:

$$Q(t) = Q(t) \cdot f_{\text{snow}}(t) + Q(t) \cdot f_{\text{rain}}(t),\ f_{snow} + f_{rain} = 1 \qquad (2.1)$$

where Q is total river discharge, f_{snow} and f_{rain} are snow and rain fractions of Q, and t is time.

$$\delta_{river}(t) = f_{snow}(t) \cdot \delta_{snow} + f_{rain}(t) \cdot \delta_{rain} \qquad (2.2)$$

δ_{river} is measured river $\delta^{18}O$, and estimates of the mean $\delta^{18}O$ of snow and rain end-members are denoted as δ_{snow} and δ_{rain}. We characterized δ_{snow} by taking the arithmetic

[1] Cherskii became an official IAEA GNIP sampling station in October 2005 and continues to collect monthly composite samples.

mean of the spring snow survey and determined δ_{rain} in two steps. First, we weighted the $\delta^{18}O$ of each individual rain event by the amount of precipitation measured at the Cherskii airport within each month to determine a weighted mean. Second, each monthly mean (May through September) was weighted by the total precipitation for that month, minimizing bias from over or under-sampling rain events during some months with respect to others.

We made a few assumptions about watershed processes other than mixing of snow and rain to use the partitioning method described above. The water budget of a river basin can be defined as,

$$Q = P - ET - \Delta S \tag{2.3}$$

where P is precipitation, ET is evapotranspiration, and ΔS is the change in groundwater storage. We assumed ΔS for one year was negligible because there is only one dam (hydroelectric) that finished filling in 1990 [*McClelland et al.*, 2004]. This simplified Equation 2.3 to:

$$Q = P - ET \tag{2.4}$$

ET is composed of evaporation (E), transpiration, and interception. Transpiration and interception do not modify the isotopic composition of surface water, and therefore, interception will be included in transpiration throughout this paper. E, however, enriches the residual water in heavy isotopes. If E was a large part of ET in this watershed, and evaporating elements (e.g., lakes) were closely linked to river flow, then δ_{river} cannot be assumed to be a simple mixture of snow and rain end-members.

To test the isotopic influence of *E* on the Kolyma, we measured δD on a subset of precipitation and all river samples. Negative d-excess (d-excess = $\delta D - 8 \cdot \delta^{18}O$) values have been used as an elimination criterion for samples suspected of *E* influence [*Kurita et al.*, 2004]. Isotopic equations derived to quantify the *E*/*P* ratio for lakes have been used to estimate evaporation from river systems [*Gibson and Edwards*, 2002; *Lee and Veizer*, 2003] (described as an appendix in section 2.6).

Finally, we estimated the contributions of snow and rain to the annual water budget using a mass balance approach.

$$Q \cdot f_{snow} = P \cdot f_{snow}^{P} - ET \cdot f_{snow}^{ET} \tag{2.5}$$

Knowing Q, f_{snow}, P and f_{snow}^{P}, one can solve for the snow fraction of ET (f_{snow}^{ET}). A similar equation can be written for the rain fraction.

2.3.4 Data sources

We obtained daily discharge records of the Kolymskoye gauge station on the Kolyma from Arctic-RIMS (Rapid Integrated Monitoring System) (http://rims.unh.edu/). We also utilized several basin-scale NCEP products from Arctic-RIMS, including rescaled *P* and *P*-ET estimates by *Serreze et al.* [2003] and elevation adjusted surface temperature [*Oelke*, 2003]. Serreze's *P* product was a rescaling of NCEP reanalysis data using measurements from a sparse precipitation gauge station network in the Arctic. We then subtracted *P*-ET from *P* to estimate the seasonal cycle of ET.

2.4 Results and Discussion

2.4.1 Stable oxygen isotope observations

We measured the Kolyma $\delta^{18}O$ from August 2002 through April 2004 (Figure 2.2). The *Q*-weighted annual mean $\delta^{18}O$ value for the Kolyma from October 2002 to September 2003 was -22.2‰. This compares remarkably well with the value of -22.4‰ mentioned in *Letolle et al.* [1993] used by *Ekwurzel et al.* [2001]. River $\delta^{18}O$ rapidly became depleted (more negative) during the spring pulse of snowmelt in late-May to early June. Minimum $\delta^{18}O$ (-24.4‰) occurred on June 7, 2003, near the seasonal maximum in *Q*, but delayed by 6 days (Figure 2.3a). The mean and standard deviation about the mean of sampled snow, -26.2 ± 5.0‰, explained the depletion during the spring thaw. From June through early July, *Q* remained high and river $\delta^{18}O$ rapidly increased due to summer rain inputs which had a weighted mean and standard deviation in the mean of -16.3 ± 3.8‰. (For reference, ice formations in the permafrost of this region range from -19‰ to -26‰ [*Vasil'chuk et al.*, 2001].) Maximum $\delta^{18}O$ occurred during October of both 2002 and 2003 (with a value of -21.0 ± 0.1‰ in both years), and then slowly decreased over the baseflow months of October through January, stabilizing by February until the spring thaw in May. Rain, snow and river measurements are archived online[2] and as an appendix in section 2.8.

[2] This data is included in the GRL paper as supplemental online material (http://www.agu.org/journals/gl/gl0514/2005GL022857/) and has been submitted to the National Science Foundation's Arctic System Science (ARCSS) database.

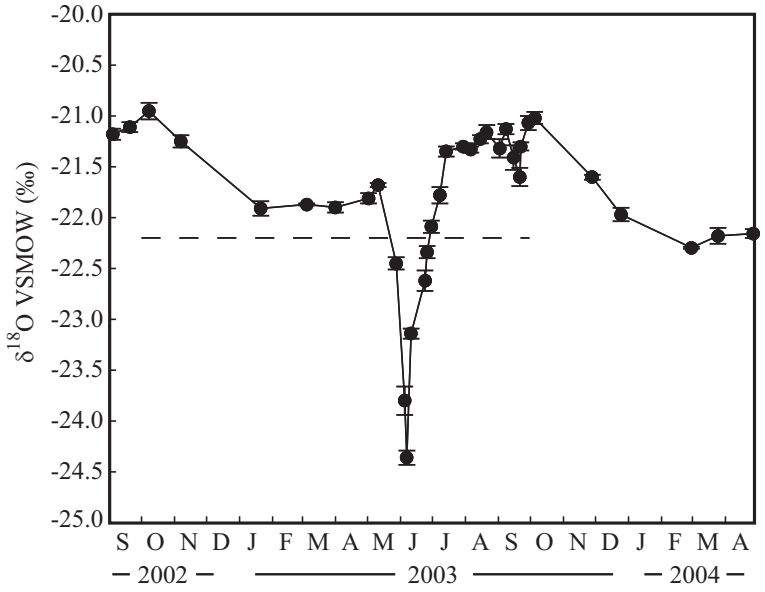

Figure 2.2 $\delta^{18}O$ of the Kolyma River sampled at Cherskii, from September 2002 through April 2004. Error bars represent the analytical standard deviation. The *Q*-weighted mean for the one-year period from October 2002 to September 2003 was -22.2‰, marked by the dashed line.

January through April baseflow $\delta^{18}O$ in 2003 was -21.9 ± 0.1‰ and was 0.3‰ lower in 2004 (-22.2 ± 0.1‰). The source of low winter *Q* (~200 m^3 s^{-1}) is assumed to be deep groundwater and controlled release from the hydroelectric dam. The cause of interannual variability in river baseflow $\delta^{18}O$ is uncertain, but may reflect more snow input to the hydroelectric reservoir in the second year. Seasonal variations in Kolyma $\delta^{18}O$ are similar to Canadian river time series of measurements during ice-free conditions, and reconstructions of winter $\delta^{18}O$ from river ice cores [*Gibson and Prowse,* 2002].

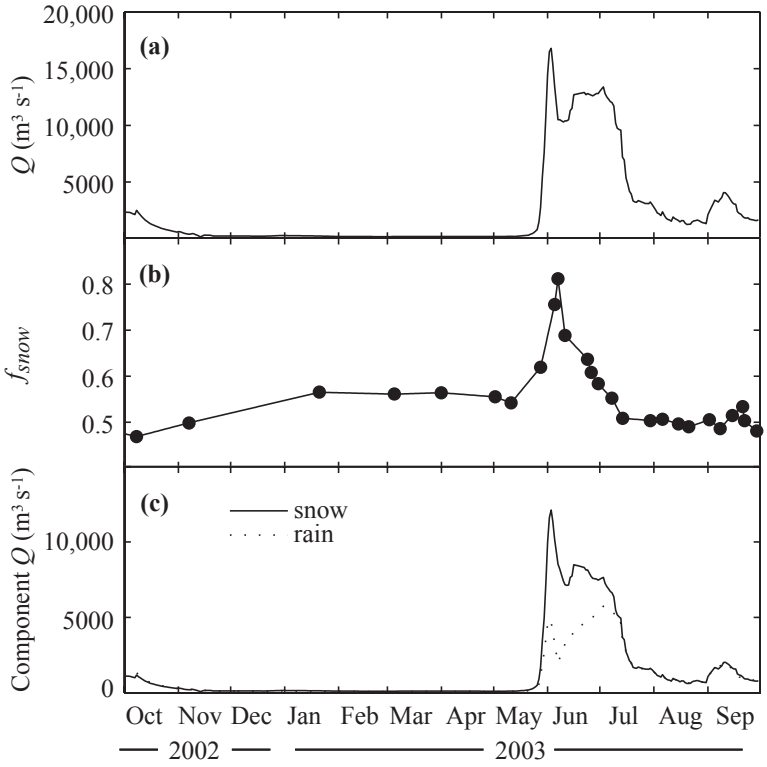

Figure 2.3 (a) Kolyma Q (m^3 s^{-1}) measured at Kolymskoye, (b) fraction of snow component calculated from $\delta^{18}O$ partitioning, and (c) the discharge (m^3 s^{-1}) associated with snow (solid line) and rain components (dotted line). The fraction of snow peaked in early June at 82%, and the rain component peak was delayed until early July.

2.4.2 Partitioning river flow into snow and rain components

We used mean snow and rain $\delta^{18}O$ end-members described above (-26.2 ± 5.0‰ and -16.3 ± 3.8‰) and measurements of the Kolyma from October 2002 to September 2003 (Figure 2.2) to partition snow and rain contributions to the river (Figure 2.3b). During the spring Q pulse, the snow component peaked at 82%. During baseflow conditions, snow and rain contributions to the river were both close to 50%. In Figure 2.3c we show the mass flux of snow and rain components. Snow dominated the river flow during spring, peaking in early June. In contrast, inputs from rain increased over the

summer and peaked during early July. Summing these curves over the year, we found 60 ± 10% of water leaving the Kolyma originally fell as snow and 40 ± 10% as rain.

2.4.3 Annual water balance

We compared our analysis of the annual snow and rain partitioning in river runoff to the proportions of annual snow and rain that fell on the watershed. Figure 2.4 shows monthly mean *P*, air temperature, and ET estimated for the Kolyma watershed, and measured air temperature and *P* at Cherskii for our study period. Cherskii airport air temperature was used to define the rain season as May through September (air temperatures above freezing) and the snow season as October through April. We estimated that 47% of annual *P* fell as snow and 53% as rain. We then used Equation 2.5 to partition the remaining loss pathway, ET, into 43% snow and 57% rain (Table 2.1).

Table 2.1 Annual water budget of the Kolyma River basin

Water Budget Component	$km^3 yr^{-1}$	Snow	Rain	Error
River Discharge	74	60%	40%	10%
Precipitation Inputs	340	47%	53%	~ 15%
Evapotranspiration	266	43%	57%	~ 18%

Water loss pathways in the Kolyma watershed are extremely seasonal. The months of May through September account for 90% of river *Q* and 83% of ET. Comparing fractions of snow and rain from incoming *P* and outgoing river *Q*, there is a higher proportion of snow in river *Q* than in *P*. This supports the assumption that much of the snowmelt immediately flows over the frozen soil surface into the river. However,

it is apparent from ET partitioning, that snow contributes substantially to the summer ET flux. This is consistent with recent studies showing Siberian larch forests utilize snowmelt water during spring leaf-out, a period of enhanced transpiration [*Sugimoto et al.*, 2002], and local scale hydrologic experiments that show about half of snowmelt is lost as runoff, and the other half recharges soil water (S. P. Davidov, unpublished data, 2004).

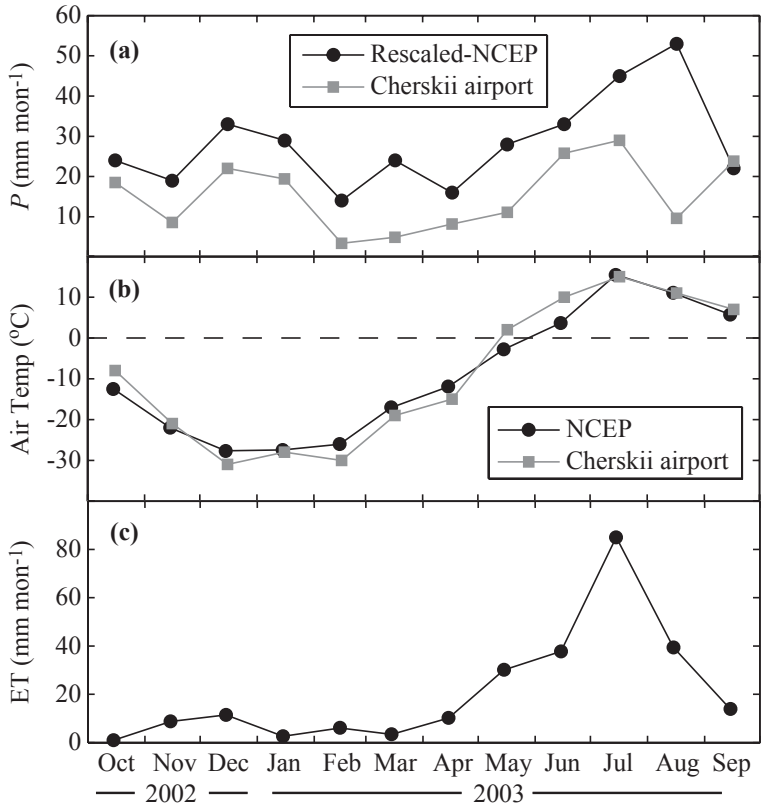

Figure 2.4 (a) Rescaled NCEP monthly mean *P* (mm mon^{-1}) [*Serreze et al.,* 2003] for the Kolyma watershed (circles) and measured at the Cherskii airport (squares). (b) Monthly mean surface air temperature from the elevation corrected NCEP reanalysis for the Kolyma watershed (circles) [*Oelke,* 2003] and measured at the Cherskii airport (squares). (c) ET estimated from *Serreze et al*. [2003].

2.4.4 Evaporation influence estimated from δD and $\delta^{18}O$

Some precipitation samples we analyzed for δD (13 out of 44) had negative d-excess values, suggesting they may have been evaporatively enriched. If we discarded these samples, δ_{rain} decreased to -16.6‰ and the resulting river *Q* partitioning shifted by 2% (f_{snow} = 58% and f_{rain} = 42%). Using only precipitation samples with positive d-excess values, the local meteoric water line (LMWL) was $\delta D = 7.0 \cdot \delta^{18}O - 11.7$, r^2=0.99, n=31 (Figure 2.5). None of the Kolyma samples had negative d-excess values. The Kolyma waterline was $\delta D = 6.8 \cdot \delta^{18}O - 19.1$, r^2=0.98, n=30.

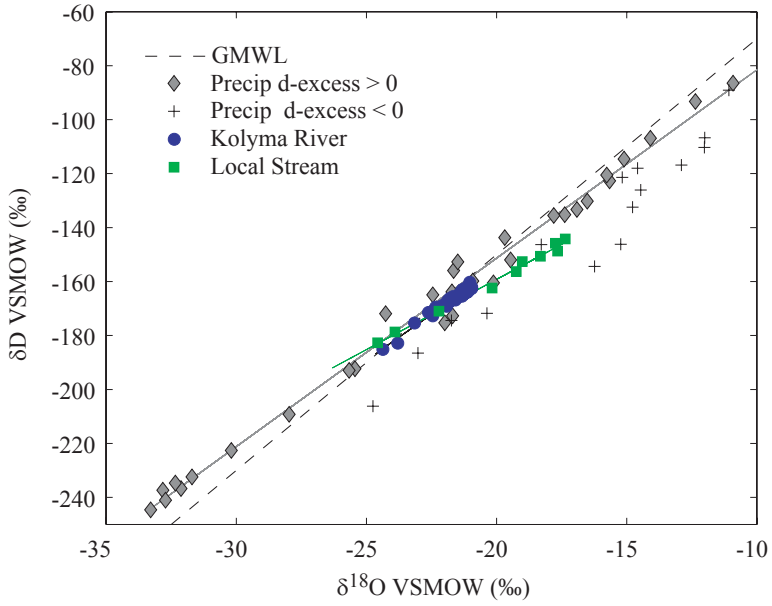

Figure 2.5 $\delta^{18}O$ versus δD relationships for precipitation (rain and snow) with d-excess values greater than zero (grey diamonds) and d-excess values less than zero (pluses), the Kolyma River (blue circles), and the local stream (green squares). A least-squares fit line for precipitation using all data (diamonds and pulses) is $\delta D = 6.6 \cdot \delta^{18}O - 23.7$ and when using only d-excess values greater than zero, the regression is $\delta D = 7.0 \cdot \delta^{18}O - 11.7$. The Kolyma River regression is $\delta D = 6.8 \cdot \delta^{18}O - 19.1$. The local stream regression is $\delta D = 5.2 \cdot \delta^{18}O - 55.1$. The global meteoric water line (GMWL) is plotted for reference, $\delta D = 8 \cdot \delta^{18}O + 10$ (dashed line). Error bars are smaller than the symbols.

The slopes of the LMWL and the river regression line were similar (7.0 ± 0.1‰ compared to 6.8 ± 0.2‰), indicating a low *E*/*P* ratio for the watershed. Using the approach described in the appendix section 2.6 of this chapter, we estimated 6% of *P* for the basin was lost through *E*. Therefore, *E* does not appear to be a major component of ET in the Kolyma and our assumption that measured $\delta^{18}O$ in river samples represent a simple mixture of snow and rain (not enriched significantly by *E*) appears valid.

2.4.5 Partitioning error and sensitivity analysis

Sources of uncertainty in this study were (1) the assumption that precipitation collected near Cherskii was representative of the entire watershed and (2) there was no enrichment of snowmelt water above measured snowpack $\delta^{18}O$ [*Laudon et al.*, 2002]. We explored sensitivity to the choice of δ_{rain} and δ_{snow} by calculating the annual river partitioning using end-members ± 1‰. Resulting f_{snow} values range from 50–70% with 6% standard deviation, which is within our estimated standard deviation of 10%. Also, statistically similar slopes for the river δD-$\delta^{18}O$ water line and the LMWL suggest there are not drastically different water vapor sources and precipitation conditions upstream.

2.5 Conclusions

We determined the Q-weighted annual average of Kolyma $\delta^{18}O$ was -22.2‰ and during the same year, 60% of water that left the basin through the river originally fell as snow and 40% as rain. Our analysis suggests not all snowmelt leaves the watershed as spring runoff, instead, a significant amount contributes to ET. We believe monitoring stable water isotopes of Arctic rivers will aid investigations of future climate change.

Increases in river $\delta^{18}O$ are expected as a result of increasing mean annual temperature. However, a shift in the seasonality of precipitation, changes in surface vegetation (type, coverage, and water status) and increases in active layer depth as a result of permafrost melt may also contribute to changes in Arctic hydrology and the water isotope budget.

Acknowledgements:

This work was supported by an NSF RAISE grant OPP-0097439. We thank H. Kristenson and S. Hayden for field sampling and J. Neff for logistical assistance. We also thank X. Xu and S. Trumbore at UCI for the use of their stable isotope facilities. LRW received support from the EPA's STAR fellowship program.

2.6 Appendix to section 2.3.3

Equations derived to quantify the evaporation/precipitation (E/P) ratio for lakes can be used as a first order estimate of evaporation from a river system [*Gibson et al.*, 1993; *Gibson and Edwards*, 2002; *Lee and Veizer*, 2003]. In this study we used the approach by Gibson et al. [1993].

$$E/P = (\delta_s - \delta_p)/(\delta^* - \delta_s) \cdot (1 - h)/h \quad (2.6)$$

Where δ_s is the weighted isotopic composition of the river and δ_p is the mean annual weighted isotopic composition of precipitation for the basin. δ_p was determined to be -24.4‰ from the intersection of the d-excess filtered LMWL and that of a local stream with a greater evaporative influence from lakes than the Kolyma River. This local stream

had a water regression line of $\delta D = 5.2 \cdot \delta^{18}O - 55.1$, $r^2=0.99$, n=10. δ^* represents the limiting isotopic composition under climate conditions and is defined by the following equation.

$$\delta^* = (h \cdot \delta_a + \varepsilon)/(h - \varepsilon) \quad (2.7)$$

δ_a is the isotopic composition of atmospheric water vapor estimated in equilibrium with precipitation at the mean air temperature, ε is the combined kinetic and equilibrium fractionation factor between liquid and vapor water ($\varepsilon^* + \varepsilon^k$), ε^* is the equilibrium fractionation factor, $(\alpha - 1)1000$ where $\ln \alpha = 1137\ T^{-2} - 0.4156\ T^{-1} - 0.00207$ [*Majoube*, 1971], and ε^k is the kinetic fractionation factor (14.2‰ $\cdot$ (1 - h) for oxygen) [*Gonfiantini*, 1986]. h is the mean relative humidity. We obtained estimates of evaporation-weighted air temperature (15°C) and relative humidity (60%) from eddy covariance micrometerologic station measurements installed near Cherskii.

2.7 References

Brabets, T. P., B. Wang, and R. H. Meade (2000), Environmental and hydrologic overview of the Yukon River Basin, Alaska and Canada., 99-4204 pp, *US Geological Survey Water Resources Report*.

Clark, P. U., N. G. Pisias, T. F. Stocker, and A. J. Weaver (2002), The role of the thermohaline circulation in abrupt climate change, *Nature*, *415*, 6874, 863-869.

Dittmar, T., and G. Kattner (2003), The biogeochemistry of the river and shelf ecosystem of the Arctic Ocean: a review, *Mar. Chem.*, *83*, 3-4, 103-120.

Ekwurzel, B., P. Schlosser, R. A. Mortlock, R. G. Fairbanks, and J. H. Swift (2001), River runoff, sea ice meltwater, and Pacific water distribution and mean residence times in the Arctic Ocean, *J. Geophys. Res.*, *106*, C5, 9075-9092.

Gat, J. R., and R. Gonfiantini (1981), *Stable isotope hydrology: Deuterium and oxygen-18 in the water cycle*, International Atomic Energy Agency, Vienna.

Gat, J. R. (1996), Oxygen and hydrogen isotopes in the hydrologic cycle, *Annual Review of Earth and Planetary Sciences*, *24*, 225-262.

Gibson, J. J., T. W. D. Edwards, G. G. Bursey, and T. D. Prowse (1993), Estimating evaporation using stable isotopes - Quantitative results and sensitivity analysis for 2 catchments in northern Canada, *Nordic Hydrology*, *24*, 2-3, 79-94.

Gibson, J. J., and T. W. D. Edwards (2002), Regional water balance trends and evaporation-transpiration partitioning from a stable isotope survey of lakes in northern Canada, *Global Biogeochem. Cycles*, *16*, 2, 1026, doi:10.1029/2001GB001839.

Gonfiantini, R. (1986), Environmental isotopes in lake studies, in *Handbook of Environmental Isotope Geochemistry*, pp. 113-168, Elsevier, New York.

Kurita, N., N. Yoshida, G. Inoue, and E. A. Chayanova (2004), Modern isotope climatology of Russia: A first assessment, *J. Geophys. Res.*, *109*, D303102, doi:10.1029/2003JD003404.

Laudon, H., H. F. Hemond, R. Krouse, and K. H. Bishop (2002), Oxygen 18 fractionation during snowmelt: Implications for spring flood hydrograph separation, *Water Resour. Res.*, *38*, 11, 1258, doi:10.1029/2002WR001510.

Lee, D. H., and J. Veizer (2003), Water and carbon cycles in the Mississippi River basin: Potential implications for the Northern Hemisphere residual terrestrial sink, *Global Biogeochem. Cycles*, *17*, 2, 1037, doi:10.1029/2002GB001984.

Letolle, R., J. M. Martin, A. J. Thomas, V. V. Gordeev, S. Gusarova, and I. S. Sidorov (1993), 18O abundance and dissolved silicate in the Lena delta and Laptev Sea (Russia), *Mar. Chem.*, *43*, 47-64.

Majoube, M. (1971), Oxygen-18 and deuterium fractionation between water and steam, *J. Chim. Phys. Phys.-Chim. Biol.*, *68*, 10, 1423-1436.

McClelland, J. W., R. M. Holmes, B. J. Peterson, and M. Stieglitz (2004), Increasing river discharge in the Eurasian Arctic: Consideration of dams, permafrost thaw, and fires as potential agents of change, *J. Geophys. Res.*, *109*, D18102, doi:10.1029/2004JD004583.

McNamara, J. P., D. L. Kane, and L. D. Hinzman (1997), Hydrograph separations in an Arctic watershed using mixing model and graphical techniques, *Water Resour. Res.*, *33*, 1707-1719.

Oelke, C., T. Zhang, M. C. Serreze, and R. L. Armstrong (2003), Regional-scale modeling of soil freeze/thaw over the Arctic drainage basin, *J. Geophys, Res.*, *108*, D10, 4314, doi:10.1029/2002JD002722.

Peterson, B. J., R. M. Holmes, J. W. McClelland, C. J. Vorosmarty, R. B. Lammers, A. I. Shiklomanov, I. A. Shiklomanov, and S. Rahmstorf (2002), Increasing river discharge to the Arctic Ocean, *Science*, *298*, 2171-2173.

Serreze, M. C., M. P. Clark, and D. H. Bromwich (2003), Monitoring precipitation over the Arctic terrestrial drainage system: Data requirements, shortcomings, and applications of atmospheric reanalysis, *J. Hydrometeorol.*, *4*, 387-407.

Sugimoto, A., N. Yanagisawa, D. Naito, N. Fujita, and T. C. Maximov (2002), Importance of permafrost as a source of water for plants in east Siberian taiga, *Ecological Research*, *17*, 493-503.

Vasil'chuk, Y. K. (1992), *Oxygen isotope composition of ground ice application to paleogeocryological reconstructions*, 420 pp., Russian Academy of Sciences and Moscow University, Moscow.

Vasil'chuk, Y. K., A. C. Vasil'chuk, D. Rank, W. Kutschera, and J. C. Kim (2001), Radiocarbon dating of delta O-18-delta D plots in Late Pleistocene ice-wedges of the Duvanny Yar (Lower Kolynia River, Northern Yakutia), *Radiocarbon*, *43*, 2B, 541-553.

2.8 Data appendix

Table 2.2 Kolyma River stable isotope data.

Collection	Lat	Long	Discharge (m^3 day^{-1})	$\delta^{18}O$ (‰) VSMOW	δD (‰) VSMOW
6-Aug-02	68° 42'	161° 22'	5480	-21.6	-166.8
20-Aug-02	68° 42'	161° 22'	3531	-21.0	-162.0
4-Sep-02	68° 42'	161° 22'	3890	-21.2	-164.2
20-Sep-02	68° 42'	161° 22'	4600	-21.1	-163.9
8-Oct-02	68° 42'	161° 22'	2510	-21.0	-162.6
7-Nov-02	68° 42'	161° 22'	398	-21.3	-164.5
21-Jan-03	68° 42'	161° 22'	199	-21.9	-169.1
5-Mar-03	68° 42'	161° 22'	189	-21.9	-168.0
1-Apr-03	68° 42'	161° 22'	195	-21.9	-167.4
2-May-03	68° 42'	161° 22'	189	-21.8	-166.3
11-May-03	68° 42'	161° 22'	205	-21.7	-165.6
28-May-03	68° 42'	161° 22'	2768	-22.5	-172.7
5-Jun-03	68° 42'	161° 22'	13500	-23.8	-182.9
7-Jun-03	68° 42'	161° 22'	10500	-24.4	-185.1
11-Jun-03	68° 42'	161° 22'	10400	-23.1	-175.3
24-Jun-03	68° 42'	161° 22'	12800	-22.6	-171.5
26-Jun-03	68° 42'	161° 22'	12667	-22.3	-169.4
30-Jun-03	68° 42'	161° 22'	12800	-22.1	-169.0
8-Jul-03	68° 42'	161° 22'	12000	-21.8	-167.2
14-Jul-03	68° 42'	161° 22'	7190	-21.4	-164.8
30-Jul-03	68° 42'	161° 22'	3230	-21.3	-164.4
6-Aug-03	68° 42'	161° 22'	2370	-21.3	-164.7
15-Aug-03	68° 42'	161° 22'	1620	-21.2	-163.6
21-Aug-03	68° 42'	161° 22'	1270	-21.2	-162.2
2-Sep-03	68° 42'	161° 22'	2438	-21.3	-165.5
8-Sep-03	68° 42'	161° 22'	3450	-21.1	---
15-Sep-03	68° 42'	161° 22'	3200	-21.4	-164.3
21-Sep-03	68° 42'	161° 22'	1960	-21.6	-165.8
22-Sep-03	68° 42'	161° 22'	1850	-21.3	-162.9
29-Sep-03	68° 42'	161° 22'	1600	-21.1	-161.8
5-Oct-03	68° 42'	161° 22'	1420	-21.0	-160.3
28-Nov-03	68° 42'	161° 22'	282	-21.6	---
25-Dec-03	68° 42'	161° 22'	216	-22.0	---
29-Feb-04	68° 42'	161° 22'	---	-22.3	---
25-Mar-04	68° 42'	161° 22'	---	-22.2	---
27-Apr-04	68° 42'	161° 22'	---	-22.2	---

Table 2.3 Cherskii rain stable isotope data.

Collection Date	Lat	Long	Precip (mm)	$\delta^{18}O$ (‰) VSMOW	δD (‰) VSMOW
30-Jun-02	68° 44'	161° 25'	0.7	-12.0	-110.3
2-Jul-02	68° 44'	161° 25'	0.3	-12.7	---
5-Jul-02	68° 44'	161° 25'	2.2	-16.9	-133.3
10-Jul-02	68° 44'	161° 25'	3.3	-15.7	-122.7
11-Jul-02	68° 44'	161° 25'	1.2	-13.4	---
15-Jul-02	68° 44'	161° 25'	2.7	-16.5	-130.2
16-Jul-02	68° 44'	161° 25'	4.9	-10.5	---
17-Jul-02	68° 44'	161° 25'	10.3	-10.3	---
18-Jul-02	68° 44'	161° 25'	2.6	-26.6	---
16-Aug-02	68° 44'	161° 25'	1.6	-12.4	-93.3
23-Aug-02	68° 44'	161° 25'	0.4	-12.4	---
24-Aug-02	68° 44'	161° 25'	4.5	-17.4	-135.2
2-Sep-02	68° 44'	161° 25'	10.4	-15.6	---
27-Sep-02	68° 44'	161° 25'	1.3	-15.8	-120.5
6-Apr-03	68° 44'	161° 25'	2.5	-21.7	-172.7
19-May-03	68° 44'	161° 25'	0.5	-20.1	-160.5
24-May-03	68° 44'	161° 25'	9.5	-15.1	-114.6
4-Jun-03	68° 44'	161° 25'	0.9	-14.5	-126.1
8-Jun-03	68° 44'	161° 25'	2.4	-15.9	---
16-Jun-03	68° 44'	161° 25'	1.3	-17.8	---
18-Jun-03	68° 44'	161° 25'	1.8	-21.7	-174.4
23-Jun-03	68° 44'	161° 25'	10.4	-14.8	---
23-Jun-03	68° 44'	161° 25'	0.5	-10.6	---
26-Jun-03	68° 44'	161° 25'	4.7	-18.3	-146.3
1-Jul-03	68° 44'	161° 25'	2.2	-14.8	-132.4
2-Jul-03	68° 44'	161° 25'	3.0	-18.9	---
3-Jul-03	68° 44'	161° 25'	7.7	-20.9	-159.8
20-Jul-03	68° 44'	161° 25'	4.5	-15.2	-121.4
21-Jul-03	68° 44'	161° 25'	3.8	-14.6	-118.0
23-Jul-03	68° 44'	161° 25'	1.8	-12.0	-106.7
29-Jul-03	68° 44'	161° 25'	6.0	-14.1	-106.9
3-Aug-03	68° 44'	161° 25'	0.3	-14.0	---
4-Aug-03	68° 44'	161° 25'	0.3	-10.9	-86.5
5-Aug-03	68° 44'	161° 25'	0.3	-11.2	---
13-Aug-03	68° 44'	161° 25'	1.7	-12.9	-116.8
19-Aug-03	68° 44'	161° 25'	3.1	-17.8	-135.5
20-Aug-03	68° 44'	161° 25'	3.3	-19.5	-152.0
24-Aug-03	68° 44'	161° 25'	0.3	-11.1	-89.1
30-Aug-03	68° 44'	161° 25'	0.3	-25.4	-192.3

Table 2.4 Cherskii snow stable isotope data

Collection Date	Lat	Long	Depth (cm)	$\delta^{18}O$ (‰) VSMOW	δD (‰) VSMOW
8-Apr-03	68° 44'	161° 25'	0	-33.3	-244.6
8-Apr-03	68° 44'	161° 25'	-51	-21.7	-155.9
8-Apr-03	68° 43'	161° 27'	0	-31.7	-232.4
8-Apr-03	68° 43'	161° 27'	-28	-20.4	-171.8
8-Apr-03	68° 42'	161° 17'	0	-32.1	-236.7
8-Apr-03	68° 42'	161° 17'	-20	-16.2	-154.4
8-Apr-03	68° 40'	161° 25'	0	-32.8	-237.3
8-Apr-03	68° 40'	161° 25'	-42	-28.0	-209.2
8-Apr-03	68° 37'	161° 38'	0	-32.1	---
8-Apr-03	68° 37'	161° 38'	-30	-25.7	---
8-Apr-03	68° 44'	161° 25'	0	-32.5	---
8-Apr-03	68° 44'	161° 25'	-44	-21.3	---
8-Apr-03	68° 42'	161° 32'	0	-32.2	---
8-Apr-03	68° 42'	161° 32'	-51	-19.8	---
8-Apr-03	68° 41'	161° 33'	0	-32.1	---
8-Apr-03	68° 41'	161° 33'	-37	-18.5	---
8-Apr-03	68° 41'	161° 33'	0	-33.4	---
8-Apr-03	68° 41'	161° 33'	-52	-19.9	---
11-Apr-03	68° 34'	161° 38'	0	-26.2	---
11-Apr-03	68° 34'	161° 38'	---	-23.6	---
11-Apr-03	69° 01'	160° 57'	0	-28.3	---
11-Apr-03	69° 01'	160° 57'	-18	-17.0	---
11-Apr-03	68° 41'	160° 13'	0	-25.6	---
11-Apr-03	68° 41'	160° 13'	-40	-25.6	---
11-Apr-03	68° 46'	158° 27'	0	-24.4	---
11-Apr-03	68° 46'	158° 27'	-55	-30.9	---
12-Apr-03	68° 47'	161° 22'	0	-24.8	---
12-Apr-03	68° 47'	161° 22'	-8	-31.0	---
12-Apr-03	68° 54'	161° 38'	0	-32.3	-234.7
12-Apr-03	68° 54'	161° 38'	-41	-23.0	-186.5
12-Apr-03	69° 00'	161° 32'	0	-30.6	---
12-Apr-03	69° 00'	161° 32'	-16	-18.5	---
13-Apr-03	67° 49'	160° 10'	0	-25.3	---
13-Apr-03	67° 49'	160° 10'	-47	-32.0	---
13-Apr-03	67° 47'	159° 18'	0	-30.2	-222.6
13-Apr-03	67° 47'	159° 18'	-40	-22.5	-164.9
13-Apr-03	67° 18'	158° 44'	0	-24.8	-206.2
15-Apr-03	67° 18'	158° 44'	-50	-32.7	-241.0
18-Apr-03	69° 26'	161° 55'	0	-28.8	---

18-Apr-03	69° 26'	161° 55'	-40	-21.2	---
18-Apr-03	69° 11'	161° 36'	0	-24.3	-171.9
18-Apr-03	69° 11'	161° 36'	-30	-21.5	-152.7
19-Apr-03	68° 34'	161° 30'	0	-27.8	---
19-Apr-03	68° 34'	161° 30'	-19	-28.3	---
19-Apr-03	68° 31'	161° 11'	0	-29.1	---
19-Apr-03	68° 31'	161° 11'	-25	-22.4	---
19-Apr-03	68° 21'	161° 33'	0	-25.7	-192.9
19-Apr-03	68° 21'	161° 33'	-42	-22.0	-175.3
25-May-03	68° 44'	161° 25'	0 (fresh)	-21.7	-163.8

Table 2.5 Cherskii local stream stable isotope data.

Date	Lat	Long	$\delta^{18}O$ (‰) VSMOW	δD (‰) VSMOW
7-May-03	68° 42'	161° 32'	-24.6	-182.7
9-May-03	68° 42'	161° 32'	-23.9	-178.7
12-May-03	68° 42'	161° 32'	-22.2	-171.0
17-May-03	68° 42'	161° 32'	-19.2	-156.3
20-May-03	68° 42'	161° 32'	-20.2	-162.4
27-May-03	68° 42'	161° 32'	-19.0	-152.6
17-Jun-03	68° 42'	161° 32'	-18.3	-150.6
15-Jul-03	68° 42'	161° 32'	-17.7	-148.7
18-Aug-03	68° 42'	161° 32'	-17.4	-144.2
16-Sep-03	68° 42'	161° 32'	-17.7	-145.8

Chapter 3

SEASONAL EXCHANGE OF CO_2 AND $\delta^{18}O$-CO_2 VARIES WITH POST-FIRE SUCCESSION IN BOREAL FOREST ECOSYSTEMS*

*Adapted from Welp, L. R., H. Liu and J. T. Randerson, (in press) *Journal of Geophysical Research-Biogeosciences*.

3.1 Abstract

Seasonal cycles of atmospheric CO_2 and $\delta^{18}O$-CO_2 at high northern latitudes have the potential to serve as indicators of ecological change in response to climate changes. Effective interpretation of these observations requires an understanding of how different species and ecosystems contribute to biosphere-atmosphere exchange. Here, we examined the effect of post-fire stand age in boreal forest ecosystems on the seasonal distribution of CO_2 and $\delta^{18}O$-CO_2 fluxes. We measured net CO_2 fluxes in a 3-year burn scar, a 15-year trembling aspen stand, and an 80-year black spruce stand in interior Alaska using eddy covariance. By combining measurements of the oxygen isotopic composition of ecosystem water pools at each stand with the measured CO_2 fluxes, we predicted half-hourly $\delta^{18}O$-CO_2 fluxes and used a 1-box atmosphere model to make relative comparisons of the effect of stand age on the shape and amplitude of the seasonal cycle of CO_2 and $\delta^{18}O$-CO_2. A shorter growing season and higher rates of net ecosystem uptake during mid-summer at the 15-year stand resulted in a larger seasonal CO_2 amplitude and also delayed the drawdown of atmospheric CO_2 compared to the 80-year stand. Reduced levels of gross primary production isoforcing from the 15-year stand during spring and early summer caused atmospheric $\delta^{18}O$-CO_2 to increase more gradually

between April and June as compared to fluxes from the 80-year stand. Our analysis suggests that increased boreal forest disturbance would delay the phase of CO_2 drawdown at high northern latitudes, but would advance the phase of $\delta^{18}O$-CO_2 drawdown.

3.2 Introduction

Climate change caused by increased greenhouse forcing over the next century is expected to be greatest in Arctic and boreal regions, in part from temperature-albedo feedbacks linked with reduced snow and ice cover [*Cess et al.*, 1991; *ACIA*, 2004]. Indeed, observed rates of warming in the Arctic over the last few decades have been 50% larger than the global mean [*IPCC*, 2001], and acceleration of this trend is predicted as greenhouse gas concentrations increase [*ACIA*, 2004]. Evidence that warmer spring temperatures during recent decades have lengthened the terrestrial growing season comes from satellite-derived observations of Normalized Difference Vegetation Index (NDVI) [*Myneni et al.*, 1997; *Tucker et al.*, 2001; *Zhou et al.*, 2001; *Bogaert et al.*, 2002; *Hicke et al.*, 2002; *Nemani et al.*, 2003; *Slayback et al.*, 2003; *Angert et al.*, 2005], passive microwave satellite observations and modeling of soil freeze/thaw transitions [*McDonald et al.*, 2004; *Smith et al.*, 2004], analysis of atmospheric carbon dioxide time series [*Keeling et al.*, 1996; *Randerson et al.*, 1999; *Angert et al.*, 2005], and phenology records [*Walther et al.*, 2002].

The increased growing season length may allow for greater rates of photosynthesis and carbon accumulation during spring and summer [*Frolking et al.*, 1996; *Randerson et al.*, 1999; *Kimball et al.*, 2001; *Myneni et al.*, 2002; *Tanja et al.*, 2003; *White and Nemani*, 2003], whereas warming air and soil temperatures may

stimulate higher rates of respiration [*Chapin et al.*, 1996; *Goulden et al.*, 1998]. Warming of northern continental interiors may also increase fire activity [*Stocks et al.*, 1998; *Gillett et al.*, 2004; *Flannigan et al.*, 2005], causing a decrease in the mean age of forests and a shift in species composition. The combined effect of these multiple changes in northern ecosystem processes on biome-level carbon fluxes remains challenging to measure or predict. In this respect, atmospheric trace gas observations have the potential to serve as an important top-down constraint of large scale ecological change.

The seasonal cycles in concentrations of atmospheric CO_2 and heavy stable isotopologues ($^{13}CO_2$ and $C^{18}OO$) at high northern latitudes integrate carbon fluxes from boreal and Arctic biomes across both North America and Eurasia. Thus, they record, and have the potential to help diagnose, terrestrial ecosystem processes and their response to climate change at the biome scale. Here, we focus on two of these tracers, CO_2 and $C^{18}OO$, and the sensitivity to species composition of the boreal forests as it varies with post-fire stand age. These two tracers are complementary; the seasonal cycle of atmospheric CO_2 is sensitive to the net carbon balance of ecosystems, whereas the seasonal cycle of $C^{18}OO$ is sensitive to the magnitude of the gross CO_2 fluxes (i.e., photosynthesis and respiration) and the hydrological cycle. Effective use of these tracers as large-scale ecological indicators of climate change [*Menzel and Fabian*, 1999; *Walther et al.*, 2002] requires improved understanding of the processes that control CO_2 and $C^{18}OO$ fluxes in northern ecosystems.

Typically, the concentration of CO_2 in northern latitudes decreases from May through August, due to photosynthetic uptake exceeding ecosystem respiration during

summer months. Increasing concentrations follow from September through April as a result of slow, continuous ecosystem respiration fluxes to the atmosphere and negligible rates of photosynthesis [*Bolin and Keeling*, 1963]. From the 1960s through the latter part of the 1990s, the seasonal cycle of atmospheric CO_2 measured at high northern latitudes has increased in amplitude (peak-to-trough) and the phase has advanced [*Conway et al.*, 1994; *Keeling et al.*, 1996; *Randerson et al.*, 1997; *McDonald et al.*, 2004].

Two classes of mechanisms have been proposed to account for the observed changed in the seasonal cycle of CO_2. The first involves direct climate controls on the timing and magnitude of northern ecosystem fluxes, including temperature, radiation, the timing of soil thaw, and drought [*Keeling et al.*, 1996; *Randerson et al.*, 1999; *McDonald et al.*, 2004; *Angert et al.*, 2005]. The second involves a change in distribution of plant functional types caused by increases in disturbance (fire, insects, logging, etc.) [*Zimov et al.*, 1999]. Measurements from Siberian shrub and forest tundra ecosystems show that species assemblages associated with early stages of succession have enhanced rates of photosynthetic uptake during the summer in addition to enhanced respiratory losses during fall, partly from the removal of the less productive and more insulating moss layer. Based on these results, *Zimov et al.* [1999] hypothesize that increased disturbance in Arctic and boreal biomes has increased the abundance of early successional ecosystems and this, in turn, has contributed to the observed increases in the CO_2 seasonal amplitude.

In contrast to the CO_2 record, the much shorter $C^{18}OO$ record (measured and reported as $\delta^{18}O\text{-}CO_2$) shows no unidirectional, fossil fuel-controlled trend (as there is for

CO_2 and $^{13}CO_2$) and the interannual variability in annual mean and seasonal amplitude is much larger [*Trolier et al.*, 1996; *Ciais and Meijer*, 1998; *CMDL*, 2000]. The seasonal cycle and latitudinal gradient of $\delta^{18}O$-CO_2 are largely controlled by gross CO_2 exchange with the terrestrial biosphere as well as isotopic fractionation of meteoric water and climatic factors such as temperature and humidity [*Francey and Tans*, 1987; *Ciais and Meijer*, 1998; *Peylin et al.*, 1999; *Riley et al.*, 2002; *Cuntz et al.*, 2003a].

When CO_2 diffuses into a leaf, it rapidly reaches isotopic equilibrium with the evaporatively enriched leaf water pool because carbonic anhydrase catalyzes CO_2 hydration [*Mills and Urey*, 1940; *Farquhar et al.*, 1993; *Yakir and Sternberg*, 2000]. Only a portion of the CO_2 entering the leaf gets fixed as organic matter before the remainder diffuses back out of the leaf and returns to the atmosphere. This retrodiffusive flux is approximately twice as large as gross primary production and carries the leaf water isotopic signature [*Francey and Tans*, 1987; *Friedli et al.*, 1987; *Farquhar et al.*, 1993]. Similarly, CO_2 produced by soil respiration is in contact with soil water for a sufficient time to equilibrate with water in the upper layers of the soil surface before diffusing out into the atmosphere [*Hesterberg and Siegenthaler*, 1991; *Tans*, 1998; *Miller et al.*, 1999]. Leaf water is isotopically enriched compared to soil water because of greater evaporation rates at the leaf surface than the soil surface. As a result, photosynthesis typically enriches atmospheric $\delta^{18}O$-CO_2 (more positive) and respiration depletes $\delta^{18}O$-CO_2 (more negative) [*Ciais et al.*, 1997]. This large difference in $\delta^{18}O$ of leaf water/photosynthetic CO_2 flux and soil water/respiratory CO_2 flux, has the potential to be used to partition net CO_2 fluxes into one-way gross flux components [*Ogee et al.*,

2004]. Successful partitioning of measured net CO_2 fluxes into foliar and soil components using $\delta^{18}O$ has been demonstrated at the site level over discrete periods of time during the growing season [*Yakir and Wang*, 1996; *Bowling et al.*, 2003b]. In principle, a similar partitioning at the global scale is possible, however photosynthetic and respiratory end-members vary widely and are incompletely known.

For both CO_2 and $\delta^{18}O$-CO_2, the role of different ecosystems and their contribution to biome-level fluxes remain poorly understood. Here we examine the effects of boreal forest post-fire stand age on the seasonal cycle of CO_2 and $\delta^{18}O$-CO_2 using a combination of CO_2 flux and oxygen isotope measurements from three stands in a fire chronosequence in interior Alaska. Species composition varies with time since fire and has the potential to influence rates of carbon uptake [*Litvak et al.*, 2003; *Bond-Lamberty et al.*, 2004], respiration rates [*Wang et al.*, 2002; *O'Neill et al.*, 2003], growing season length [*Falge et al.*, 2002], leaf diffusion properties such as stomatal conductance [*Ewers et al.*, 2005], as well as the use and cycling of meteoric water by the ecosystem [*Flanagan et al.*, 1997]. Each of these differences could lead to changes in the seasonality of CO_2 or $\delta^{18}O$-CO_2 fluxes. We estimate atmospheric isoforcing for each of our three stands following the approach described by *Flanagan et al.* [2005]. We examine, in detail, differences in biosphere-atmosphere exchange between a deciduous broadleaf forest and an evergreen conifer forest. In a final step, we investigate stand age effects on the seasonal cycles of CO_2 and $\delta^{18}O$-CO_2 using a 1-box atmospheric model. This allowed us to explore the *Zimov et al.* [1999] hypothesis in the context of changes in species composition within boreal forest ecosystems.

3.3 Site description

We measured water isotopes and CO_2 fluxes at three stands that were part of a fire chronosequence in interior Alaska, near the town of Delta Junction (63°54'N, 145°40'W). This is an area of discontinuous permafrost that experiences seasonal extremes in climate. Temperature measurements at nearby Big Delta (64°00'N, 145°44'W), from 1937 to 2004 by the Western Regional Climate Center, show the average daily minimum temperature in January was -24°C and the average daily maximum during July was 21°C [*WRCC*, 2004]. For the 30 year period, from 1971 to 2000, the average annual precipitation in this region was 303 mm and the growing season length (air temperatures above freezing) was approximately 115 days from mid-May to early September [*WRCC*, 2004]. Our sites were located on relatively well-drained silty loam soil [*King et al.*, 2002], and were burned 3 years, 15 years, and approximately 80 years prior to the 2002 growing season. During the summer of 2002, rainfall measured by two tipping bucket rain gauges was 12 mm in May, 66 mm in June, 45 mm in July, 97 mm in August, and 53 mm in September [*Liu et al.*, 2005]. Total precipitation during the 2002 calendar year was approximately 305 mm. Time series of average daily maximum photosynthetic photon flux density (PPFD) above the canopy, relative humidity, and 2 m air temperature are shown in Figure 3.1, along with soil temperatures at a depth of 10 cm at each stand. Differences in soil temperature between stands were caused partly by differences in canopy structure and leaf area that controlled the amount of shortwave radiation absorbed by the soil/moss surface.

The most recently disturbed stand (the 3-year stand) was burned during the 1999 Donnelly Flats fire (63°54'N, 145°44'W) [*Liu et al.*, 2005]. In 2002, 30% of the ground surface was covered by bunch grasses (*Festuca altaica*) and deciduous shrubs less than 1 m tall. Charred dead spruce boles remained standing and partial moss cover consisted of *Polytrichum* ssp. and *Ceratodon* ssp.

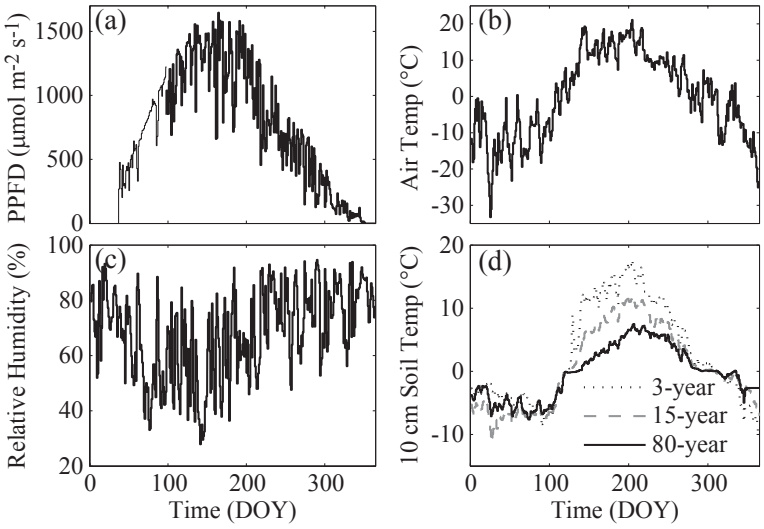

Figure 3.1 Daily micrometeorological data from Delta Junction during 2002. (a) Daily maximum photosynthetic photon flux density (*PPFD*), (b) daily mean above canopy air temperature averaged across all stands, (c) daily mean above canopy relative humidity averaged across all stands, and (d) daily mean soil temperature measured 10 cm below the surface at each stand.

The intermediate aged stand (the 15-year stand) burned during the 1987 Granite Creek fire (63°55'N 145°23'W), and by 2002, was dominated by an overstory of deciduous aspen trees (*Populous tremuloides*) with a mean canopy height of 5 m and willow shrubs (*Salix* spp.). The understory vegetation included smaller shrubs (*Ledum palustre*, *Rosa acicularis*, *Vaccinium uliginosum* and *Vaccinium vitisidaea*), grasses

(*Festuca* spp. and *Calamagrostis lapponica*) and moss (*Polytrichum* ssp.) [*Liu et al.*, 2005]. The understory also included regrowing black spruce (*Picea mariana*). By 2002, some of the dead spruce boles remained standing, but most had fallen over.

The mature conifer end-member of our study (the 80-year stand) was an approximately 80 year old stand of black spruce (*Picea mariana*) (63°53'N, 145°44'W), 5 km south of the 3-year stand and less than 20 km southwest of the 15-year stand [*Liu et al.*, 2005]. The mean canopy height was 4 m and the sparse understory consisted of shrubs (*Ledum palustre*, *Vaccinium uliginosum* and *Vaccinium vitisidaea*). The dominant ground cover was feathermoss (*Pleurozium schreberi* and *Rhytidium rugosum*) and lichen (*Cladonia* spp. and *Stereocaulon* spp.). Moss and fibrous organic layer thickness was approximately 11 cm [*Manies et al.*, 2004].

3.4 Methods

3.4.1 Eddy covariance and micrometeorological measurements

Eddy covariance measurements of net ecosystem exchange (NEE) CO_2 fluxes were made using an open-path CO_2 analyzer (LiCor 7500, LI-COR, Inc., Lincoln, Nebraska) and a 3-D sonic anemometer (CSAT3, Campbell Scientific, Inc., Logan, Utah) at each stand. Vertical and horizontal wind velocity, sonic temperature, and CO_2 and water vapor concentrations were recorded at 10 Hz on a Campbell CR5000 data logger. Corrections were made to the CO_2 fluxes to account for density effects [*Webb et al.,* 1980] and buoyancy temperature and crosswind effects [*Liu et al.,* 2001]. Energy balance closure during the summer of 2002 (June–August) was 80% at the 3-year stand,

83% at the 15-year stand, and 86% at the 80-year stand [*Liu et al.*, 2005]. Instrument configuration and sampling heights are summarized in Table 1 of *Liu et al.* [2005].

Micrometeorological observations that we used to develop and drive the CO_2 flux partitioning and isoflux models included CO_2 and latent heat fluxes, wind speed above and inside the canopy, PPFD (LI 190, LI-COR, Inc., Lincoln, Nebraska), precipitation, air temperature and relative humidity above and inside the canopy, and soil temperature at 10 cm depth. Micrometeorological data was 86% complete at the 3-year stand, nearly 100% at the 15-year stand and 95% at the 80-year stand. Air and soil temperature, relative humidity, PPFD, and wind speed data were gap filled using linear interpolation of points surrounding the missing data for short gaps (e.g., less than 3 hours), or using measurements recorded at one of the other nearby tower locations for extended periods of missing data (with the exception of soil temperature which was linearly interpolated for multi-day periods of missing data). We filtered NEE measurements for periods of low turbulence using a minimum u^* threshold of 0.2 m s^{-1} [*Goulden et al.,* 1997]. We also excluded periods with rain or dust that potentially interfered with the operation of the infrared gas analyzer. Combined with instrument data gaps, the filtering procedure yielded 30-minute NEE measurements for 51% of the growing season (April–September) at the 3-year stand, 46% at the 15-year stand, and 57% at the 80-year stand.

3.4.2 Isotopic measurements

We collected precipitation using rain collectors that consisted of a 7.5 cm diameter funnel with 20 cm of ¼ inch ID Tygon tubing feeding into a 500 mL Nalgene bottle. The funnel and bottle were supported inside a PVC pipe. We constructed a vent

from 30 cm of ¼ inch ID Tygon tubing, allowing for rapid filling of the bottle while minimizing fractionation due to evaporation. We emptied the collectors weekly into borosilicate glass vials with screw caps sealed with Parafilm. The vials were stored in a refrigerator until analysis. We collected snow samples from both the top and bottom of the snow pack weekly during winter and stored them in the same way as the summer rain samples. We analyzed precipitation and extracted leaf, stem, and soil water samples for $\delta^{18}O$-H_2O by continuous flow GC-IRMS on a Finnigan MAT Delta S mass spectrometer (Thermo Finnigan, Bremen, Germany) following the method described by [*Fessenden et al.*, 2002]. We injected sample sizes of 0.5 mL of water by syringe into 7 mL headspace vials flushed with 10% CO_2 in N_2. The vials were capped with Hycar rubber stoppers and allowed to equilibrate by shaking in a 25°C constant temperature water bath for a minimum of 12 hours. We prepared isotopic standards in the same manner as the unknown samples. We used a gas-tight syringe to inject 200–300 μL of headspace into a HP/Agilent Technologies 6890 Series Gas Chromatograph G1530A with a 25 m Poroplot-Q capillary column (0.32 mm diameter). The CO_2 effluent from the GC passed through a Finnigan GC Combustion III and Nafion drying trap before entering the mass spectrometer.

We collected atmospheric water vapor cryogenically by pulling air through a 9 mm OD glass tube cold finger (with a inner 6 mm OD tube) sitting in crushed dry ice. We maintained the flow rate through the cold finger at 0.3 L min^{-1} for approximately 2 hours [*Helliker et al.*, 2002]. Water condensed on the inner portion of the 9 mm tube and the outer portion of the 6 mm tube. Both glass tubes were removed from the dry ice and

sampling apparatus and sealed with a rubber stopper/septum and wrapped with Parafilm. Samples were stored in a freezer until analysis. To measure the $\delta^{18}O$ of the condensed water vapor, the sample tubes were removed from the freezer and allowed to reach room temperature over a period of 1 to 3 hours. We injected ~1 mL of pure CO_2 through the stopper/septum to bring the internal CO_2 concentration to ~10%. Standards were prepared in 7 mL headspace vials, as previously described, and both standards and samples were allowed to equilibrate at room temperature for at least 48 hours. We used a gas-tight syringe to inject 80 μL of the headspace from the water vapor tubes into the Delta S GC-IRMS. Sample $\delta^{18}O$-H_2O values were calculated relative to known standards equilibrated at the same time. The reproducibility for this method was ±0.5‰.

We collected bulk soil water samples from soil pits at 2.5, 5, 10, 15, and 30 cm depths, using borosilicate glass vials sealed with Parafilm. We also sampled dominant tree species for stem (xylem) and leaf water isotopic composition. Stems, leaves, and needles collected for isotopic analysis were stored in 25 mL screw-cap borosilicate glass vials and sealed with Parafilm. We collected stem samples from non-green, woody stems to minimize effects of evaporative enrichment. Stems were cut into 1 cm sections to facilitate water extraction. Petioles were removed from the broadleaf leaves to minimize the effects of non-evaporatively enriched stem water contributions. Samples were frozen until water was extracted by cryogenic vacuum distillation [*Ehleringer et al.*, 2000].

3.4.3 Isotopic modeling of water pools

We measured $\delta^{18}O$ of atmospheric and ecosystem water pools on two field campaigns in 2002, although to predict the seasonal and annual isoforcing of $\delta^{18}O$-CO_2,

we needed continuous estimates of the isotopic composition of the water pools. Therefore, it was necessary to model the $\delta^{18}O$ of precipitation, water vapor, soil and xylem water, and leaf water at 30-minute intervals. We used the measured $\delta^{18}O$ of precipitation collected at Delta Junction during 2002 to create a temperature regression based on the mean air temperatures of the week prior to sample collection (because samples were collected weekly) (Figure 3.2). We compared our isotopic data to four IAEA GNIP stations at Fort Smith (60°02'N, 111°97'W), Mayo (63°37'N, 135°52'W), Whitehorse (60°72'N, 135°52'W), and Yellowknife (62°28'N, 114°27'W), spanning the years 1961–1993 [*IAEA/WMO*, 2004]. These stations were chosen because they are at similar latitudes as our field sites and also are interior (non-coastal) locations. The regression of weighted monthly $\delta^{18}O$ of precipitation on the monthly mean air temperature was nearly identical to that calculated from our own isotopic measurements (Figure 3.2a). The isotopic temperature dependence from Delta Junction was then applied to the monthly mean air temperature measured at the stands to construct an estimated seasonal cycle of $\delta^{18}O$ of meteoric water (Figure 3.2b). In our model, soil water $\delta^{18}O$ was set equal to the $\delta^{18}O$ of precipitation. As will be discussed later, this assumption ignores short-term isotopic variations in the top soil layers due to natural variability in precipitation and evaporation between rain events [*Riley et al.*, 2002].

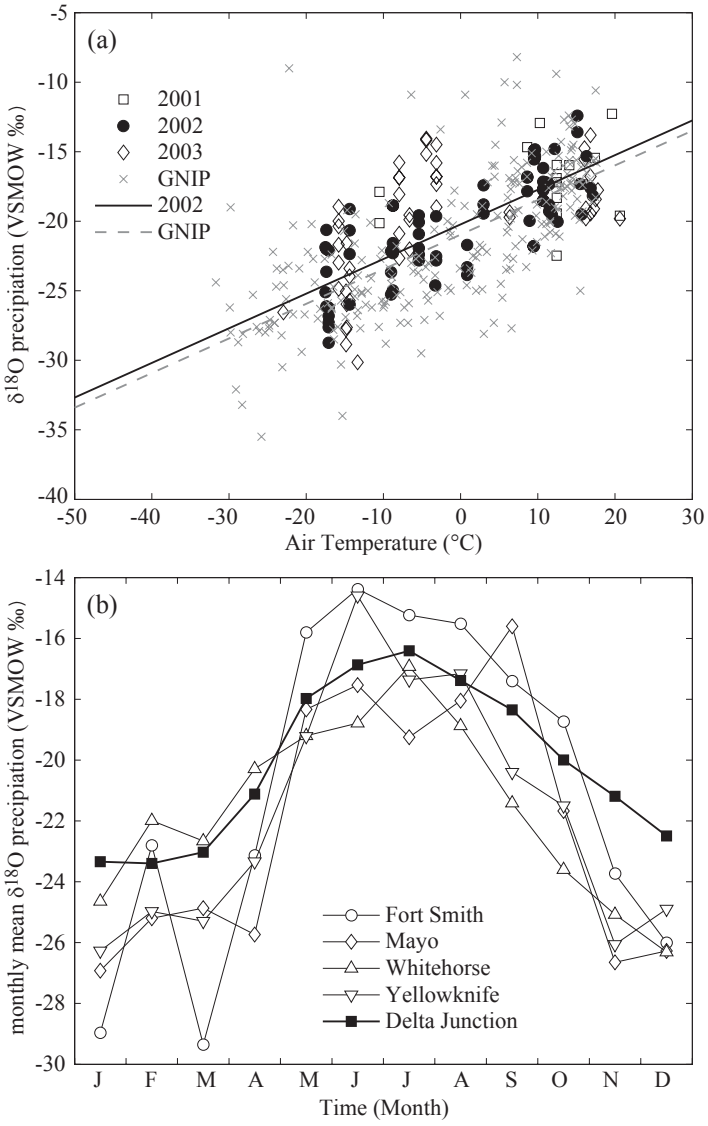

Figure 3.2 (a) $\delta^{18}O$ of precipitation collected at Delta Junction during 2001–2003 as a function of mean surface air temperature for the week preceding collection. Monthly precipitation data from the GNIP IAEA network stations Fort Smith, Mayo, Whitehorse and Yellowknife are plotted as a function of monthly mean air temperature. GNIP station time series are intermittent and span from 1961 to 1993. Regressions are shown for 2002 Delta Junction measurements (solid line) and GNIP measurements (dashed line). The temperature regression for 2002 Delta Junction precipitation yielded a slope of 0.25‰/°C and an intercept of -20.22‰, r^2=0.62, n=75, p<0.001. This was similar to the regression for the combined GNIP stations which had a slope of 0.25‰/°C and an intercept of -20.96‰, r^2=0.47, n=236, p<0.001. (b) Monthly mean $\delta^{18}O$ of precipitation for each GNIP station and the estimate for Delta Junction (derived from the temperature regression shown in the upper panel). Standard deviations about the GNIP monthly means are ~3‰ at all locations, but were excluded from the figure for clarity.

Atmospheric water vapor $\delta^{18}O$ was assumed to be depleted relative to modeled precipitation $\delta^{18}O$ by -8‰ based on the mean difference between water vapor and precipitation isotopic measurements made during June and August (Figure 3.3). We also assumed that there was no diurnal cycle in water vapor $\delta^{18}O$ based on our measured water vapor $\delta^{18}O$ profiles that showed considerable variability, but no clear diurnal trends (data not presented).

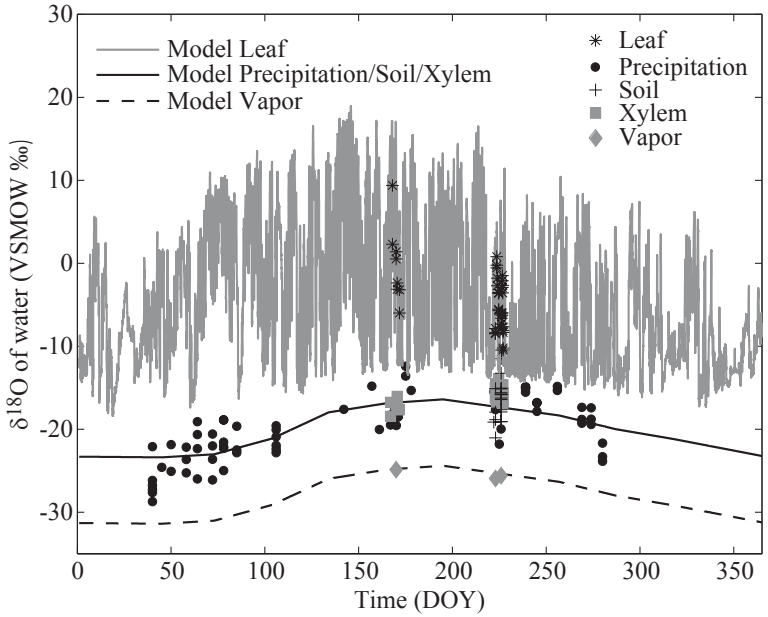

Figure 3.3 Measured (symbols) and modeled (lines) $\delta^{18}O$ of leaf water, precipitation, soil and xylem water and water vapor for the year 2002.

Leaf water $\delta^{18}O$ becomes enriched during the day due to evaporative enrichment during transpiration. The level of leaf water enrichment was estimated first using the Craig-Gordon steady state model of isotopic fractionation [*Craig and Gordon*, 1965], expanded to include leaf boundary layer effects [*Flanagan et al.*, 1991]. The steady state

$^{18}O/^{16}O$ ratio of leaf water ($H_2{}^{18}O/H_2{}^{16}O$) at the sites of evaporative enrichment (R_{ss}) is given by:

$$R_{ss} = \alpha^* \left[\alpha_k R_{wx} \left(\frac{e_i - e_s}{e_i} \right) + \alpha_{kb} R_{wx} \left(\frac{e_s - e_a}{e_i} \right) + R_a \left(\frac{e_a}{e_i} \right) \right] \quad (3.1)$$

where R_a and R_{wx} are the $^{18}O/^{16}O$ ratios of water vapor in the atmosphere and xylem water respectively and e is the water vapor pressure (subscripts a, s, and i correspond to the free atmosphere, leaf surface and intercellular spaces respectively), α^* is the temperature-dependent equilibrium fractionation factor between liquid water and water vapor, α_k is the kinetic fractionation associated with diffusion of water vapor in air (1.032) [*Cappa et al.*, 2003] and α_{kb} in the kinetic fractionation associated with diffusion through the boundary layer ($\alpha_{kb} = \alpha_k^{2/3}$). We used the mean 30-minute air temperature and relative humidity measured at each stand above the canopy to drive this model of predicted leaf water enrichment.

Measurements of leaf water $\delta^{18}O$ tend to show a few hour lag relative to that calculated with the Craig-Gordon steady state approximation [*Dongmann et al.*, 1974; *Lai et al.*, 2006]. Leaf water $\delta^{18}O$ can be thought of as always approaching some steady state, but rarely reaching it because of the relatively large reservoir of water in the leaf compared to the flux of transpiration through the leaf. Therefore, we also employed a transitory model where the $\delta^{18}O$ of leaf water is a mixture of the Flanagan modified Craig-Gordon steady state prediction at that time and at the previous time step [*Dongmann et al.*, 1974; *Cuntz et al.*, 2003a; *Lai et al.*, 2006].

$$R_{nss}(t) = R_{ss}(t) - \left[R_{ss}(t) - R_{nss}(t-1)\right] \cdot e^{\left(-\zeta \frac{\Delta t}{\tau}\right)} \quad (3.2)$$

Where $R_{nss}(t)$ is the non-steady state prediction of the isotopic ratio of leaf water at time t, $R_{ss}(t)$ is the Craig-Gordon steady state solution at time t, $R_{nss}(t\text{-}1)$ is the isotopic ratio of leaf water at time t-1, and ζ is represented by the following equation:

$$\zeta = \alpha^* \alpha_{kv} (1-h) \quad (3.3)$$

where h is the humidity in the canopy air. α_{kv} is the effective kinetic fractionation through the stomata and boundary layer, $\alpha_{kv} = 1 - (0.032\ r_s + 0.021\ r_b)/(r_s + r_b)$, where r_s and r_b are the stomatal and boundary layer resistances to water vapor diffusion and 0.032 and 0.021 are scalars corresponding to the respective isotopic fractionation factors) [*Cappa et al.*, 2003].

The turnover time of leaf water (τ in Equation 3.1) is proportional to the volume of leaf water divided by the transpiration rate and Δt is the 30-minute time step of the model. We used a τ of 2 hours based on reducing residuals between measured and modeled leaf water values. Leaf water turnover time probably varies with species and should vary diurnally with transpiration rate; however, we had limited data to make this evaluation and therefore, decided to use a constant τ for all stands. For comparison, *Cuntz et al*. [2003a] used a τ of ~3 hours globally and *Lai et al*. [2006] solved for a τ of 11 hours for conifers in the Pacific Northwest.

3.4.4 Partitioning CO_2 fluxes

NEE measurements at each stand were partitioned into ecosystem respiration (R_e) and gross primary productivity (GPP) components using Q_{10} and Michalis-Menten

models, respectively. We used a temperature dependent Q_{10} respiration model that was mathematically equivalent to a Van't Hoff exponential model [*Lloyd and Taylor,* 1994].

$$R_e = R_o Q_{10}^{\left(\frac{T-T_o}{10}\right)} \tag{3.4}$$

Where T is the 10 cm soil temperature, T_o = 10 °C, R_o is the base respiration rate and Q_{10} is a temperature sensitivity parameter. Nighttime growing season (April–September) NEE measurements and 10 cm soil temperatures from three years of combined measurements (2002–2004) were used to solve for stand-specific Q_{10} values. Using these Q_{10} values and nighttime NEE measurements, we then solved for R_o values during 15-day windows moving by 5-day increments during the growing season (April–September). Winter R_e was predicted by using the growing season Q_{10} and half the mean growing season R_o. For each stand, these R_o and Q_{10} values were used with 10 cm soil temperature to estimate respiration at the half-hourly time step of our model.

Gross primary production (GPP) was modeled after *Zha et al.* [2004],

$$GPP = \left(\frac{A_{\max} \cdot \alpha \cdot APAR}{A_{\max} + \alpha \cdot APAR)} \right) \cdot VPD_{scalar} \tag{3.5}$$

where $APAR$ (μmol photons m^{-2} s^{-1}) is absorbed photosynthetically active radiation ($APAR = PPFD \cdot FPAR$, where $FPAR$ is the fraction of PAR absorbed by the vegetation), GPP and A_{max} (maximum photosynthetic capacity) are both in μmol CO_2 m^{-2} s^{-1} and α is a quantum efficiency (mol CO_2/mol photons). Many studies have explored the effect of vapor pressure deficit (VPD) and humidity levels on leaf-level gas exchange [*Jarvis and McNaughton*, 1986], therefore, we included a dependence on VPD in the assimilation

model to better represent diurnal variations in water stress. (This VPD_{scalar} was not included in *Zha et al.* [2004].)

$$VPD_{scalar} = 1 - 0.5\left(\frac{VPD}{VPD_{\max}}\right) \tag{3.6}$$

The value of VPD_{scalar} (unitless) decreased linearly with increasing VPD until reaching VPD_{max}, above which it remained constant at 0.5. For each stand, we fixed VPD_{max} at 3 kPa. This resulted in a very conservative reduction of GPP during afternoon periods of high VPD. The GPP model behaves linearly when $\alpha \bullet APAR$ is much smaller than A_{max} and saturates when $\alpha \bullet APAR$ approaches A_{max}. A_{max} and α were solved for every week during the growing season using *PPFD* data recorded by the micrometeorological towers and *FPAR* derived from MODerate Resolution Imaging Spectroradiometer (MODIS) observations [*Myneni et al.*, 2002]. Table 3.1 lists values of the model parameters for each stand used to calculate GPP and R_e fluxes for 2002.

Table 3.1 Model parameters used to partition NEE into GPP and R_e components.

Stand	Q_{10}[1] (unitless)	R_o[1,2] (μmol CO_2 m^{-2} s^{-1})	$AMAX$[3] (μmol CO_2 m^{-2} s^{-1})	α[3] (mol CO_2 mol photons^{-1})[4]	$FPAR$[3] (%)
3-year	2.1	1.0	-3.6	-0.04	60
15-year	3.9	2.3	-11.2	-0.08	84
80-year	4.7	5.0	-9.6	-0.09	84

[1] Q_{10} and R_o are solved using 10 cm soil temperatures.
[2] R_o was separately estimated for 5-day intervals during the growing season – here we report the mean over the growing season.
[3] $AMAX$, α and $FPAR$ are June–Aug means.
[4] The units are per mol of absorbed *PPFD* (incident $PPFD \bullet FPAR$).

3.4.5 Atmospheric modeling

We used a simple 1-box atmosphere model to isolate the relative effect ecosystem exchange from each forest type has on the seasonal cycle of CO_2 and $\delta^{18}O$-CO_2 of the atmosphere. The atmospheric box represents the high-northern latitude atmosphere in which one age-class of forest (e.g., the 3-year stand, the 15-year stand, or the 80-year stand) interacts with the atmosphere in each model run. The mass of air in the atmospheric box (M_a in Equation 3.7) was defined so that the amplitude of the seasonal cycle of CO_2, when forced with the fluxes from the 80-year stand, matched the amplitude at the Pt. Barrow station of the NOAA CMDL network [*CMDL*, 2000]. M_a was the same for each stand and model simulation. The conceptual experiment presented here is roughly equivalent to covering the entire boreal forest land area with a single age-class of forest, and mixing the resulting biospheric fluxes into the entire atmosphere contained between 59°N and 70°N. Observations at the Pt. Barrow station represent well-mixed background values of CO_2 and $\delta^{18}O$-CO_2 at high northern latitudes (because gases are sampled from ocean wind sectors under well-mixed conditions) and will be used later to give a reference framework for our results. No atmospheric boundary conditions were imposed (i.e. there was no mixing from other latitudes). The change in atmospheric CO_2 is predicted from modeled R_e and GPP fluxes (mol m^{-2} 30 min^{-1}) starting with an atmospheric CO_2 concentration at 370 ppm.

$$\frac{d(C_a M_a)}{dt} = GPP + R_e \tag{3.7}$$

where C_a is the molar ratio of CO_2 in the 1-box model, and M_a is the mass of air in the atmospheric box (equivalent to 5.4 x 10^5 mol air m^{-2}).

To determine the total isotopic effect of biospheric CO_2 fluxes on the atmosphere, net isofluxes (in units of moles C ‰) were calculated at half-hour time steps as:

$$\frac{d\left(C_a M_a \delta_a^{CO_2}\right)}{dt} = GPP\left(\delta_{a,i}^{CO_2} - \Delta_A\right) + R_e\left(\delta_{soil}^{CO_2} - \varepsilon_{diff}\right) \quad (3.8)$$

Where $\delta_a^{CO_2}$ is the $\delta^{18}O$ of CO_2 in the 1-box model (initialized at -1.4‰ VPDB-CO_2), $\delta_{a,i}^{CO_2}$ is the $\delta^{18}O$ of atmospheric CO_2 used in calculating the isofluxes and was estimated using the mean seasonal cycle of observations from the Pt. Barrow NOAA CMDL station, Δ_A is the discrimination against $C^{18}OO$ during photosynthesis (defined later in Equation 3.9), $\delta_{soil}^{CO_2}$ is the $\delta^{18}O$ of CO_2 in equilibrium with soil water (‰ VPDB-CO_2), and ε_{diff} is the fractionation associated with diffusion of CO_2 out of the soil (‰).

The seasonal cycle of $\delta_a^{CO_2}$ was determined by dividing Equation 3.8 by Equation 3.7. For this modeling study, ε_{diff} was assumed to be -7.2‰ [*Miller et al.*, 1999]. We assumed that the abiotic retrodiffusion isoflux [*Stern et al.*, 2001] did not contribute to the seasonality in $\delta^{18}O$-CO_2 [*Cuntz et al.*, 2003b]. The discrimination associated with GPP, Δ_A, was first presented by *Farquhar et al.* [1993] and has been modified by *Gillon and Yakir* [2001] to include the effect of incomplete isotopic equilibration of CO_2 with H_2O by carbonic anhydrase. *Gillon and Yakir* [2001] showed that in most cases, hydration of CO_2 by carbon anhydrase is not 100% efficient, and some of the CO_2 that diffuses into the leaf, returns to the atmosphere without isotopically equilibrating with leaf water. Although this effect is more pronounced in C_4 grasses, where carbonic

anhydrase is only about 40% efficient, it is estimated to be approximately 88–99% for broadleaf and conifer C_3 trees.

$$\Delta_A = \overline{a} + \varepsilon\left[\theta_{eq}\left(\delta_c^{CO_2} - \delta_{a,i}^{CO_2}\right) - \overline{a}\frac{\left(1-\theta_{eq}\right)}{\left(\varepsilon+1\right)}\right] \tag{3.9}$$

$$\varepsilon = \frac{C_c}{(C_a - C_c)} \tag{3.10}$$

Here $\overline{a}$ is the weighted mean of discrimination occurring during diffusion from ambient air to the sites of carboxylation in the chloroplast (estimated to be 7.4‰) and $\delta_c^{CO_2}$ is the oxygen isotopic composition of CO_2 (‰ VPDB-CO_2) in the chloroplast. $\delta_c^{CO_2}$ is assumed to be in isotopic equilibrium with enriched leaf water at the ambient air temperature (close to leaf temperature). The fraction of CO_2 entering the leaf that fully equilibrates with the leaf water pool before exiting is denoted as θ_{eq}. For the 3-year and 15-year stands, we used the mean of the ranges of values given for trees/shrubs in *Gillon and Yakir* [2001], $\theta_{eq} = 0.96$. Likewise for the 80-year stand, the mean for conifers was $\theta_{eq} = 0.93$. C is the partial pressure of CO_2 and the subscripts a and c correspond to the CO_2 in ambient air and inside the choloroplast. We used the internal stomatal CO_2 ratio with the ambient CO_2 mixing ratio (C_i/C_a) as an estimate of C_c/C_a used to calculate $C_c/(C_a\text{-}C_c)$ in Equation 3.10. We recognize that this is a simplification given that there is evidence that C_i and C_c can differ by $0.1 \cdot C_a$ to $0.2 \cdot C_a$ [*Lloyd and Farquhar*, 1994; *Yakir and Sternberg*, 2000; *Cuntz et al.*, 2003a]. To address this, we conducted a sensitivity analysis in which we varied C_i and examined the impacts on δ^{18}O-CO_2 isofluxes. C_i/C_a ratios were estimated from δ^{13}C of plant tissue collected in the summer of 2002 using the

relationship for C_3 plants derived by *Farquhar et al.* [1989]. The discrimination ($\Delta^{13}C$) was estimated at 20.9‰ for dominant grasses at the 3-year stand, 22.0‰ for aspen at the 15-year stand, and 21.2‰ for black spruce at the 80-year stand. This translates to C_i/C_a ratios (or C_c/C_a estimates) of 0.71, 0.76 and 0.73 respectively. These estimates are broadly consistent with *Dang et al.* [1997] measurements of 0.81 for aspen and 0.71 for black spruce. Because the value of C_c/C_a sets the magnitude of the retrodiffusive flux of CO_2 out of the leaf and to the atmosphere, we wanted to include the effects of the diurnal cycle of C_c/C_a in our isoforcing calculations. We introduced a diurnal cycle in C_i/C_a (used to estimate C_c/C_a) using the Ball-Berry equation [*Ball*, 1988].

$$\frac{1}{r_s} = \frac{m \cdot GPP \cdot h_s \cdot P}{C_s} + b \tag{3.11}$$

and a rearrangement of the diffusion representation of photosynthesis.

$$\frac{C_i}{C_a} = 1 + \frac{GPP \cdot P \cdot (1.65 r_s + 1.37 r_b)}{LAI \cdot C_a} \tag{3.12}$$

In the preceding two equations, r_s is the resistance of water through the stomata (m^2 s μmol^{-1} H_2O), and r_b is resistance through the laminar leaf boundary layer (m^2 s μmol^{-1} H_2O). C_s and C_a are the partial pressures of CO_2 at the leaf surface (including the effect of r_b) and in the atmosphere, h_s is relative humidity at the leaf surface, b is the residual conductance when GPP is zero, P is the atmospheric pressure and LAI is the unitless leaf area index which varies seasonally (from MODIS observations) and m is a constant. We solved for parameters m and b in Equation 3.11 such that when entered into Equation 3.12, the GPP-weighted annual mean C_i/C_a for each stand matched our estimates from the

$\Delta^{13}C$ measurements. The sensitivity of the seasonal cycle of $\delta^{18}O\text{-}CO_2$ to the diurnal cycle of C_i/C_a will be explored further in this paper.

In previous modeling studies, $\delta_a^{CO_2}$ and $\delta_{a,i}^{CO_2}$ have been 'coupled' so that the model predicted $\delta^{18}O\text{-}CO_2$ from the previous time step was used to calculate the discrimination in the next time step. We found it necessary to fix $\delta_{a,i}^{CO_2}$ in Equations 3.8 and 3.9 with observations from Point Barrow (rather than allowing it to change in response to the stand model isoforcing. This was necessary because atmospheric CO_2 is not in isotopic equilibrium with the extremely negative $\delta^{18}O$ of water pools at high northern latitudes. In the coupled simulations that we first attempted, $\delta_{a,i}^{CO_2}$ would reach values as negative as -4 to -5‰ (VPDB-CO_2) by the end of one year because our model did not include mixing with air enriched in $\delta^{18}O\text{-}CO_2$ from the tropics. Because the calculated isofluxes were dependent on $\delta_{a,i}^{CO_2}$, (through Δ_A in Equation 3.9) it was necessary to keep $\delta_{a,i}^{CO_2}$ consistent with current high-latitude observations to produce realistic fluxes. The discussions of our model results will be based on the resulting model-predicted $\delta_a^{CO_2}$. Note that removing the seasonal cycle and using a constant value for $\delta_{a,i}^{CO_2}$ for the entire year (Pt. Barrow annual mean of -1.4‰) yielded nearly identical results and did not change any of the conclusions of this study.

The purpose of the simple atmospheric model was to examine in isolation how biosphere-atmosphere fluxes that vary with stand age influence the atmospheric record. This approach provides insight about the role of species composition in boreal forests, and is not meant to replace a more realistic coupled biosphere-atmosphere model that

includes atmospheric transport and fluxes from the ocean, stratosphere, fossil fuels, and other terrestrial ecosystems.

We linearly detrended our model results of seasonal cycles of CO_2 and $\delta_a^{CO_2}$ (referred to as modeled $\delta^{18}O$-CO_2) to allow us to compare seasonal phasing across stands and with atmospheric observations. This is a common first step in the analysis of the seasonal cycle for atmospheric trace gases that also have a secular trend; it was required here because our local ecosystem fluxes were not in steady state with the atmosphere.

3.5 Results

3.5.1 CO_2 fluxes

Measurements of NEE from the 3 stands are shown in Figure 3.4. In the spring, the onset of photosynthesis and net CO_2 uptake was delayed by approximately 3 weeks at the 15-year stand as compared with the 80-year stand. Leaf emergence of aspen at the 15-year stand occurred between 18–24 May 2002, day of year (DOY) 138–144. By DOY 146, the daily net CO_2 flux was negative. The carbon uptake period, as defined by negative daily net CO_2 fluxes, was significantly shorter at the younger stands; the 3-year stand was reduced by 9 weeks as compared to the 80-year stand and the 15-year stand was reduced by 7 weeks.

In mid-summer from 18 June to 15 July 2002 (DOY 169–196), mean mid-day NEE (10 am – 2 pm local solar time) was -1.2 μmol m^{-2} s^{-1} at the 3-year stand, -5.7 μmol m^{-2} s^{-1} at the 15-year stand, and -4.2 μmol m^{-2} s^{-1} at the 80-year stand. For this same period, integrated daily NEE was -0.3 g C m^{-2} day^{-1} at the 3-year stand, -2.4 g C m^{-2} day^{-1}

at the 15-year stand, and -1.3 g C m^{-2} day^{-1} at the 80-year stand. Both the mid-day minima and daily NEE were reduced at the 3-year stand because of low leaf area. Mid-day NEE (10 am – 2 pm) was 36% more negative at the 15-year stand than at the 80-year stand. Integrated over 24 hours, the difference was even larger. The daily NEE for the 15-year stand was 85% more negative because during the night, NEE fluxes from the two stands were similar in magnitude and offset the differences measured during mid-day.

The R_e and GPP models described in the methods section were combined to form modeled half-hour NEE flux estimates. Weekly composite averages of the modeled fluxes are plotted with tower NEE diurnal averages in Figure 3.4. The model slightly under-predicted the nighttime NEE maxima and the daytime NEE minima (Figure 3.4). Our calculated Q_{10} values (Table 3.1) were between 2.1 to 4.7, and are within the range of Q_{10} values reported for other boreal forest ecosystems [Wang et al., 2002].

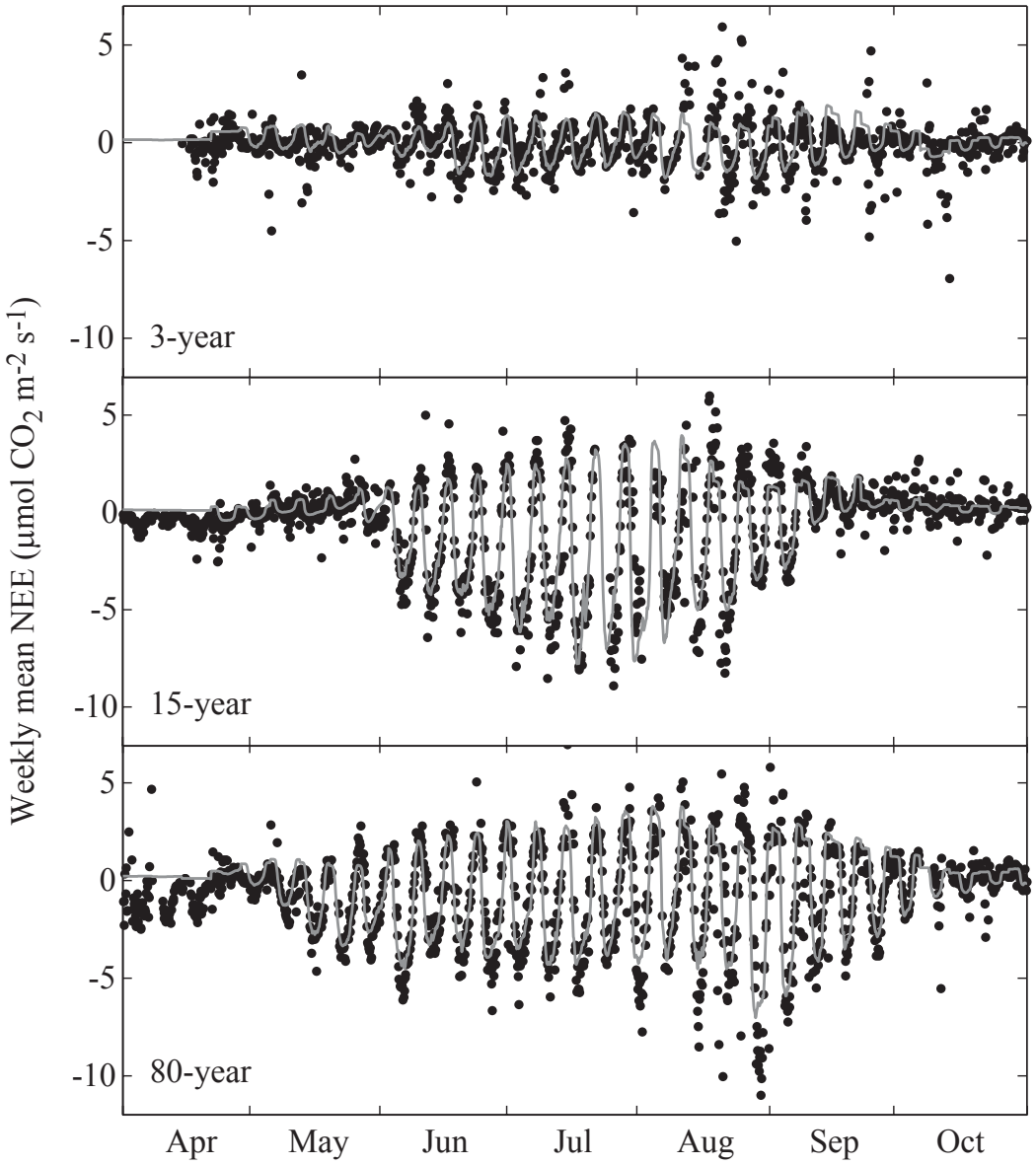

Figure 3.4 Measured (black filled circles) and modeled (solid grey line) weekly mean NEE for the three stands in 2002. This plot shows mean diurnal cycles constructed from 7-day intervals of 30-minute NEE data. The mean diurnal cycles are plotted sequentially to allow examination of the seasonality in GPP (indicated partly by the daytime minima) and R_e (indicated partly by the nighttime maxima). The growing season at the 15-year stand is shorter and more intense (with a larger diurnal cycle in mid-summer). Linear regression slopes between modeled and measured (weekly mean) NEE are 0.18 at the 3-year stand (r^2=0.35), 0.75 at the 15-year stand (r^2=0.76) and 0.59 at the 80-year stand (r^2=0.72). CO_2 fluxes at the 3-year stand are small making them difficult to measure and model and resulting in poor correlation statistics.

The magnitude of the potential bias between the modeled and measured NEE during the growing season was examined by comparing differences in the cumulative NEE (DOY 100–300) of the model fluxes with tower-measured NEE (Figure 3.5a). These results showed that the modeled NEE fluxes under-predicted the carbon uptake at each stand, however, without adding more complexity to our partitioning model, we considered this a reasonable fit to observations because it captured most of the seasonal change in net CO_2 fluxes (shape of the curves in Figure 3.5a) as well as variations in the diurnal cycle (Figure 3.4). Although the modeled NEE fluxes should be used cautiously, especially in the winter, the integrated annual sums provided an estimate of the magnitude of the source or sink of CO_2 at each stand for the entire year (Figure 3.5b). Annual integrated sums of GPP and R_e, in addition to NEE, are summarized in Table 3.2.

Table 3.2 Annual ecosystem fluxes, isofluxes, and other model parameters.

Annual Value (Flux-weighted)[1]	3-year	15-year	80-year	Units
GPP	-16.1	-36.3	-41.2	mol m^{-2} yr^{-1}
R_e	19.5	26.8	35.5	mol m^{-2} yr^{-1}
NEE	3.4	-9.5	-5.8	mol m^{-2} yr^{-1}
$\delta^{18}O$ leaf water (GPP)	-0.6	-1.4	-0.5	‰ (VSMOW)
$\delta^{18}O$ soil water (R_e)	-18.3	-17.8	-18.1	‰ (VSMOW)
$\delta^{18}O$ leaf CO_2 (GPP)	1.6	0.3	1.6	‰ (VPDB-CO_2)
$\delta^{18}O$ soil CO_2 (R_e)	-15.4	-14.5	-14.1	‰ (VPDB-CO_2)
C_c/C_a (GPP)	0.71	0.76	0.73	unitless
Δ_A (GPP)	9.3	5.1	7.5	‰
GPP•($\delta_{a,i}^{CO_2} - \Delta_A$)	170	227	360	mol m^{-2} yr^{-1} ‰
R_e•($\delta_{soil}^{CO_2} - \varepsilon_{soil}$)	-441	-581	-753	mol m^{-2} yr^{-1} ‰
Net Isoflux	-271	-354	-393	mol m^{-2} yr^{-1} ‰

[1]Gross fluxes used for parameter flux-weighting are in parentheses.

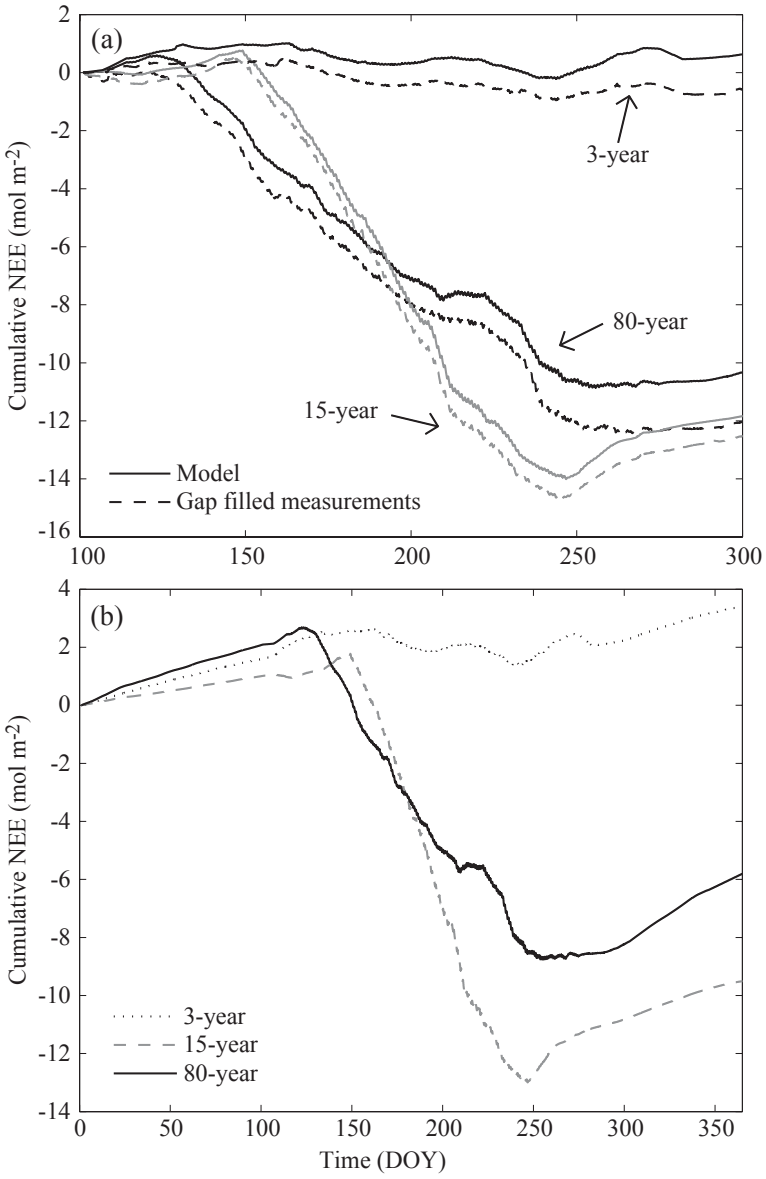

Figure 3.5 (a) A comparison between modeled NEE and measured NEE during the growing season, DOY 100–300. The solid lines are cumulative modeled NEE estimates and the dotted lines are measured NEE values that were gap filled with modeled estimates during periods of missing data. Modeled NEE has a bias towards decreased net carbon uptake at each stand. (b) Cumulative modeled NEE for the entire year (DOY 1–365) for each stand. The sign convention is such that positive values are fluxes to the atmosphere and negative values are uptake by the ecosystem. The 3-year stand was a source with a flux of approximately 3.4 mol CO_2 m^{-2} yr^{-1} (40.8 g C m^{-2} yr^{-1}) while the 15-year stand was a sink with a flux of approximately -9.5 mol CO_2 m^{-2} yr^{-1} (-114 g C m^{-2} yr^{-1}). The mature 80-year stand was a smaller sink of CO_2 with a flux of approximately -5.8 mol CO_2 m^{-2} yr^{-1} (-69.6 g C m^{-2} yr^{-1}).

3.5.2 Observations and modeling of the $\delta^{18}O$ of water pools

Figure 3.3 shows the range of precipitation, soil, xylem, leaf and water vapor isotope measurements from field campaigns in 2002, along with model estimates. During the day, bulk leaf water $\delta^{18}O$ was substantially enriched as compared to $\delta^{18}O$ of precipitation. At night, non-steady state estimates of leaf water $\delta^{18}O$ decreased but did not fully return to xylem water values. Field measurements of $\delta^{18}O$ of water vapor during mid-summer ranged between -18‰ to -29‰ and the daily averages were approximately 6–9‰ less than the model predicted $\delta^{18}O$ of precipitation (Figure 3.3). Each vapor $\delta^{18}O$ value plotted is an average of vertical canopy profiles measured four times over the course of one day. To examine the model performance, measurements of leaf and xylem water from field campaigns in June and August are expanded along with model predictions in Figure 3.6. The different stand ages show similar modeled leaf water $\delta^{18}O$ because of similarities in climate driver datasets (i.e., air temperatures, wind speeds, and relative humidity levels were similar at all three stands). The model did reasonably well at capturing the magnitude and diurnal variability of leaf water $\delta^{18}O$, but overestimated enrichment levels on several days. This is partly due to comparing predicted $\delta^{18}O$ at the site of evaporative enrichment with bulk leaf water measurements that contain some portion of non-enriched xylem water. Relative humidity contributed the most to variability in the leaf water $\delta^{18}O$ model predictions over weekly to monthly timescales. The seasonal maximum in leaf water isotopic enrichment (DOY ~150 in Figure 3.3) was linked to the seasonal minimum in relative humidity (DOY ~150 in

Figure 3.1) and not to the seasonal maximum in $\delta^{18}O$ of modeled plant source water (precipitation) $\delta^{18}O$ maximum which occurred near DOY 200 in Figure 3.3.

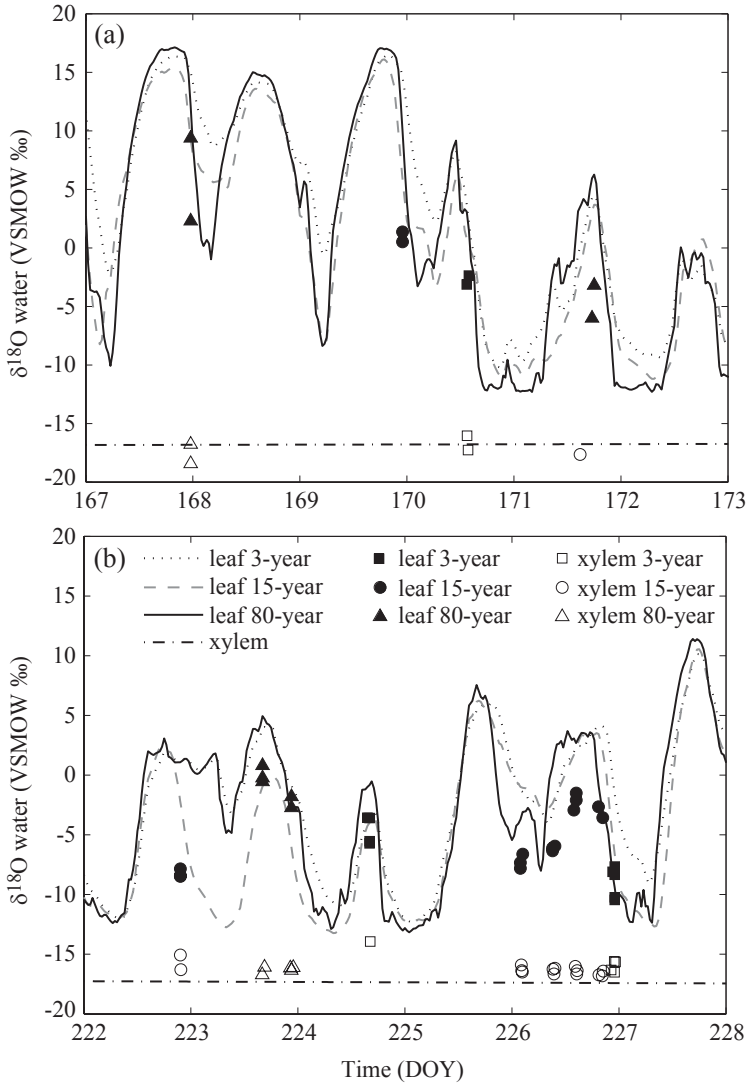

Figure 3.6 Measured $\delta^{18}O$ of leaf water and xylem water (symbols) are shown with model predictions (lines) during intensive field campaigns during (a) 16–22 June 2002 and (b) 10–16 August 2002. The leaf water model used in this study was a non-steady state model with a leaf water turnover time of 2 hours. Modeled xylem water was set equal to the $\delta^{18}O$ of precipitation.

3.5.3 Atmospheric modeling

The shorter and more intense growing season at the 15-year deciduous aspen stand caused a 30% increase in the peak-to-trough CO_2 seasonal amplitude, a delay in maximum CO_2 concentration, and an advance in minimum CO_2 concentration compared to the 80-year stand (Figure 3.7a). The 'downward zero crossing time' of the phase (the day which the CO_2 concentration crosses the mean value of the seasonal cycle in its descending phase) was delayed by 13 days at the 15-year stand as compared with the 80-year stand. The amplitude of the seasonal cycle at the 3-year stand was small and was difficult to separate from the secular trend. The downward zero crossing time analysis for the 3-year stand yielded a delay of 9 days compared to the 80-year stand, however, small NEE fluxes at the 3-year stand substantially increased the error of the model prediction.

Although we did not necessarily expect the 1-box model results to match atmospheric observations because of the lack of transport in the model, we compared the box model results of CO_2 (and later $\delta^{18}O$-CO_2) with the mean seasonal cycle of flask measurements from Pt. Barrow, Alaska [*CMDL*, 2000] in Figure 3.7a. The 80-year stand exhibited a maximum in CO_2 in April close to the atmospheric observations, but the predicted minimum in September was delayed from observations by one month. The 15-year stand most closely matched the atmospheric observations with an identical spring maximum in May and minimum in August. The seasonal amplitude in CO_2 agreed well with observations because the mass of air in the 1-box model was chosen so that the 80-

year stand fluxes matched this feature of the atmospheric record. We used the same mass for the other two model simulations.

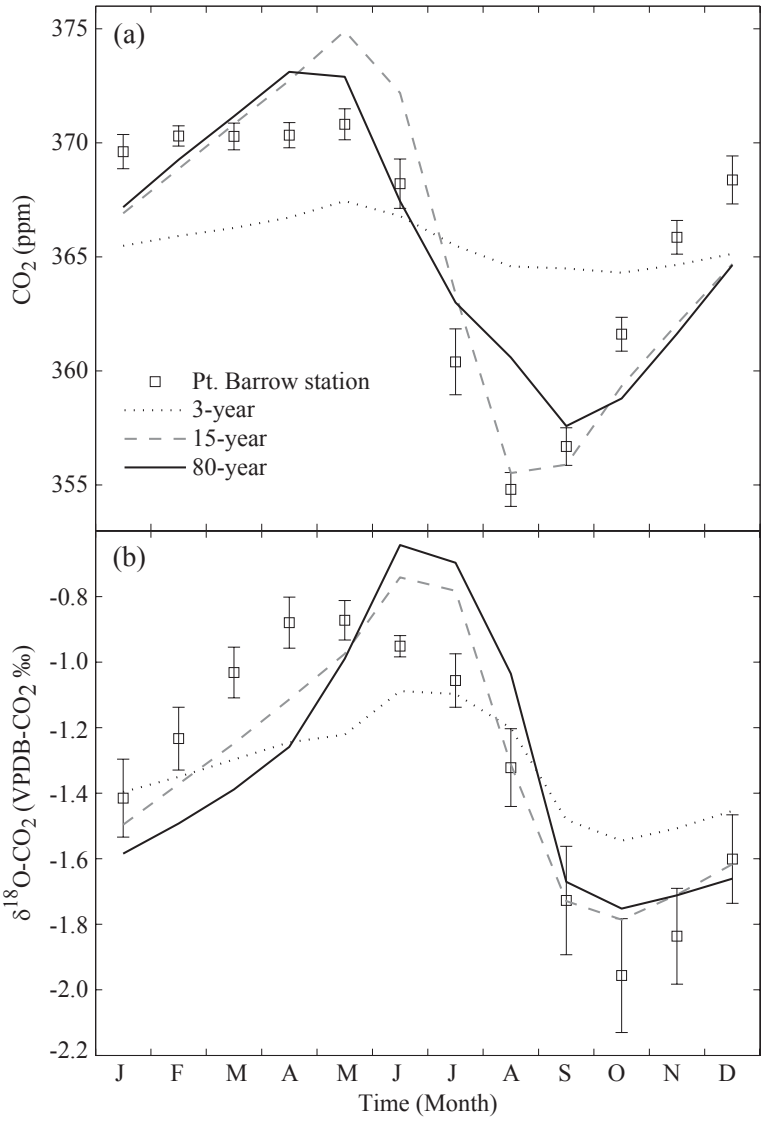

Figure 3.7 Predicted seasonal cycles of (a) CO_2 and (b) δ^{18}O-CO_2 for fluxes from each stand compared to the mean seasonal cycle of the NOAA CMDL flask network observations at Pt Barrow (1990–1997). Error bars on the Pt. Barrow observations represent the standard deviation about each mean monthly value for the entire data record. The phase of the 15-year CO_2 seasonal cycle was delayed relative to that at the 80-year stand and the amplitude is increased. In contrast, the phase of 15-year δ^{18}O-CO_2 seasonal cycle was advanced relative to that predicted for the 80-year stand.

To understand effects of photosynthesis and respiration on atmospheric $\delta^{18}O$-CO_2, we considered the isotopic flux (or isoforcing) of each component separately (Figure 3.8). As described previously, photosynthesis normally enriches the atmosphere in $\delta^{18}O$-CO_2, and respiration depletes the atmosphere. The large changes in isoforcing were constrained to periods of the year where there were large CO_2 fluxes, as the isoflux is the product of the one-way CO_2 flux and the isotopic composition of this flux. The combined net isoforcing on the atmosphere is shown in Figure 3.9. In terms of total net isoforcing, the 3-year stand had the effect of relative enrichment compared to the mature 80-year stand (also see Table 3.2). Although the recent fire disturbance at the 3-year stand decreased the atmospheric enrichment due to reduced assimilation, it diminished the depletion by reducing respiration even more. The overall effect was to enrich the atmosphere in $\delta^{18}O$-CO_2 relative to the 80-year stand. The intermediate 15-year stand had a less negative net isoforcing, but it was not substantially different from the 80-year stand.

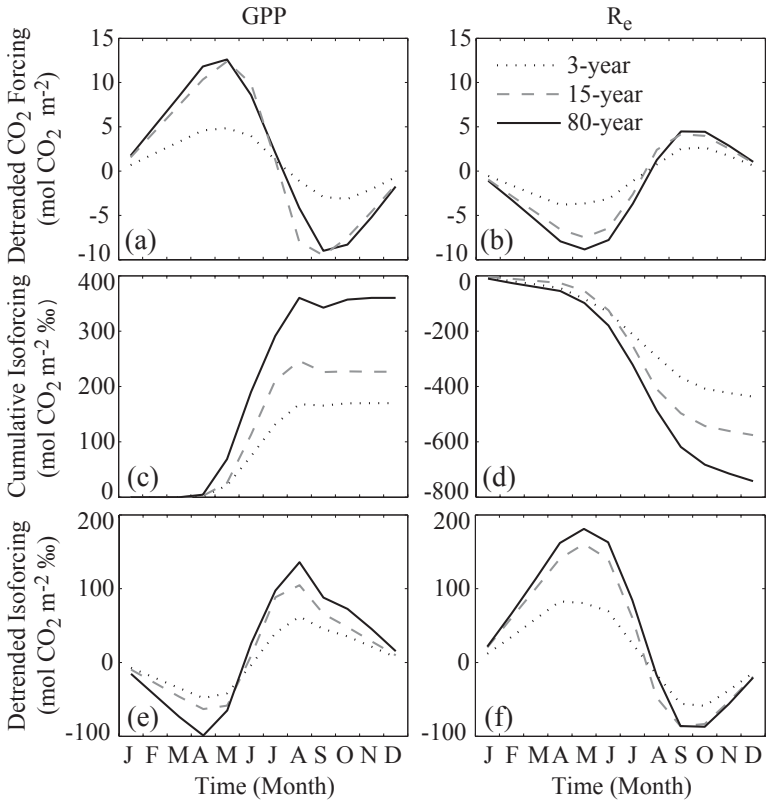

Figure 3.8 Cumulative (a) GPP and (b) R_e components of CO_2 forcing with the annual trend removed, (c) GPP and (d) R_e cumulative isoforcing, and (e) GPP and (f) R_e cumulative isoforcing with the annual trend removed. Note that the y-axis units in panels a,b,e, and f are relative units – they are not absolute values. At no time during the year was the cumulative GPP isoforcing negative (c) nor was the cumulative R_e isoforcing positive (d).

Using the modeled isofluxes for each forest, a seasonal cycle of $\delta^{18}O\text{-}CO_2$ was predicted using the simple 1-box model ($\delta_a^{CO_2}$) (Figure 3.7b). Since this is not a fully coupled model, the model results of $\delta^{18}O\text{-}CO_2$ reflect isoforcing by each forest age stand prior to feedbacks with the atmosphere. All three stands exhibited maximum $\delta^{18}O\text{-}CO_2$ in June and minimum in October. The zero crossing point of the seasonal cycle of the younger stands was advanced by 12 days relative to the 80-year stand (Figure 3.7b). The shape of the $\delta^{18}O\text{-}CO_2$ seasonal cycle during spring and early summer is also noticeably

different between the 15-year and 80-year stands. In part because of the earlier onset of photosynthesis at the 80-year stand (Figure 3.4) that coincided with relatively low levels of humidity (Figure 3.1), this stand had substantially greater GPP isoforcing during May and June (Figure 3.8). As a consequence, $\delta^{18}O\text{-}CO_2$ increased more rapidly from April to June for the 80-year stand than for the 15-year stand. Figure 3.7b also compares model predictions to atmospheric observations at Pt. Barrow, Alaska, the same values ($\delta_{a,i}^{CO_2}$) used to calculate the photosynthetic discrimination in Equations 3.8 and 3.9. By comparing the detrended seasonal cycles of GPP and R_e components of the net isoforcing (Figure 3.8ef), it is clear that isotopic exchange associated with R_e has a larger effect on the seasonal cycle than isotopic exchange associated with GPP.

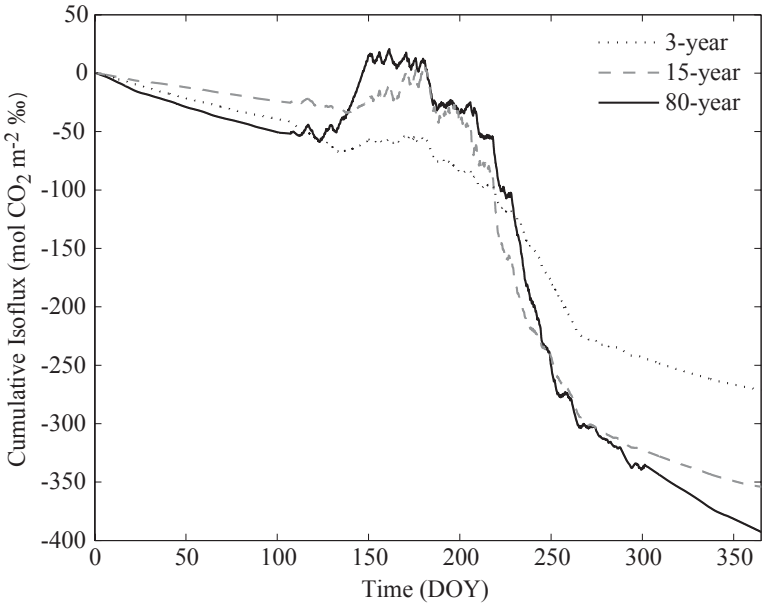

Figure 3.9 Cumulative net annual isoflux at each stand. All stands were predicted to deplete the atmosphere in $\delta^{18}O\text{-}CO_2$ because ecosystem water pools in the far north are extremely depleted in $\delta^{18}O$. The atmospheric $\delta^{18}O\text{-}CO_2$ was not in steady state with surface water pools at this latitude due to mixing with southern air masses with higher $\delta^{18}O\text{-}CO_2$.

3.5.4. Sensitivity of the $\delta^{18}O\text{-}CO_2$ seasonal cycle to C_c/C_a

We examined the sensitivity of the predicted seasonal cycle of $\delta^{18}O\text{-}CO_2$ amplitude and phase to the C_c/C_a ratio used in our model. For clarity, we present results for the 15-year stand only, however similar results were obtained for the other stands. First, we tested the importance of the diurnal cycle in C_c/C_a by comparing model results from our standard approach (that included a diurnally variable C_c/C_a predicted using the Ball-Berry equation) with a model run that had a time-invariant C_c/C_a value set at the GPP-weighted annual average of the variable case (i.e., GPP weighted C_c/C_a was the same in both runs). The constant C_c/C_a case enriched the atmosphere $\delta^{18}O\text{-}CO_2$ compared to the variable C_c/C_a case by doubling the GPP isoforcing and decreased the amplitude by 33% (Table 3.3). The increased GPP isoforcing component also delayed the zero point crossing by 17 days.

Table 3.3 Sensitivity analysis of the $\delta^{18}O\text{-}CO_2$ seasonal cycle

Model simulation	GPP Isoforcing (mol m^{-2} yr^{-1} ‰)	R_e Isoforcing (mol m^{-2} yr^{-1} ‰)	Net Isoforcing (mol m^{-2} yr^{-1} ‰)	$\delta^{18}O\text{-}CO_2$ Amplitude (‰)	Percent amplitude change	Zero crossing point	Day shift
Control C_c/C_a = 0.76 time varying	227	-581	-354	1.2	0%	229	0
C_c/C_a = 0.76 constant	457	-581	-124	0.8	-33%	256	-17
C_c/C_a = 0.66 time varying	226	-581	-355	1.0	-17%	224	5
C_c/C_a = 0.86 time varying	213	-581	-368	1.9	58%	233	-4

This sensitivity was a result of the covariance of leaf water $\delta^{18}O$ enrichment and C_c/C_a over a diurnal cycle. During mid-day when leaf water was most enriched, there were two negative feedbacks that limited GPP isoforcing. First, if there was no change in stomatal conductance, as GPP rates increased, C_c/C_a decreased, reducing the magnitude of the retrodiffusive flux. Second, stomatal conductance often decreased during mid-day in response to low levels of atmospheric humidity, and this also reduced C_c/C_a. Diurnal covariance between afternoon leaf water enrichment and decreased C_c/C_a was critical for predicting the GPP isoforcing component (Equations 3.9 and 3.10) and hence, the seasonal cycle of $\delta^{18}O$-CO_2. *Cuntz et al.* [2003a] also recognized the importance of C_c/C_a (or similarly, C_i/C_a) and noted that reasonable values of C_c/C_a could easily adjust the magnitude of the GPP isoforcing (through ε in Equation 3.10) by a factor of 2 ($C_c/C_a = 0.67$) or 3 ($C_c/C_a = 0.75$). We show here that it is possible to increase the GPP isoforcing by a factor of 2 without changing the GPP weighted C_c/C_a annual mean, but by simply removing the diurnal cycle in C_c/C_a.

The results from the sensitivity tests where we adjusted the C_c/C_a weighted mean value by ±0.1 were unexpected. Instead of increased C_c/C_a leading to an increase in the GPP isoforcing through the ε factor, it led to a small decrease. This was because for part of the year, $\delta^{18}O$ of leaf CO_2 was greater than the $\delta^{18}O$ of the atmosphere (positive GPP isoforcing) and for part of the year $\delta^{18}O$ of leaf CO_2 was less than $\delta^{18}O$ of the atmosphere (negative GPP isoforcing) (Figure 3.10). In effect, the C_c/C_a adjustments to the GPP isoforcing were canceled out when integrated over the growing season.

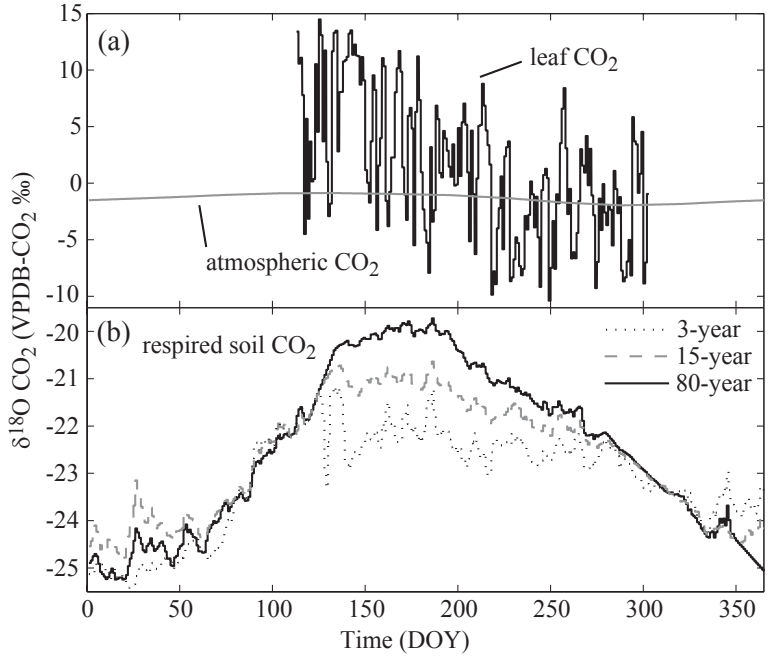

Figure 3.10 (a) Daily GPP-weighted leaf δ^{18}O-CO_2 and δ^{18}O of atmospheric CO_2 ($\delta_{a,i}^{CO_2}$) and (b) daily R_e-weighted respired soil δ^{18}O-CO_2 (diffusion fractionation of -7.2‰ has been included, $\delta_{soil}^{CO_2} - \varepsilon_{diff}$) for the 15-year stand. High δ^{18}O values of leaf CO_2 (and leaf water) in the beginning of the growing season (around DOY 150) were due to low relative humidity levels during this period (Figure 3.1c). This resulted in more positive Δ_A values on average earlier in the growing season and decreasing Δ_A towards the end of the season. Differences in the magnitude and seasonal distribution of GPP at each stand resulted in variations in the isoforcing among stands, even though the modeled δ^{18}O of leaf water was similar across stands. Soil temperature differences resulted in different equilibrium fractionation factors between CO_2 and water, and therefore, δ^{18}O of soil respired CO_2 at each stand.

3.6 Discussion

3.6.1 Disturbance induced changes in CO_2 seasonal amplitude and phase

We compared seasonal carbon exchange from the 15-year and 80-year stands to test the *Zimov et al*. [1999] hypothesis that disturbance could contribute substantially to the observed increase in the seasonal amplitude of atmospheric CO_2. Previous work from

a boreal forest chronosequence in Canada showed that light-saturated CO_2 uptake in mid-summer is greatest in intermediate stand ages [*Litvak et al.*, 2003]. *Falge et al.* [2002] found that in temperate regions, broadleaf deciduous forest stands have a substantially shorter growing season that is characterized by high rates of net carbon uptake as compared with evergreen conifer forest stands. We measured an 85% increase in carbon uptake at the 15-year stand compared to the 80-year stand during the 31 day period from 18 June to 15 July (DOY 169–196). Together, these observations provide qualitative support for the *Zimov et al.* [1999] hypothesis, and the idea that plant functional type plays a key role in shaping the seasonal cycle of atmospheric CO_2 at high northern latitudes.

In terms of explaining observed increases in the CO_2 amplitude in the Arctic from 1961–1994 [*Keeling et al.*, 1996], several factors suggest that disturbance-driven change in plant functional type within boreal ecosystems is probably not the dominant mechanism. From our 1-box conceptual atmospheric model, replacing fluxes from the 80-year stand with fluxes from the 15-year stand caused an increase in the seasonal amplitude of CO_2 of 30%. This change represents a rough first guess at the expected effect of replacing all northern evergreen conifer forests with deciduous broadleaf forests. There is growing evidence that disturbance rates have increased in recent decades within the boreal forests of North America [*Kurz and Apps*, 1999; *Kasischke and Stocks*, 2000; *Gillett et al.*, 2004] and Eurasia [*Conard et al.*, 2002; *Sukhinin et al.*, 2004]; however, actual shifts in the distribution of stand ages and plant functional types have been far more modest than the total stand replacement represented by our model simulations. In

addition, only 42% of the seasonal cycle at Pt. Barrow and other Arctic observation stations originates from biosphere-atmosphere exchange with boreal forests; tundra ecosystems contribute another 14%, deciduous forests 12%, and grassland ecosystems further to the south contribute another 16% [*Randerson et al.*, 1997].

Another metric of seasonal cycle change is the phase, which is often measured by the DOY that the seasonal cycle crosses from a positive value to a negative value in the spring (for a time series of CO_2 for which the secular trend from fossil fuel emissions has been removed). This 'downward zero crossing time' of the atmospheric CO_2 seasonal cycle has advanced 7 days from 1975 to 1994 [*Keeling et al.*, 1996]. The leading candidate for explaining both the advanced CO_2 phase as well as increased amplitude is increasing spring and summer air temperature at high northern latitudes [*Keeling et al.*, 1996; *McDonald et al.*, 2004; *Angert et al.*, 2005]. A warmer climate simultaneously increases growing season length through earlier initiation of photosynthetic activity [*Black et al.*, 2000; *Tanja et al.*, 2003; *White and Nemani*, 2003] and net uptake rates during summer, and provides greater substrate for respiratory losses during fall, winter, and spring [*Goulden et al.*, 1998]. However, deciduous broadleaf trees must grow new leaves each spring, and hence, there is a delay in start of the carbon uptake period compared to evergreen conifers that retain needles year-round. This directly delays the phase of the CO_2 seasonal cycle, by 13 days at the 15-year stand compared to the 80-year. Using arguments similar to those discussed earlier for the CO_2 amplitude, we present this as an upper bound of expected atmospheric change if all boreal evergreen forests were replaced by deciduous forests. Assuming a modest increase in the rate of disturbance, we

predict a shift toward deciduous forest species should have delayed the seasonal CO_2 phase by perhaps a day or two. This suggests that spring warming may have had an even stronger effect on ecosystem fluxes and advanced the phase of the seasonal cycle of CO_2 more than previous estimates that did not account for disturbance-induced changes in forest stand age and plant functional type.

3.6.2 Factors controlling the seasonal cycle of $\delta^{18}O$-CO_2

The modeled amplitudes of the $\delta^{18}O$-CO_2 seasonal cycle imposed by surface fluxes at the 15-year stand and the 80-year stand were comparable (Figure 3.7b). Nonetheless, the phase and shape of the seasonal cycle was considerably different as a result of differences in isotopic exchange between the two stands. The $\delta^{18}O$-CO_2 phase was advanced by 9 days at the 15-year stand relative to the 80-year stand (Figure 3.7b). Stand-level differences in both the GPP and R_e isotopic fluxes contributed to differences in the phase and shape of the seasonal cycle (Figures 3.8ef).

Because precipitation is considerably depleted in ^{18}O at high northern latitudes, CO_2 in equilibrium with leaf water is very close to atmospheric $\delta^{18}O$-CO_2 (Figure 3.10a). The GPP isoforcing was only slightly positive and was even negative at times (when the $\delta^{18}O$ of leaf CO_2 is less than $\delta_{a,i}^{CO_2}$), depleting the atmosphere in $\delta^{18}O$-CO_2. The flux-weighted annual mean Δ_A was +5.1‰ for the 15-year stand, much smaller than the +7.5‰ for the 80-year stand. For comparison, these Δ_A values were lower than other widely variable high-latitude estimates. *Farquhar et al*. [1993] predicted approximately +14‰ at 60°N and *Flanagan et al*. [1997] estimated Δ_A was +21‰ for the Canadian

boreal forest during mid-day in July which was also higher than our model predictions of mid-day Δ_A during July of approximately +17‰.

In the Delta Junction study region, low spring relative humidity (Figure 3.1c) led to enriched leaf waters that gradually became more depleted as humidity increased throughout the summer (Figure 3.10a). Earlier initiation of GPP at the 80-year stand during the period of more enriched leaf water resulted in a more positive Δ_A at that stand. Delays in leaf-out at the 15-year stand led to less atmospheric enrichment associated with GPP in the early part of the growing season (Figure 3.8c). Thus, the increase in $\delta^{18}O$-CO_2 between April and June was considerably smaller for the 15-year stand as compared with the 80-year stand (Figures 3.7b and 3.8e). Changes in the phase also reflected differences in isotopic fluxes associated with R_e (Figure 3.8f). Specifically, the advance in phase of R_e at the 15-year stand (Figure 3.8b) led to an advance in the phase of the R_e isoforcing (Figure 3.8f).

The phase of the seasonal cycle of $\delta^{18}O$-CO_2, most notably the minimum, is delayed from that of CO_2 by 1 to 2 months in the atmosphere at high northern latitudes [*Ciais and Meijer*, 1998; *Peylin et al.*, 1999]. Reproducing this phase lag in global models has been challenging and has been attributed in part to errors associated with atmospheric transport [*Cuntz et al.*, 2003b]. Our analysis suggests that ecosystem processes (as well as transport not considered here) may contribute to phase delays between $\delta^{18}O$-CO_2 and CO_2. Specifically, with our 1 box atmospheric model, seasonal phases from the 80-year and 15-year stands showed a one or two month lag, respectively, between CO_2 and $\delta^{18}O$-CO_2 minima (Figure 3.7), matching the phase lag observed at Pt.

Barrow. Preliminary analysis suggests that key controls on the phase at the ecosystem level include the isotopic composition of precipitation and seasonal patterns of plant water use.

3.6.3 Future work

We developed a simple model for $\delta^{18}O\text{-}CO_2$ isoforcing to extend the interpretation of our field measurements and to specifically investigate some of the effects of stand age on the seasonal cycle of $\delta^{18}O\text{-}CO_2$. In this analysis, we simplified or omitted a number of processes that should be considered in future work. First, there is an active area of research currently focusing on non-steady state leaf water enrichment models and observations [*Cernusak et al.*, 2004; *Farquhar and Cernusak*, 2005] and the effects on canopy vapor $\delta^{18}O$ [*Lai et al.*, 2006] and surface isofluxes [*Seibt et al.*, 2005]. Differences in leaf morphology are likely to lead to different leaf water turnover times among broadleaves and conifer needles. More field experiments are required to accurately determine differences in the τ parameter (Equation 3.2). Recent work suggests non-zero nighttime stomatal conductance rates may have consequences for $\delta^{18}O\text{-}CO_2$ isofluxes and that the magnitude of the effect may be different for broadleaf and conifer species [*Barbour et al.*, 2005]. However, the degree to which concurrent increases in nighttime leaf and canopy boundary layer resistances offsets the impact of this mechanism for ecosystem $\delta^{18}O\text{-}CO_2$ isofluxes remains unexplored.

A more complete representation of R_e isoforcing may be obtained, in future, by partitioning foliar and stem components of R_e [*Flanagan et al.*, 1997; *Bowling et al.*, 2003a; 2003b; *Riley et al.*, 2003] and by including the effects of moss water on soil R_e

isoforcing [e.g., *Flanagan et al.,* [1997]. R_e isoforcing estimates could also be improved by including a more detailed representation of equilibration of CO_2 with surface soil water pools [*Riley et al.*, 2002] and fluxes associated with abiotic atmosphere-soil CO_2 exchange [*Tans*, 1998; *Miller et al.*, 1999; *Stern et al.*, 2001]. A key factor that contributes to uncertainty in the GPP isoforcing term is our limited understanding of seasonal patterns of plant water use, including the use of snowmelt water by different plant species throughout the growing season [*Sugimoto et al.*, 2002; *Welp et al.*, 2005].

3.7 Conclusions

We measured NEE and the isotopic composition of atmosphere and ecosystem water pools at three stands in a boreal forest fire chronosequence. Our measurements and model analysis provide evidence that species composition exerts a strong control on the shape of both the CO_2 and $\delta^{18}O$-CO_2 seasonal cycles at high northern latitudes. An expansion of the areas covered by deciduous forests in the boreal region, as a result of increased forest fire frequency, would increase the amplitude and delay the phase of the seasonal cycle of CO_2. Increases in high-latitude disturbance and spring warming have been proposed as potential explanations of observed increases in the amplitude of the seasonal cycle of atmospheric CO_2 [*Keeling et al.*, 1996; *Zimov et al.*, 1999; *McDonald et al.*, 2004; *Angert et al.*, 2005]. Here we argued that it must be a combination of these processes. Changes in the boreal disturbance regime over the last few decades, though not well characterized, seem too small to drive large changes in the seasonal amplitude, based on our NEE measurements.

Our analysis suggests that the seasonal cycle of $\delta^{18}O\text{-}CO_2$ is also sensitive to the seasonal timing of GPP and R_e surface fluxes, both of which are controlled by plant functional type (and thus stand age) within the boreal forest. In contrast to CO_2, an expansion of the areas covered by deciduous forests would advance the phase of the $\delta^{18}O\text{-}CO_2$ seasonal cycle. An increase in deciduous forest area would also weaken GPP isoforcing during the early part of the growing season and cause $\delta^{18}O\text{-}CO_2$ to increase more gradually between April and June. Important next steps include improving our understanding winter and summer precipitation use by different plant functional types and investigating the impact of changing plant functional types and climate on the $\delta^{18}O\text{-}CO_2$ seasonal cycle using a coupled model that includes atmospheric transport and mixing.

Acknowledgements

The authors would like to thank J. Fessenden for assistance in the field and $\delta^{13}C$ foliage measurements, J. Lindfors for help developing the eddy covariance systems, F.S. Chapin for logistical support through the University of Alaska, Fairbanks, and J. Garron for data collection. NOAA CMDL flask data was generously made available by P. Tans, J. White and B. Vaughn. D. Noone, W. Riley and C. Still contributed many useful $\delta^{18}O$-CO_2 discussions. We thank two anonymous reviewers for thoughtful comments that substantially improved the quality of this manuscript. We also thank S.A. Zimov and F.S. Chapin for providing insight about species effects on biosphere-atmosphere exchange in northern ecosystems. This work was supported by grants from NSF's Office of Polar Programs (NSF OPP-0097439), NOAA's Office of Global Programs (NA03OAR4310059), the Powell Foundation, and by a gift from the Davidows to Caltech. LRW was supported by a NCER STAR EPA graduate fellowship.

3.8 References

ACIA (2004), *Impacts of a Warming Arctic: Arctic Climate Impact Assessment*, Cambridge University Press, http://www.acia.uaf.edu.

Angert, A., S. Biraud, A. Bonfils, C. C. Henning, W. Buermann, J. Pinzon, C. J. Tucker, and I. Fung (2005), Drier summer cancel out the CO_2 uptake enhancement induced by warmer springs, *Proc. Natl. Acad. Sci. U. S. A.*, *102*, 31, 10823-10827.

Ball, J. T. (1988), An analysis of stomatal conductance, Ph.D. thesis, Stanford University, Stanford, California.

Barbour, M. M., L. A. Cernusak, D. Whitehead, K. L. Griffin, M. H. Turnbull, D. T. Tissue, and G. D. Farquhar (2005), Nocturnal stomatal conductance and implications for modeling delta O-18 of leaf-respired CO_2 in temperate tree species, *Functional Plant Biology*, *32*, 12, 1107-1121.

Black, T. A., W. J. Chen, A. G. Barr, M. A. Arain, Z. Chen, Z. Nesic, E. H. Hogg, H. H. Neumann, and P. C. Yang (2000), Increased carbon sequestration by a boreal deciduous forest in years with a warm spring, *Geophys. Res. Lett.*, *27*, 9, 1271-1274.

Bogaert, J., L. Zhou, C. J. Tucker, R. B. Myneni, and R. Ceulemans (2002), Evidence for a persistent and extensive greening trend in Eurasia inferred from satellite vegetation index data, *J. Geophys. Res.*, *107*, D11, 4119, doi:10.1029/2001JD001075.

Bolin, B., and C. D. Keeling (1963), Large-scale atmospheric mixing as deduced from seasonal and meridional variations of carbon dioxide, *J. Geophys. Res.*, *68*, 13, 3899-3920.

Bond-Lamberty, B., C. K. Wang, and S. T. Gower (2004), Net primary production and net ecosystem production of a boreal black spruce wildfire chronosequence, *Global Change Biol.*, *10*, 4, 473-487.

Bowling, D. R., N. G. McDowell, J. M. Welker, B. J. Bond, B. E. Law, and J. R. Ehleringer (2003a), Oxygen isotope content of CO_2 in nocturnal ecosystem respiration: 1. Observations in forests along a precipitation transect in Oregon, USA, *Global Biogeochem. Cycles*, *17(4)*, 1120, doi:10.1029/2003GB002081.

Bowling, D. R., N. G. McDowell, J. M. Welker, B. J. Bond, B. E. Law, and J. R. Ehleringer (2003b), Oxygen isotope content of CO_2 in nocturnal ecosystem respiration: 2. Short-term dynamics of foliar and soil component fluxes in an old-growth ponderosa pine forest, *Global Biogeochem. Cycles*, *17(4)*, 1124, doi:10.1029/2003GB002082.

Cappa, C. D., M. B. Hendricks, D. J. DePaolo, and R. C. Cohen (2003), Isotopic fractionation of water during evaporation, *J. Geophys. Res.*, *108*, D16, 4525, doi:4510.1029/2003JD003597.

Cernusak, L. A., G. D. Farquhar, S. C. Wong, and H. Stuart-Williams (2004), Measurement and interpretation of the oxygen isotope composition of carbon dioxide respired by leaves in the dark, *Plant Physiol.*, *136*, 2, 3350-3363.

Cess, R. D., et al. (1991), Interpretation of snow-climate feedback as produced by 17 general-circulation models, *Science*, *253*, 5022, 888-892.
Chapin, F. S., S. A. Zimov, G. R. Shaver, and S. E. Hobbie (1996), CO2 fluctuation at high latitudes, *Nature*, *383*, 6601, 585-586.
Ciais, P., et al. (1997), A three-dimensional synthesis study of delta O-18 in atmospheric CO_2.1. Surface fluxes, *J. Geophys. Res.*, *102*, D5, 5857-5872.
Ciais, P., and H. A. J. Meijer (1998), The $^{18}O/^{16}O$ isotope ratio of atmospheric CO_2 and its role in global carbon cycle research, in *Stable Isotopes*, pp. 409-431, BIOS Scientific Publishers Ltd, Oxford.
CMDL (2000), National Oceanic and Atmospheric Administration, Climate Monitoring and Diagnostics Laboratory (CMDL)/ Institute of Arctic and Alpine Research, http://www.cmdl.noaa.gov/ccgg.
Conard, S. G., A. I. Sukhinin, B. J. Stocks, D. R. Cahoon, E. P. Davidenko, and G. A. Ivanova (2002), Determining effects of area burned and fire severity on carbon cycling and emissions in Siberia, *Climatic Change*, *55*, 1-2, 197-211.
Conway, T. J., P. P. Tans, L. S. Waterman, and K. W. Thoning (1994), Evidence for interannual variability of the carbon cycle from the National Oceanic and Atmospheric Administration/Climate Monitoring and Diagnostics Laboratory Global Air Sampling Network, *J. Geophys. Res.*, *99*, D11, 22831-22855.
Craig, H., and L. I. Gordon (1965), Deuterium and oxygen-18 variations in the ocean and the marine atmosphere, paper presented at Proceedings of a Conference on Stable Isotopes in Oceanographic Studies and Paleotemperatures, Spoleto, Italy.
Cuntz, M., P. Ciais, G. Hoffmann, C. E. Allison, and W. Knorr (2003a), A comprehensive global three-dimensional model of delta O-18 in atmospheric CO_2: 1. Validation of surface processes, *J. Geophys. Res.*, *108*, D17, 4527, doi:10.1029/2002JD003153.
Cuntz, M., P. Ciais, G. Hoffmann, C. E. Allison, R. J. Francey, W. Knorr, P. P. Tans, J. W. C. White, and I. Levin (2003b), A comprehensive global three-dimensional model of delta O-18 in atmospheric CO_2: 2. Mapping the atmospheric signal, *J. Geophys. Res.*, *108*, D17, 4528, doi:10.1029/2002JD003154.
Dang, Q. L., H. A. Margolis, M. R. Coyea, M. Sy, and G. J. Collatz (1997), Regulation of branch-level gas exchange of boreal trees: roles of shoot water potential and vapor pressure difference, *Tree Phyisol.*, *17*, 8-9, 521-535.
Dongmann, G., H. W. Nurnberg, H. Forstel, and K. Wagener (1974), Enrichment of $H_2{}^{18}O$ in leaves of transpiring plants, *Radiation and Environmental Biophysics*, *11*, 1, 41-52.
Ehleringer, J. R., J. Roden, and T. E. Dawson (2000), Assessing ecosystem-level water relations through stable isotope ratio analysis, in *Methods in Ecosystem Science*, pp. 181-198, Springer Verlag, New York.
Ewers, B. E., S. T. Gower, B. Bond-Lamberty, and C. K. Wang (2005), Effects of stand age and tree species on canopy transpiration and average stomatal conductance of boreal forests, *Plant Cell Environ.*, *28*, 5, 660-678.

Falge, E., et al. (2002), Phase and amplitude of ecosystem carbon release and uptake potentials as derived from FLUXNET measurements, *Agric. For. Meteorol.*, *113*, 1-4, 75-95.

Farquhar, G. D., J. R. Ehleringer, and K. T. Hubick (1989), Carbon isotope discrimination and photosynthesis, *Annu. Rev. Plant Physiol. Plant Mol. Biol.*, *40*, 503-537.

Farquhar, G. D., J. Lloyd, J. A. Taylor, L. B. Flanagan, J. P. Syvertsen, K. T. Hubick, S. C. Wong, and J. R. Ehleringer (1993), Vegetation effects on the isotope composition of oxygen in atmospheric CO_2, *Nature*, *363*, 6428, 439-443.

Farquhar, G. D., and L. A. Cernusak (2005), On the isotopic composition of leaf water in the non-steady state, *Functional Plant Biology*, *32*, 4, 293-303.

Fessenden, J. E., C. S. Cook, M. J. Lott, and J. R. Ehleringer (2002), Rapid ^{18}O analysis of small water and CO_2 samples using a continuous-flow isotope ratio mass spectrometer, *Rapid Commun. Mass Spectrom.*, *16*, 1257-1260.

Flanagan, L. B., J. P. Comstock, and J. R. Ehleringer (1991), Comparison of modeled and observed environmental-influences on the stable oxygen and hydrogen isotope composition of leaf water in *Phaseolus vulgaris* L., *Plant Physiol.*, *96*, 2, 588-596.

Flanagan, L. B., J. R. Brooks, G. T. Varney, and J. R. Ehleringer (1997), Discrimination against (COO)-O-18-O-16 during photosynthesis and the oxygen isotope ratio of respired CO_2 in boreal forest ecosystems, *Global Biogeochem. Cycles*, *11*, 1, 83-98.

Flanagan, L. B. (2005), Ecosystem CO_2 exchange and variation in the $\delta^{18}O$ of atmospheric CO_2, in *Stable isotopes and biosphere-atmosphere interactions: Processes and biological controls*, pp. 171-181, Elsevier, San Diego.

Flannigan, M. D., K. A. Logan, B. D. Amiro, W. R. Skinner, and B. J. Stocks (2005), Future area burned in Canada, *Climatic Change*, *72*, 1-2, 1-16.

Francey, R. J., and P. P. Tans (1987), Latitudinal variation in O-18 of atmospheric CO_2, *Nature*, *327*, 6122, 495-497.

Friedli, H., U. Siegenthaler, D. Rauber, and H. Oeschger (1987), Measurements of concentration, $^{13}C/^{12}C$ and $^{18}O/^{16}O$ ratios of tropospheric carbon dioxide over Switzerland, *Tellus, Ser. B*, *39*, 80-88.

Frolking, S., et al. (1996), Modelling temporal variability in the carbon balance of a spruce/moss boreal forest, *Global Change Biol.*, *2*, 4, 343-366.

Gillett, N. P., A. J. Weaver, F. W. Zwiers, and M. D. Flannigan (2004), Detecting the effect of climate change on Canadian forest fires, *Geophys. Res. Lett.*, *31*, L18211, doi:10.1029/2004GL020876.

Gillon, J., and D. Yakir (2001), Influence of carbonic anhydrase activity in terrestrial vegetation on the O-18 content of atmospheric CO_2, *Science*, *291*, 5513, 2584-2587.

Goulden, M. L., B. C. Daube, S. M. Fan, D. J. Sutton, A. Bazzaz, J. W. Munger, and S. C. Wofsy (1997), Physiological responses of a black spruce forest to weather, *J. Geophys. Res.*, *102*, D24, 28987-28996.

Goulden, M. L., et al. (1998), Sensitivity of boreal forest carbon balance to soil thaw, *Science*, *279*, 5348, 214-217.

Helliker, B. R., J. S. Roden, C. Cook, and J. R. Ehleringer (2002), A rapid and precise method for sampling and determining the oxygen isotope ratio of atmospheric water vapor, *Rapid Commun. Mass Spectrom.*, *16*, 10, 929-932.

Hesterberg, R., and U. Siegenthaler (1991), Production and stable isotopic composition of CO_2 in a soil near Bern, Switzerland, *Tellus, Ser. B*, *43*, 2, 197-205.

Hicke, J. A., G. P. Asner, J. T. Randerson, C. Tucker, S. Los, R. Birdsey, J. C. Jenkins, and C. Field (2002), Trends in North American net primary productivity derived from satellite observations, 1982-1998, *Global Biogeochem. Cycles*, *16*, 2, 1018, doi:10.1029/2001GB001550.

IAEA/WMO (2004), Global network of isotopes in precipitation, The GNIP database, http://isohis.iaea.org.

IPCC (2001), *Intergovernmental Panel on Climate Change, Climate change 2001*, Cambridge Univ. Press, New York.

Jarvis, P. G., and K. G. McNaughton (1986), Stomatal control of transpiration: Scaling up from leaf to region, in *Advances in Ecological Research*, pp. 1-49, Academic Press, Inc., London.

Kasischke, E. S., and B. J. Stocks (2000), *Fire, Climate Change, and Carbon Cycling in the Boreal Forest.*, 461 pp., Springer, New York.

Keeling, C. D., J. F. S. Chin, and T. P. Whorf (1996), Increased activity of northern vegetation inferred from atmospheric CO_2 measurements, *Nature*, *382*, 6587, 146-149.

Kimball, J. S., K. C. McDonald, A. R. Keyser, S. Frolking, and S. W. Running (2001), Application of the NASA scatterometer (NSCAT) for determining the daily frozen and nonfrozen landscape of Alaska, *Remote Sens. Environ.*, *75*, 1, 113-126.

King, S., J. Harden, K. L. Manies, J. Munster, and D. L. White (2002), Fate of carbon in Alaskan landscapes project - Database for soils from eddy covariance tower sites, Delta Junction, AK, *Open File Rep. 02-62*, U.S Geol. Surv., Menlo Park, CA.

Kurz, W. A., and M. J. Apps (1999), A 70-year retrospective analysis of carbon fluxes in the Canadian forest sector, *Ecol. Appl.*, *9*, 526-547.

Lai, C. T., J. R. Ehleringer, B. J. Bond, and K. T. P. U (2006), Contributions of evaporation, isotopic non-steady state transpiration and atmospheric mixing on the delta O-18 of water vapour in Pacific Northwest coniferous forests, *Plant Cell Environ.*, *29*, 1, 77-94.

Litvak, M., S. Miller, S. C. Wofsy, and M. Goulden (2003), Effect of stand age on whole ecosystem CO_2 exchange in the Canadian boreal forest, *J. Geophys. Res.*, *108*, D3, 8225, doi:10.1029/2001JD000854.

Liu, H. P., G. Peters, and T. Foken (2001), New equations for sonic temperature variance and buoyancy heat flux with an omnidirectional sonic anemometer, *Boundary Layer Meteorol.*, *100*, 3, 459-468.

Liu, H. P., J. T. Randerson, J. Lindfors, and F. S. Chapin (2005), Changes in the surface energy budget after fire in boreal ecosystems of interior Alaska: An annual perspective, *J. Geophys. Res.*, *110*, D13101, doi:10.11029/12004JD005158.

Lloyd, J., and G. D. Farquhar (1994), C-13 discrimination during CO_2 assimilation by the terrestrial biosphere, *Oecologia*, *99*, 3-4, 201-215.

Lloyd, J., and J. A. Taylor (1994), On the temperature-dependence of soil respiration, *Functional Ecology*, *8*, 3, 315-323.

Manies, K. L., J. W. Harden, S. R. Silva, P. H. Briggs, and B. M. Schmid (2004), Soil data from *Picea mariana* stands near Delta Junction, Alaska of different ages and soil drainage type, *U.S. Geol. Surv. Open File Rep.*, *2004-1271*.

McDonald, K. C., J. S. Kimball, E. Njoku, R. Zimmermann, and Z. Maosheng (2004), Variability in springtime thaw in the terrestrial high latitudes: Monitoring a major control on the biospheric assimilation of atmospheric CO_2 with spaceborne microwave remote sensing, *Earth Interactions*, *8*, 20, 1-23.

Menzel, A., and P. Fabian (1999), Growing season extended in Europe, *Nature*, *397*, 6721, 659-659.

Miller, J. B., D. Yakir, J. W. C. White, and P. P. Tans (1999), Measurement of O-18/O-16 in the soil-atmosphere CO2 flux, *Glob. Biogeochem. Cycle*, *13*, 3, 761-774.

Mills, G. A., and H. C. Urey (1940), The kinetics of isotopic exchange between carbon dioxide, bicarbonate ion, carbonate ion and water, *J. Am. Chem. Soc.*, *62*, 1019-1026.

Myneni, R. B., C. D. Keeling, C. J. Tucker, G. Asrar, and R. R. Nemani (1997), Increased plant growth in the northern high latitudes from 1981 to 1991, *Nature*, *386*, 6626, 698-702.

Myneni, R. B., et al. (2002), Global products of vegetation leaf area and fraction absorbed PAR from year one of MODIS data, *Remote Sens. Environ.*, *83*, 1-2, 214-231.

Nemani, R. R., C. D. Keeling, H. Hashimoto, W. M. Jolly, S. C. Piper, C. J. Tucker, R. B. Myneni, and S. W. Running (2003), Climate-driven increases in global terrestrial net primary production from 1982 to 1999, *Science*, *300*, 5625, 1560-1563.

O'Neill, K. P., E. S. Kasischke, and D. D. Richter (2003), Seasonal and decadal patterns of soil carbon uptake and emission along an age sequence of burned black spruce stands in interior Alaska, *J. Geophys. Res.*, *108*, D1.

Ogee, J., P. Peylin, M. Cuntz, T. Bariac, Y. Brunet, P. Berbigier, P. Richard, and P. Ciais (2004), Partitioning net ecosystem carbon exchange into net assimilation and respiration with canopy-scale isotopic measurements: An error propagation analysis with (CO2)-C-13 and (COO)-O-18 data, *Global Biogeochem. Cycles*, *18*, GB2019, doi:10.1029/2003GB002166.

Peylin, P., P. Ciais, A. S. Denning, P. P. Tans, J. A. Berry, and J. W. C. White (1999), A 3-dimensional study of delta O-18 in atmospheric CO_2: contribution of different land ecosystems, *Tellus, Ser. B*, *51*, 3, 642-667.

Randerson, J. T., M. V. Thompson, T. J. Conway, I. Y. Fung, and C. B. Field (1997), The contribution of terrestrial sources and sinks to trends in the seasonal cycle of atmospheric carbon dioxide, *Global Biogeochem. Cycles*, *11*, 4, 535-560.

Randerson, J. T., C. B. Field, I. Y. Fung, and P. P. Tans (1999), Increases in early season ecosystem uptake explain recent changes in the seasonal cycle of atmospheric CO_2 at high northern latitudes, *Geophys. Res. Lett.*, *26*, 17, 2765-2768.

Riley, W. J., C. J. Still, M. S. Torn, and J. A. Berry (2002), A mechanistic model of (H_2O)-O-18 and (COO)-O-18 fluxes between ecosystems and the atmosphere: Model description and sensitivity analyses, *Global Biogeochem. Cycles*, *16, 4*, 1095, doi:10.1029/2002GB001878.

Riley, W. J., C. J. Still, B. R. Helliker, M. Ribas-Carbo, and J. A. Berry (2003), O-18 composition of CO_2 and H_2O ecosystem pools and fluxes in a tallgrass prairie: Simulations and comparisons to measurements, *Global Change Biol.*, *9*, 1567-1581.

Seibt, U., L. Wingate, J. A. Berry, and J. Lloyd (2006), Non-steady state effects in diurnal ^{18}O discrimination by *Picea sitchensis* branches in the field, *Plant, Cell Environ.*, *29*, 5, doi:10.1111/j.1365-3040.2005.01474.x.

Slayback, D. A., J. E. Pinzon, S. O. Los, and C. J. Tucker (2003), Northern Hemisphere photosynthetic trends 1982-99, *Global Change Biol.*, *9*, 1, 1-15.

Smith, N. V., S. S. Saatchi, and J. T. Randerson (2004), Trends in high northern latitude soil freeze and thaw cycles from 1988 to 2002, *J. Geophys. Res.*, *109*, D12101, doi:10.1029/2003JD004472.

Stern, L. A., R. Amundson, and W. T. Baisden (2001), Influence of soils on oxygen isotope ratio of atmospheric CO2, *Global Biogeochem. Cycles*, *15*, 3, 753-759.

Stocks, B. J., et al. (1998), Climate change and forest fire potential in Russian and Canadian boreal forests, *Climatic Change*, *38*, 1, 1-13.

Sugimoto, A., N. Yanagisawa, D. Naito, N. Fujita, and T. C. Maximov (2002), Importance of permafrost as a source of water for plants in east Siberian taiga, *Ecological Research*, *17*, 4, 493-503.

Sukhinin, A. I., et al. (2004), AVHRR-based mapping of fires in Russia: New products for fire management and carbon cycle studies, *Remote Sens. Environ.*, *93*, 4, 546-564.

Tanja, S., et al. (2003), Air temperature triggers the recovery of evergreen boreal forest photosynthesis in spring, *Global Change Biol.*, *9*, 10, 1410-1426.

Tans, P. P. (1998), Oxygen isotopic equilibrium between carbon dioxide and water in soils, *Tellus, Ser. B*, *50*, 2, 163-178.

Trolier, M., J. W. C. White, P. P. Tans, K. A. Masarie, and P. A. Gemery (1996), Monitoring the isotopic composition of atmospheric CO_2: Measurements from the NOAA Global Air Sampling Network, *J. Geophys. Res.*, *101*, D20, 25897-25916.

Tucker, C. J., D. A. Slayback, J. E. Pinzon, S. O. Los, R. B. Myneni, and M. G. Taylor (2001), Higher northern latitude normalized difference vegetation index and growing season trends from 1982 to 1999, *International Journal of Biometeorology*, *45*, 4, 184-190.

Walther, G. R., E. Post, P. Convey, A. Menzel, C. Parmesan, T. J. C. Beebee, J. M. Fromentin, O. Hoegh-Guldberg, and F. Bairlein (2002), Ecological responses to recent climate change, *Nature*, *416*, 6879, 389-395.

Wang, C. K., B. Bond-Lamberty, and S. T. Gower (2002), Soil surface CO_2 flux in a boreal black spruce fire chronosequence, *J. Geophys. Res.*, *108*, D3, 8224, doi:10.1029/2001JD000861.

Webb, E. K., G. I. Pearman, and R. Leuning (1980), Correction of flux measurements for density effects due to heat and water-vapor transfer, *Quarterly Journal of the Royal Meteorological Society*, *106*, 447, 85-100.

Welp, L. R., J. T. Randerson, J. C. Finlay, S. P. Davydov, G. M. Zimova, A. I. Davydova, and S. A. Zimov (2005), A high-resolution time series of oxygen isotopes from the Kolyma River: Implications for the seasonal dynamics of discharge and basin-scale water use, *Geophys. Res. Lett.*, *32*, LI4401, doi:10.1029/2005GL022857.

White, M. A., and A. R. Nemani (2003), Canopy duration has little influence on annual carbon storage in the deciduous broad leaf forest, *Global Change Biol.*, *9*, 7, 967-972.

WRCC (2004), Western Regional Climate Center, http://www.wrcc.dri.edu/climsum.html.

Yakir, D., and X. F. Wang (1996), Fluxes of CO_2 and water between terrestrial vegetation and the atmosphere estimated from isotope measurements, *Nature*, *380*, 6574, 515-517.

Yakir, D., and L. Sternberg (2000), The use of stable isotopes to study ecosystem gas exchange, *Oecologia*, *123*, 297-311.

Zha, T., S. Kellomaki, K. Y. Wang, and I. Rouvinen (2004), Carbon sequestration and ecosystem respiration for 4 years in a Scots pine forest, *Global Change Biol.*, *10*, 9, 1492-1503.

Zhou, L. M., C. J. Tucker, R. K. Kaufmann, D. Slayback, N. V. Shabanov, and R. B. Myneni (2001), Variations in northern vegetation activity inferred from satellite data of vegetation index during 1981 to 1999, *J. Geophys. Res.*, *106*, D17, 20069-20083.

Zimov, S. A., S. P. Davidov, G. M. Zimova, A. I. Davidova, F. S. Chapin, M. C. Chapin, and J. F. Reynolds (1999), Contribution of disturbance to increasing seasonal amplitude of atmospheric CO_2, *Science*, *284*, 5422, 1973-1976.

Chapter 4

ECOSYSTEM CARBON FLUX RESPONSE TO SPRING WARMING AND SUMMER DROUGHT DEPENDS ON PLANT FUNCTIONAL TYPE IN BOREAL FOREST ECOSYSTEMS*

*Adapted from Welp, L. R., J. T. Randerson and H. Liu, in preparation for submission to *Global Change Biology*.

4.1 Abstract

We measured net ecosystem exchange (NEE) at a deciduous (aspen and willow) forest and an evergreen conifer (black spruce) forest that were part of a fire chronosequence in interior Alaska. We partitioned NEE into gross primary production (GPP) and ecosystem respiration (R_e) components and then assessed the effects of interannual variability in spring air temperatures and summer drought on these fluxes over a 3 year period. We found that interannual variability in both spring and summer NEE was greatest at the deciduous forest. Increases in spring air temperatures between 2002 and 2004 caused GPP to increase during the early part of the growing season (April, May, and June), with a 74% increase at the deciduous forest and a 16% increase at the evergreen forest. R_e increased in parallel, by 61% and 15% respectively. In contrast, summer drought during 2004 changed August GPP by -12% at the deciduous forest and by -9% at the evergreen forest. Parallel increases in R_e, by 21% and 8% for the two forests, led to a substantial reduction in net carbon uptake during the drought. These results suggest that deciduous forests may contribute disproportionately more to variability in atmospheric CO_2 concentrations within the Northern Hemisphere, and that

the carbon balance of deciduous forests may have a greater sensitivity to future changes in climate.

4.2 Introduction

With the increases in air temperatures that are predicted over the next several centuries [*IPCC*, 2001], there are potentially large feedbacks associated with the biosphere's ability to sequester CO_2 [*Braswell et al.*, 1997]. It is still unclear for many biomes, however, whether these feedbacks are positive or negative. In northern forests, there are multiple competing effects of increasing air temperatures on gross primary productivity (GPP) and ecosystem respiration (R_e). Warmer springs lead to an earlier onset of photosynthesis [*Black et al.*, 2000; *Tanja et al.*, 2003], enhance GPP during spring months [*Goulden et al.*, 1996; *Arain et al.*, 2002; *Angert et al.*, 2005] and often increase annual net carbon uptake (C-uptake) [*Chen et al.*, 1999; *Black et al.*, 2000; *Barr et al.*, 2002; *Chen et al.*, 2006]. However, increased temperatures can also increase microbial soil R_e [*Kirschbaum*, 1995] and increase the depth of soil thaw, exposing more soil organic matter to decomposition [*Goulden et al.*, 1998], causing a net loss of carbon from ecosystems [*Goulden et al.*, 1998; *Lindroth et al.*, 1998; *Valentini et al.*, 2000].

Low moisture conditions during drought (often associated with intervals of anomalously high air temperature) causes both GPP and soil R_e to decline [*Ciais et al.*, 2005; *Kljun et al.*, *in press*]. There is still debate about whether GPP or R_e is most adversely affected and thus the sign of the NEE response at regional and biome scales. An extreme drought in Europe during 2003, for example, caused multiple ecosystems to lose carbon [*Ciais et al.*, 2005]. In contrast, *Goulden et al.* [1996] found that R_e was

more sensitive to reduced soil moisture availability than GPP, and this caused carbon to accumulate at a faster rate during a late-summer drought in a temperate deciduous forest. Similarly, decreases in soil respiration from limited moisture availability causes net ecosystem carbon uptake to increase during the dry season in moist tropical forest ecosystems [*Saleska et al.*, 2003]. The net effect of drought may depend on the severity of moisture limitation. *Reichstein et al.* [2002] hypothesizes that during conditions when only the surface soil layers are affected, heterotrophic R_e will be impacted more than GPP (increasing net C-uptake) and that it is not until severe drought conditions substantially lower the water table that GPP will be affected adversely through plant water stress.

Physiological differences are likely to modulate the response of deciduous and evergreen conifer forests to climate variability. *Monson et al.* [2005], for example, proposed that annual carbon balance of deciduous forests is limited by the fraction of the year that leaves are still expanding and have not reached maximum leaf area. This fraction is reduced in years with early spring leaf-out, thereby increasing GPP. In contrast, the annual carbon balance of evergreen conifers may be regulated more strongly by a reduction in GPP caused by high mid-summer temperature and low soil moisture which typically increases in years with earlier springs [*Monson et al.*, 2005].

Interannual eddy covariance measurements in the boreal zone show that warm springs increase GPP substantially in deciduous aspen forests and to a lesser degree in evergreen black spruce forests [*Black et al.*, 2000; *Arain et al.*, 2002]. During warm summers, in the absence of drought, aspen forest R_e remains largely unchanged [*Arain et al.*, 2002; *Griffis et al.*, 2003; *Kljun et al.*, *in press*], whereas black spruce R_e increases

substantially [*Goulden et al.*, 1998; *Arain et al.*, 2002]. Therefore, warm years appear to increase annual net C-uptake in aspen forests [*Black et al.*, 2000; *Arain et al.*, 2002], and may decrease annual net C-uptake in black spruce forests [*Goulden et al.*, 1998]. *Kljun et al.* [*in press*] is the only interannual boreal study to investigate drought effects simultaneously on both deciduous and evergreen forests but they found differences in rainfall distribution and soil drainage buffered the effect of drought in the evergreen conifer forest.

Here, we report measurements of NEE at a deciduous aspen forest and an evergreen black spruce forest using the eddy covariance technique over three years (2002–2004) in interior Alaska. Our objective was to determine how plant functional type (deciduous versus evergreen) modulates ecosystem carbon flux response to interannual climate variability. These forests were part of a fire chronosequence that has been used in the past to examine the effects of post-fire forest age on microbial community changes [*Treseder et al.*, 2004], variability in burn severity [*Kasischke and Johnstone*, 2005], surface energy fluxes [*Liu et al.*, 2005], and the seasonal cycle of atmospheric CO_2 and $\delta^{18}O$-CO_2 [*Welp et al.*, *in press*]. Spring air temperatures increased progressively during 2002 through 2004. The summer of 2004 was one of the hottest and driest on record for Alaska, contributing to the worst fire season on record [*AFS*, 2006]. Because of the close proximity of the sites to one another, it was possible to directly compare the relative effects of the same climate variability on net C-uptake caused by plant functional type. We found that the deciduous aspen forest was much more sensitive to variability in weather and climate than the evergreen black spruce forest.

4.3 Methods

We measured NEE using the eddy covariance technique at three sites in interior Alaska near Delta Junction (63°54'N, 145°40'W). The oldest forest (*evergreen forest*) was a *Picea mariana* (black spruce) forest that last burned in ~1920. The intermediate-aged *deciduous forest*, less than 20 km away from the evergreen forest, had an overstory comprised primary of *Populous tremuloides* (aspen) and *Salix* spp. (willow) that burned in 1987. The youngest forest (*recent burn*), ~5 km away from the evergreen forest, burned in 1999 and has a sparse canopy cover comprised of grasses and small shrubs. Soils in this area are well-drained with ~ 30 cm of loess covering a moraine gravel layer [*Manies et al.*, 2004; *Neff et al.*, 2005]. Permafrost was not present at our sites even though it is within a region of discontinuous permafrost [*Treseder et al.*, 2004]. Eddy covariance towers were equipped with LI-7500 (Li-Cor, Inc., Lincoln, Nebraska) open path infrared gas analyzers and CSAT3 (Campbell Scientific, Inc., Logan, Utah) sonic anemometers. Instrument heights are summarized in *Liu et al.* [2005].

We filtered NEE measurements using a u* threshold of 0.2 m s^{-1} [*Goulden et al.*, 1997]. Considering low u* conditions and temporary equipment malfunctions, the percent availability of observations during April – September (2002, 2003 and 2004) was 51%, 56%, and 49% at the recent burn; 47%, 60%, and 54% at the deciduous forest; and 56%, 59%, and 50% at the evergreen forest. Gaps in the NEE observations were filled with modeled NEE using measured microclimate variables as drivers of R_e and GPP models.

$$NEE = R_e + GPP \quad (1)$$

A detailed description of the approach used to model R_e and GPP is given in *Welp et al.* [*in press*]. Briefly, daytime and nighttime R_e during periods of missing data were estimated from a temperature dependent R_e model. Temperature dependence (Q_{10}) was solved using growing season (April – September) nighttime NEE measurements and 10 cm soil temperatures from the three years of combined data. Baseline R_e rates were solved for each forest during 15-day windows moving by 5-day increments during the growing season allowing the R_e model to effectively respond to changes in substrate availability and soil moisture.

GPP was modeled using a Michaeles-Menton model with a vapor pressure deficit (VPD) response [*Welp et al.*, *in press*]. Modeled R_e was subtracted from available daytime NEE observations, and the residual CO_2 uptake was used to solve for maximum photosynthetic uptake rate and quantum efficiency during 7-day intervals throughout the growing season. The 7-day time step of the GPP model indirectly responded to variability in light conditions, moisture stress and temperature variations at each forest. The onset of the growing season for each forest was defined as the day when the gap-filled sum of daily NEE became negative (indicating net uptake of CO_2 by the ecosystem on that day) and stayed negative for at least 3 days following.

4.4 NEE measurements and partitioning results

Eddy covariance NEE measurements at each of the three forests are presented for 2002–2004 in Figure 4.1. The mean growing season was shorter in the deciduous forest because of a delay in leaf-out and the amplitude of the diurnal cycle was substantially larger in mid-summer as compared with that measured in the evergreen conifer forest.

Gap-filled NEE measurements (at a 30-minute temporal resolution) were used to construct weekly mean NEE fluxes and are presented along with modeled fluxes of GPP and R_e in Figure 4.2. During June and July, mean daily NEE at the deciduous forest (-2.3 to -3.2 g C m^{-2} day^{-1}) was 2 to 3 times as large as that measured at the conifer forest (-1.0 to -1.2 g C m^{-2} day^{-1}), a difference similar in magnitude to that reported by *Arain et al.* [2002] for the same two forest types in central Canada.

There was a decline in net C-uptake observed at the spruce forest from late-June through early-August that was not seen at the aspen forest (more positive NEE values in Figure 4.2a). This pattern has been previously reported for a black spruce forest in Canada and was attributed to seasonal differences in the relative rates of R_e and GPP [*Goulden et al.*, 1998; *Arain et al.*, 2002; *Griffis et al.*, 2003]. During this mid-summer period, R_e was increasing while GPP remained fairly constant, resulting in a decrease in the carbon uptake by the evergreen forest. By August, R_e rates started to decrease before photosynthetic rates were reduced, therefore, the carbon sink increased again briefly (more negative NEE in Figure 4.2a) before fall senescence. This is confirmed in our analysis; maximum R_e rates at the spruce site in Figure 4.2c corresponded to the July minimum in net C-uptake. GPP fluxes peaked slightly later, in August (Figure 4.2c). Differences in seasonal chlorophyll content of aspen and spruce measured by *Middleton et al*. [1997] may explain differences in seasonal GPP and NEE. They found an early (late-May to early-June) and late (mid-September) peak in chlorophyll content whereas the aspen forest chlorophyll peaked once in late-July to early-August [*Middleton et al.*, 1997; *Griffis et al.*, 2003].

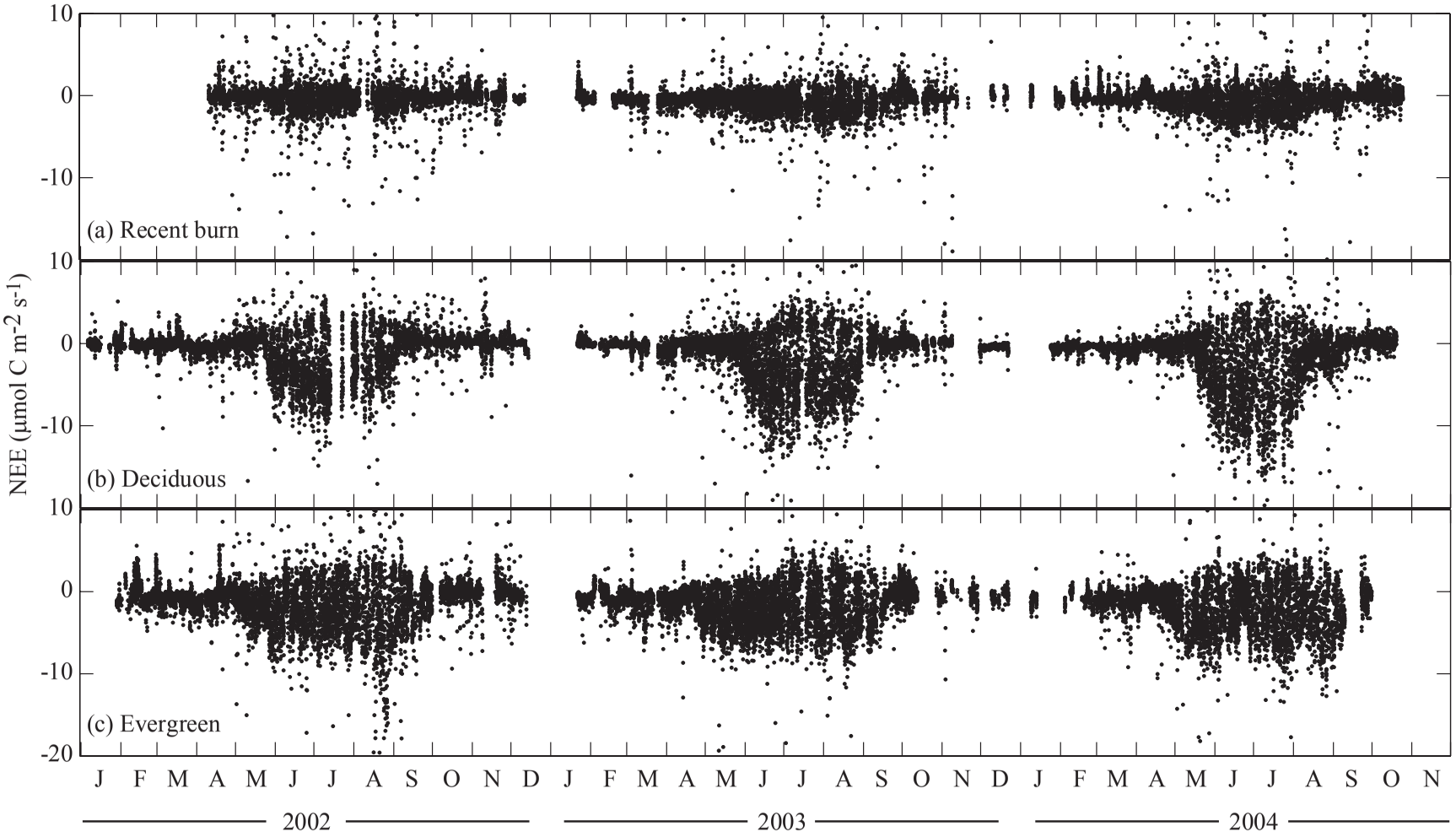

Figure 4.1: NEE measurements from 2002 - 2004. The recent burn (a) occurred in 1999, the deciduous forest (b) burned in 1987 and the evergreen (c) burned in approximately 1920. Positive values represent a release of CO_2 from the ecosystem into the atmosphere and negative values denote uptake of CO_2 by the ecosystem.

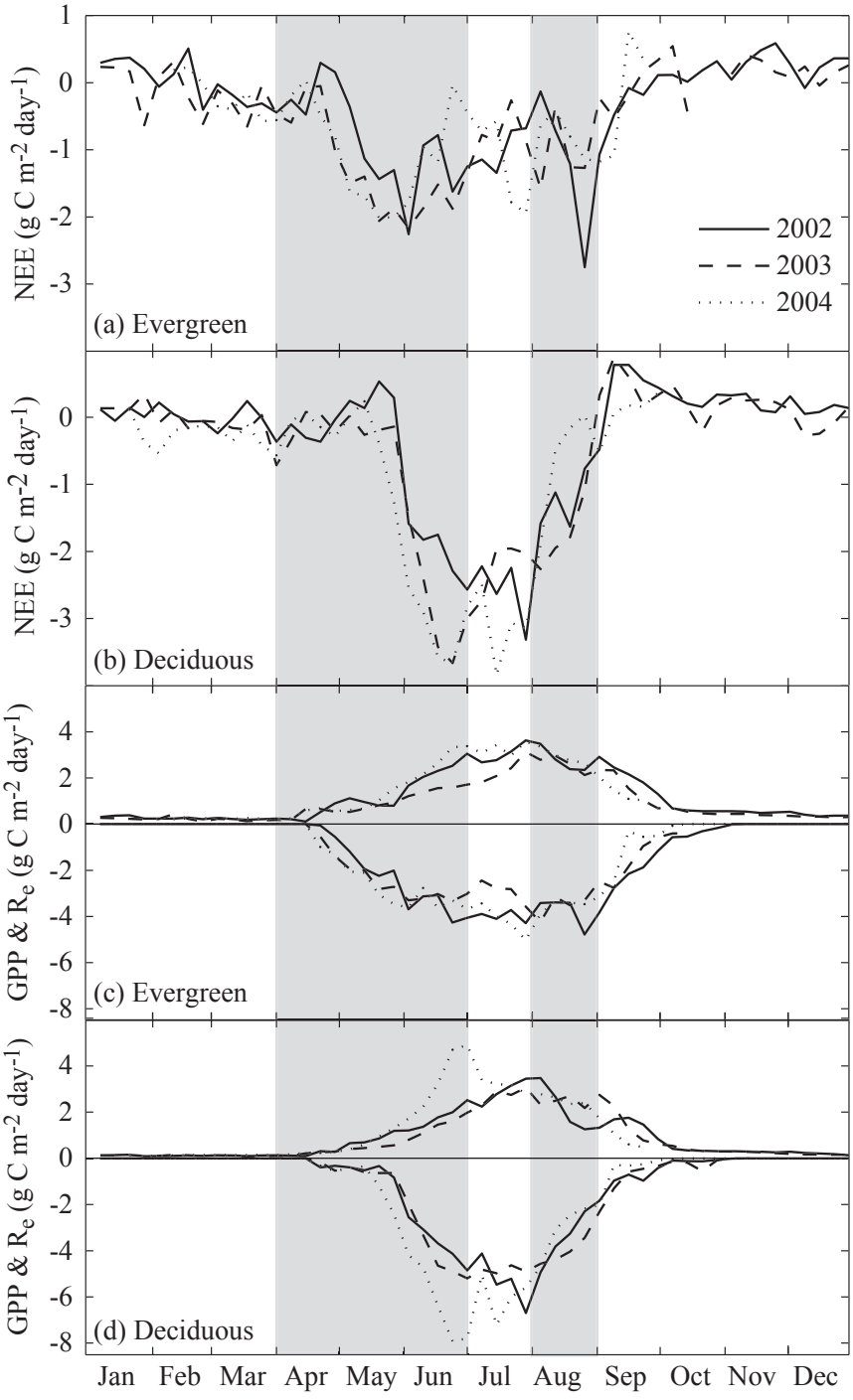

Figure 4.2 Weekly mean NEE, GPP and R_e. Positive values in panels (c) and (d) are R_e fluxes to the atmosphere and negative values are GPP uptake by the forests. Spring temperatures increased from 2002 through 2004 and a severe drought occurred during August of 2004 (shaded intervals).

4.5 Early season warming

This region experienced considerable interannual variability in climate during 2002–2004 (Figure 4.3). Air temperatures increased progressively during the springs of 2002, 2003, and 2004 (Figure 4.3a and Table 4.1). Spring soil moisture in 2002 was intermediate, 2003 was dry, and 2004 was wet due to differences in winter snow accumulation and spring rain (Figures 4.3 and Table 4.1).

At both forests, spring photosynthetic uptake responded positively to air temperatures and, to a lesser extent, to soil moisture (Table 4.1). The increase in photosynthetic uptake (more negative GPP values) was substantially greater at the deciduous forest (74% between 2002 and 2004) than the evergreen forest (only 16% between 2002 and 2004). In contrast, the onset of the growing season advanced by only 9 days at the deciduous forest as compared with 14 days at the evergreen. (The start of the growing season occurred on 26 May 2002, 23 May 2003, and 17 May 2004 at the deciduous forest and 1 May 2002, 22 April 2003, and 17 April 2004 at the evergreen forest.) This can be explained by the differences in plant functional type response of GPP to temperature increases. Evergreen forests show a slow GPP response that starts earlier than deciduous, and the deciduous forests have a delayed, but much sharper increase in photosynthetic uptake in response to warmer temperatures [*van Dijk et al.*, 2005]. The relative delay in leaf-out at the deciduous forest during early springs is presumably a strategy to avoid damage by spring frost events. A similar study by *Arain et al.* [2002] also found that warm springs enhance net C-uptake, and there was greater variability in GPP at an aspen forest in Canada compared to a nearby black spruce forest.

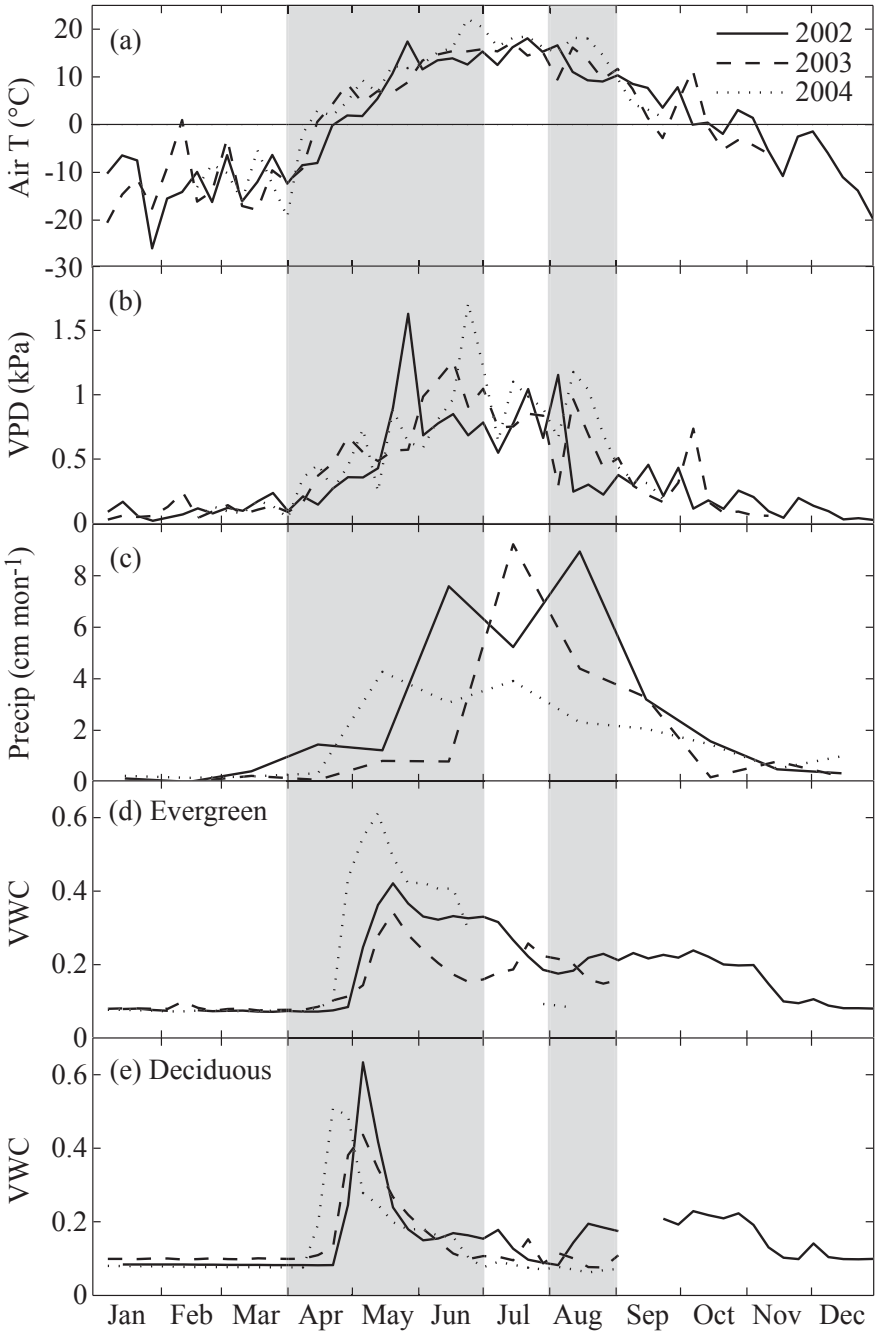

Figure 4.3 Weekly mean climate conditions. (a) Air temperature measured above the canopy, (b) vapor pressure deficit calculated from temperature and relative humidity measurements above the canopy, (c) monthly mean precipitation, (d) volumetric water content (VWC) measured at 4 cm at the evergreen site and (e) VWC measured at 2 cm at the deciduous site.

Table 4.1 Seasonal summary of climate and carbon fluxes for each year of the study.

Year	Air T[1] (°C)	VPD[1,2] (kPa)	Soil T[3] (°C)	Soil moisture[4] (VWC*1000)	PPFD (mmol m^{-2} day^{-1})	NEE[5] (g C m^{-2})		GPP[6] (g C m^{-2})		R_e[6] (g C m^{-2})	
						Deciduous	Evergreen	Deciduous	Evergreen	Deciduous	Evergreen
					April, May, and June						
2002	6.4	1.0	2.3	5.2	16.0	-65	-79	-143	-179	89	116
2003	7.7	1.0	2.2	4.6	15.7	-104	-121	-156	-188	66	85
2004	9.9	1.1	4.0	6.3	15.1	-122	-93	-249	-207	143	133
					August						
2002	11.1	0.8	9.1	4.6	9.1	-34	-39	-98	-116	62	84
2003	12.4	1.0	8.7	3.5	11.4	-45	-28	-117	-105	76	79
2004	15.5	1.3	10.9	1.9	11.8	-15	-24	-86	-105	75	86
					Growing Season (April – September)						
2002	8.9	0.9	5.4	5.0	13.3	-162	-152	-432	-482	285	356
2003	9.0	0.9	4.9	4.2	13.5	-200	-172	-446	-432	267	282
2004	10.8	1.0	6.5	4.9	13.1	-227	-156	-529	-474	336	353

1. Measured above the canopy and averaged across forests.
2. Mid-day (noon – 4 pm) measurements only.
3. Measured at 10 cm depth and averaged across forests.
4. Mean volumetric water content (VWC) measured at 2 cm depth at the deciduous site and 4 cm depth at the evergreen site.
5. Integrated gap filled eddy covariance NEE observations over the time period listed.
6. Integrated modeled fluxes over the time period listed.

Soil moisture appeared to have a strong control on spring R_e and caused a decrease in R_e at both sites during the dry spring of 2003 (Table 4.1). (Although the R_e model did not explicitly include moisture effects, low moisture effects were captured because R_o was solved for using 15-day moving windows.) Warm and wet conditions during spring 2004 increased R_e at both sites but had a larger effect on R_e at the deciduous site (61% compared to 15% at the evergreen).

Spring NEE at the deciduous forest followed trends in GPP; net C-uptake was enhanced with increased air temperature and earlier leaf-out. Spring GPP was less variable at the evergreen forest, and spring NEE variability reflected interannual differences in R_e. Increased net C-uptake at the evergreen forest in 2003 was the result of decreased R_e in response to relatively low soil moisture conditions.

4.6 Late-summer drought

Early springs were followed by warmer and drier summer conditions during this study. Mean August air temperatures and vapor pressure deficit (VPD) increased each year of our study, and soil moisture levels decreased substantially (Figure 4.3 and Table 4.1). Total April–September precipitation in our study region was 20% greater than the record mean (1937–2005) during 2002, 20% less during 2003 and 30% less during 2004. Although soil moisture was consistently higher at the evergreen forest than the deciduous forest, both saw a 50% reduction in soil moisture in August of 2004 compared to 2002. As in the spring, interannual differences in GPP were larger at the deciduous forest than at the evergreen forest (Table 4.1). Photosynthetic uptake increased (more negative GPP values) in 2003 with warmer air temperatures (19% over 2002), but the severe drought in

2004 decreased GPP to levels below 2002 (-12%) in spite of the warmer temperatures. GPP at the evergreen forest was almost unchanged during the 2004 drought (-9% change in 2003 and 2004 compared to 2002).

R_e was not depressed at either the deciduous or evergreen forest during the 2004 summer drought (Table 4.1). R_e increased with warmer temperatures at the deciduous site (23% and 21% in 2003 and 2004 respectively); however, R_e varied much less at the evergreen site (-6% and 2% respectively). The effects of increased temperature on microbial and plant respiration appeared to offset any moisture limitations and reduced carbon substrates that might have decreased microbial and plant respiration respectively.

At both sites, net C-uptake was reduced during August of 2004 compared to previous (cooler and wetter) years, resulting in a relative source of CO_2 to the atmosphere. *Ciais et al.* [2005] reported the same effect across Europe for an entire year. Late-summer net C-uptake during the 2004 drought was reduced more at the deciduous forest (56% compared to 2002 NEE) than the evergreen forest (only 38%). *Goulden et al.* [1997] predicted from eddy covariance measurements in Canada that high evaporative demand would have little effect on the GPP of black spruce ecosystems. Although we observed more sensitivity of mid-day NEE (during favorable light and temperature conditions) to VPD than was found by *Goulden et al.* [1997], seasonal GPP totals were affected. The observed drought response at the deciduous forest supported the predictions of *Hogg et al.* [2000] and *Dang et al.* [1997] that the photosynthetic uptake of aspen forests decreases as high VPD lowers aspen stomatal conductance. Our results showed greater sensitivity of GPP to high VPD conditions at the deciduous forest

compared to the evergreen which is consistent with *Ewers et al*. [2005] leaf and canopy-level gas exchange measurements which showed that aspen regulate stomatal conductance to maintain a minimum leaf water potential to prevent xylem cavitation whereas black spruce do not.

4.7 Net growing season

Now we consider the combined effects of the spring warming and summer drought on the total growing season (April–September), net C-uptake increased as temperatures warmed each year of our study at the deciduous forest (23% and 40% in 2003 and 2004), but was relatively conservative at the spruce forest (13% and 3% respectively) (Table 4.1). The increased spring photosynthetic uptake (more negative GPP) at the deciduous forest dominated the interannual variability in growing season NEE, whereas, it was the reduced spring R_e in 2003 that appeared to dominate at the evergreen forest. This was consistent with *Bond-Lamberty et al.* [2004], which showed that interannual variability in net primary productivity (NPP) is the greatest at the youngest deciduous forests of a black spruce chronosequence in Canada.

4.8 Conclusions

Simultaneous eddy covariance NEE measurements of a deciduous and evergreen forest in years experiencing very different seasonal weather, showed that warm springs and summer drought resulted in much greater variability in NEE at deciduous forests than evergreen forests. This is consistent with the findings of *Arain et al.* [2002] and *Kljun et al.* [*Kljun et al.*, *in press*]. This result implies that (1) the current variability in

atmospheric CO_2 in the Northern Hemisphere may have a much stronger contribution from the deciduous plant functional type than the evergreen and (2) including results from *Zimov et al.* [1999] and *Welp et al.* [*in press*] which show that deciduous plant functional types increase the seasonal amplitude of atmospheric CO_2, a shift towards more deciduous forests will impact the magnitude of the interannual variability as well as the mean amplitude and phase of the seasonal cycle.

Currently, it appears that increased net C-uptake during warmer springs is dominating the interannual variability at the deciduous sites, resulting in increased sinks of CO_2 as the spring warming trend continues. However, both forests showed a reduction in net C-uptake during the August drought. This indicates that a severe warming and drying trend could turn forests comprising both plant functional types into CO_2 sources in the future.

4.9 Acknowledgements

This work was supported by grants from NSF's Office of Polar Programs (NSF OPP-0097439), NOAA's Office of Global Programs (NA03OAR4310059), the Powell Foundation, and the Davidow discovery fund at Caltech. We thank J. Lindfors for help developing eddy covariance systems, F.S. Chapin for logistical support through the University of Alaska, Fairbanks, and J. Garron for data collection. LRW received support from the NCER STAR EPA fellowship program.

4.10 References

AFS (2006), Alaska Fire Service database, http://agdc.usgs.gov/data/blm/fire/.

Angert, A., S. Biraud, C. Bonfils, C. C. Henning, W. Buermann, J. Pinzon, C. J. Tucker, and I. Fung (2005), Drier summers cancel out the CO_2 uptake enhancement induced by warmer springs, *Proc. Natl. Acad. Sci. U. S. A.*, *102*, 31, 10823-10827.

Arain, M. A., T. A. Black, A. G. Barr, P. G. Jarvis, J. M. Massheder, D. L. Verseghy, and Z. Nesic (2002), Effects of seasonal and interannual climate variability on net ecosystem productivity of boreal deciduous and conifer forests, *Can. J. For. Res.*, *32*, 5, 878-891.

Barr, A. G., T. J. Griffis, T. A. Black, X. Lee, R. M. Staebler, J. D. Fuentes, Z. Chen, and K. Morgenstern (2002), Comparing the carbon budgets of boreal and temperate deciduous forest stands, *Can. J. For. Res.*, *32*, 5, 813-822.

Black, T. A., W. J. Chen, A. G. Barr, M. A. Arain, Z. Chen, Z. Nesic, E. H. Hogg, H. H. Neumann, and P. C. Yang (2000), Increased carbon sequestration by a boreal deciduous forest in years with a warm spring, *Geophys. Res. Lett.*, *27*, 9, 1271-1274.

Bond-Lamberty, B., C. K. Wang, and S. T. Gower (2004), Net primary production and net ecosystem production of a boreal black spruce wildfire chronosequence, *Global Change Biol.*, *10*, 4, 473-487.

Braswell, B. H., D. S. Schimel, E. Linder, and B. Moore (1997), The response of global terrestrial ecosystems to interannual temperature variability, *Science*, *278*, 5339, 870-872.

Chen, J. M., B. Chen, K. Higushi, J. Liu, D. Chan, D. Worthy, P. Tans, and A. Black (2006), Boreal ecosystems sequestered more carbon in warmer years, *Geophys. Res. Lett.*, *33*, L10803, doi:10.1029/2006GL025919.

Chen, W. J., et al. (1999), Effects of climatic variability on the annual carbon sequestration by a boreal aspen forest, *Global Change Biol.*, *5*, 1, 41-53.

Ciais, P., et al. (2005), Europe-wide reduction in primary productivity caused by the heat and drought in 2003, *Nature*, *437*, 7058, 529-533.

Dang, Q. L., H. A. Margolis, M. R. Coyea, M. Sy, and G. J. Collatz (1997), Regulation of branch-level gas exchange of boreal trees: roles of shoot water potential and vapor pressure difference, *Tree Physiol.*, *17*, 8-9, 521-535.

Ewers, B. E., S. T. Gower, B. Bond-Lamberty, and C. K. Wang (2005), Effects of stand age and tree species on canopy transpiration and average stomatal conductance of boreal forests, *Plant Cell Environ.*, *28*, 5, 660-678.

Goulden, M. L., J. W. Munger, S. M. Fan, B. C. Daube, and S. C. Wofsy (1996), Exchange of carbon dioxide by a deciduous forest: Response to interannual climate variability, *Science*, *271*, 5255, 1576-1578.

Goulden, M. L., B. C. Daube, S. M. Fan, D. J. Sutton, A. Bazzaz, J. W. Munger, and S. C. Wofsy (1997), Physiological responses of a black spruce forest to weather, *J. Geophys. Res.*, *102*, D24, 28987-28996.

Goulden, M. L., et al. (1998), Sensitivity of boreal forest carbon balance to soil thaw, *Science*, *279*, 5348, 214-217.

Griffis, T. J., T. A. Black, K. Morgenstern, A. G. Barr, Z. Nesic, G. B. Drewitt, D. Gaumont-Guay, and J. H. McCaughey (2003), Ecophysiological controls on the carbon balances of three southern boreal forests, *Agric. For. Meteorol.*, *117*, 1-2, 53-71.

Hogg, E. H., B. Saugier, J. Y. Pontailler, T. A. Black, W. Chen, P. A. Hurdle, and A. Wu (2000), Responses of trembling aspen and hazelnut to vapor pressure deficit in a boreal deciduous forest, *Tree Physiol.*, *20*, 11, 725-734.

IPCC (2001), *Intergovernmental Panel on Climate Change, Climate change 2001*, Cambridge Univ. Press, New York.

Kasischke, E. S., and J. F. Johnstone (2005), Variation in postfire organic layer thickness in a black spruce forest complex in interior Alaska and its effects on soil temperature and moisture, *Can. J. For. Res.*, *35*, 9, 2164-2177.

Kirschbaum, M. U. F. (1995), The temperature-dependence of soil organic-matter decomposition, and the effect of global warming on soil organic-C storage, *Soil Biology & Biochemistry*, *27*, 6, 753-760.

Kljun, N., T. A. Black, T. J. Griffis, A. G. Barr, D. Gaumont-Guay, K. Morgenstern, J. H. McCaughey, and Z. Nesic (*in press*), Response of net ecosystem productivity of three boreal forest stands to drought, *Ecosystems*.

Lindroth, A., A. Grelle, and A. S. Moren (1998), Long-term measurements of boreal forest carbon balance reveal large temperature sensitivity, *Global Change Biol.*, *4*, 4, 443-450.

Liu, H. P., J. T. Randerson, J. Lindfors, and F. S. Chapin (2005), Changes in the surface energy budget after fire in boreal ecosystems of interior Alaska: An annual perspective, *J. Geophys. Res.*, *110*, D13, doi:10.1029/2004JD005158.

Manies, K. L., J. W. Harden, S. R. Silva, P. H. Briggs, and B. M. Schmid (2004), Soil data from *Picea mariana* stands near Delta Junction, AK of different ages and soil drainage type, *U.S. Geological Survey Open File Report 2004-1271*, 19 pp.

Middleton, E. M., J. H. Sullivan, B. D. Bovard, A. J. Deluca, S. S. Chan, and T. A. Cannon (1997), Seasonal variability in foliar characteristics and physiology for boreal forest species at the five Saskatchewan tower sites during the 1994 Boreal Ecosystem-Atmosphere Study, *J. Geophys. Res.*, *102*, D24, 28831-28844.

Monson, R. K., et al. (2005), Climatic influences on net ecosystem CO_2 exchange during the transition from wintertime carbon source to springtime carbon sink in a high-elevation, subalpine forest, *Oecologia*, *146*, 1, 130-147.

Neff, J. C., J. W. Harden, and G. Gleixner (2005), Fire effects on soil organic matter content, composition, and nutrients in boreal interior Alaska, *Can. J. For. Res.*, *35*, 9, 2178-2187.

Reichstein, M., et al. (2002), Severe drought effects on ecosystem CO_2 and H_2O fluxes at three Mediterranean evergreen sites: Revision of current hypotheses? *Global Change Biol.*, *8*, 10, 999-1017.

Saleska, S. R., et al. (2003), Carbon in Amazon forests: Unexpected seasonal fluxes and disturbance-induced losses, *Science*, *302*, 5650, 1554-1557.

Tanja, S., et al. (2003), Air temperature triggers the recovery of evergreen boreal forest photosynthesis in spring, *Global Change Biol.*, *9*, 10, 1410-1426.

Treseder, K. K., M. C. Mack, and A. Cross (2004), Relationships among fires, fungi, and soil dynamics in Alaskan boreal forests, *Ecological Applications*, *14*, 6, 1826-1838.

Valentini, R., et al. (2000), Respiration as the main determinant of carbon balance in European forests, *Nature*, *404*, 6780, 861-865.

van Dijk, A., A. J. Dolman, and E. D. Schulze (2005), Radiation, temperature, and leaf area explain ecosystem carbon fluxes in boreal and temperate European forests, *Global Biogeochem. Cycles*, *19*, GB2029, doi:2010.1029/2004GB002417.

Welp, L. R., J. T. Randerson, and H. P. Liu (*in press*), The influence of stand age on seasonal exchange of CO_2 and $\delta^{18}O$-CO_2 from a boreal forest fire chronosequence, *J. Geophys. Res.*

Zimov, S. A., S. P. Davidov, G. M. Zimova, A. I. Davidova, F. S. Chapin, M. C. Chapin, and J. F. Reynolds (1999), Contribution of disturbance to increasing seasonal amplitude of atmospheric CO_2, *Science*, *284*, 5422, 1973-1976.

Chapter 5

PREDICTIONS FOR FUTURE CHANGES IN $\delta^{18}O$ OF ATMOSPHERIC CO_2

5.1 New hypothesis

If temperatures continue to increase in the Arctic, we can expect substantial changes in the ways carbon and water cycles interact. Already there are observations of changes to the seasonal cycle of atmospheric CO_2 concentrations [*Keeling et al.*, 1996] and Arctic river discharge [*Peterson et al.*, 2002]. Chapter 3 discussed the role of plant functional type in determining the phase and amplitude of CO_2 and $\delta^{18}O$-CO_2. The results of this work lead to two predictions for the seasonal cycle of $\delta^{18}O$-CO_2 as Arctic and global mean temperatures rise. (1) Based on temperature controls of the $\delta^{18}O$ of precipitation, the seasonal cycle of $\delta^{18}O$-CO_2 should decrease in amplitude and shift phase substantially with increased air temperatures. (2) It may be possible to use these changes in the $\delta^{18}O$-CO_2 seasonal cycle to diagnose wide-spread changes in air temperature across boreal ecosystems.

The seasonal cycle of $\delta^{18}O$-CO_2 was explained in Chapter 3 as being controlled not only by gross biospheric CO_2 fluxes but also the $\delta^{18}O$ of soil and plant source waters, that are the starting point for the isotopic forcing (isoforcing) by respiration and photosynthesis. Soil and stem water $\delta^{18}O$ are controlled by the annual mean and seasonal cycle of the $\delta^{18}O$ of precipitation, and stem water is further modified by the fraction of summer to winter precipitation taken up by the plants.

5.2 Warmer air temperatures are correlated with increased $\delta^{18}O$ of precipitation

From early measurements of the $\delta^{18}O$ of precipitation globally, *Dansgaard* [1964] realized that there was a positive relationship between the mean annual $\delta^{18}O$ of precipitation and mean annual air temperatures, 0.695‰/°C. *Yurtsever and Gat* [1981] calculated the global mean sensitivity to monthly temperature changes, 0.338 ± 0.028‰/°C. The seasonal gradient in $\delta^{18}O$ changes with temperature is less than the mean annual spatial gradient because of seasonal changes in the temperatures of the source water regions [*Aristarain et al.*, 1986; *Hoffmann et al.*, 2000]. For comparison, the seasonal gradient observed at Delta Junction, Alaska was 0.25‰/°C. The $\delta^{18}O$ - temperature relationship has been widely used to construct paleotemperatures from preserved proxies of the $\delta^{18}O$ of precipitation including ice cores [*Jouzel et al.*, 1987] and tree rings [*Libby and Pandolfi*, 1974; *Epstein and Yapp*, 1976].

Isotopes have recently been introduced into general circulation models (GCM's) allowing for future predictions of changes in the $\delta^{18}O$ of precipitation as CO_2 concentrations and air temperatures increase. (A summary of these GCM's is presented in *Hoffmann et al.* [2000].) Model experiments comparing modern conditions to those during cooler times (Last Glacial Maximum, 21 kyr BP) and warmer times (Holocene optimum, 6 kyr BP) both showed gradients in northern regions of 0.5 – 1.0‰/°C [*Hoffmann et al.*, 2000]. A 2 x CO_2 model run also showed strong warming at high latitudes and increasing $\delta^{18}O$ of precipitation [*Hoffmann et al.*, 2000]. The Arctic Climate Impact Assessment predicts temperature changes over the Arctic region of 5 –

7°C by the end of the 21st century [*ACIA*, 2004]. This warming trend could lead to changes in precipitation $\delta^{18}O$ of 2.5 – 7‰ if GCM predictions are correct.

5.3 Sensitivity of the $\delta^{18}O$-CO_2 seasonal cycle to the mean $\delta^{18}O$ of precipitation

A sensitivity test of the model used in Chapter 3 showed that increasing the $\delta^{18}O$ of precipitation (and plant source water) by 1 – 3‰, while preserving the seasonality, made a large difference in the seasonal cycle of $\delta^{18}O$-CO_2 (Figure 5.1). For comparison, Figure 5.2 shows the seasonality of GPP and R_e isoforcing on the atmosphere (as shown by the model used in Chapter 3). The large shift in the $\delta^{18}O$-CO_2 seasonal cycle with changes in $\delta^{18}O$ precipitation is because the $\delta^{18}O$ of CO_2 exiting the leaf, after equilibrating with leaf water, is very close to the background atmospheric $\delta^{18}O$-CO_2 (Figure 5.3). If the $\delta^{18}O$ of plant source water (in the model case this is the same as precipitation) varies by as little as a few ‰, it can change the sign of the effect of the photosynthetic (GPP) isoflux through Δ_A which is proportional to $\delta_c^{CO_2} - \delta_{a,i}^{CO_2}$ (leaf – atmosphere) as shown in Equations 3.8 and 3.9. In most areas of the world the effect of GPP isoforcing is strongly positive, but at high latitudes, the similarity of atmospheric $\delta^{18}O$-CO_2 and that of the GPP isoforcing reduces the effect of GPP isoforcing on the seasonal cycle of $\delta^{18}O$-CO_2 in the atmosphere. Currently, the seasonal cycle of $\delta^{18}O$-CO_2 is controlled primarily by respiration (R_e) isoforcing [*Peylin et al.*, 1999].

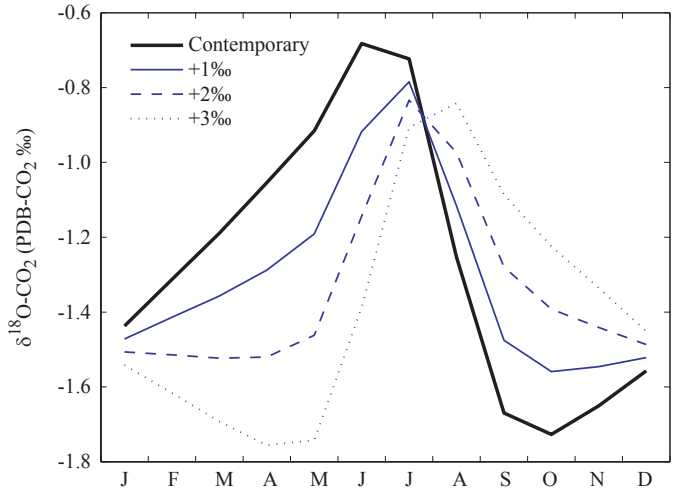

Figure 5.1 The modeled seasonal cycle of $\delta^{18}O\text{-}CO_2$ at the 15-year forest in Chapter 3 (contemporary, solid black) and the sensitivity to a +1, +2, and +3‰ change in precipitation or plant source water (solid, dashed, and dotted blue). The contemporary seasonal cycle most closely resembles that of the R_e isoforcing (Figure 5.2b), however, as precipitation $\delta^{18}O$ increases, the seasonal cycle transitions to reflect stronger GPP isoforcing (Figure 5.2a).

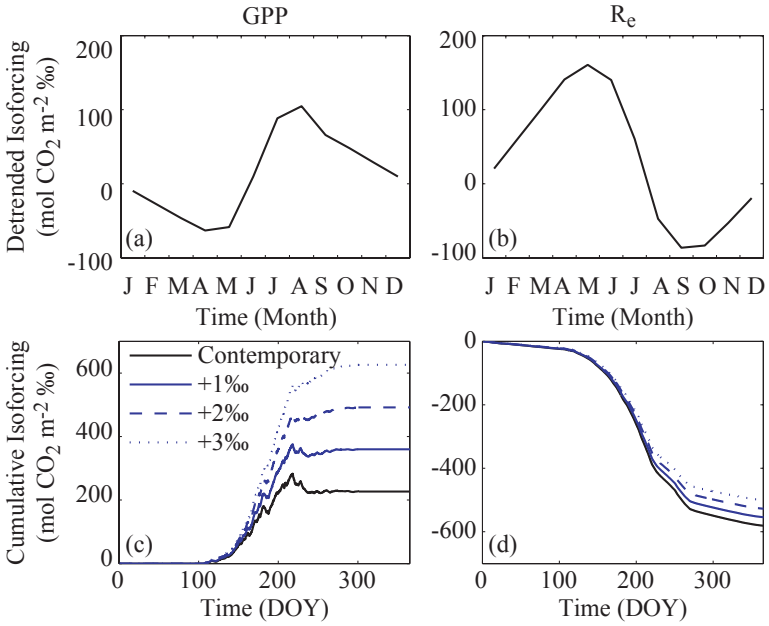

Figure 5.2 The effects of (a) GPP and (b) R_e isoforcing on the seasonal cycle of monthly mean $\delta^{18}O\text{-}CO_2$ as predicted by the model in Chapter 3. The contemporary atmosphere resembles the R_e seasonal isoforcing. Also, the cumulative annual (c) GPP and (d) R_e isoforcing for a +1, +2, and +3‰ change in $\delta^{18}O$ of precipitation. The increase in GPP isoforcing was much larger than the decrease in R_e isoforcing.

As the $\delta^{18}O$ of precipitation increases, the relative effect of the GPP isoforcing increases, and the seasonal cycle first decreases in amplitude because of the competing effects of GPP and R_e isoforcing (+1‰ case in Figure 5.1). As the $\delta^{18}O$ of precipitation increases further, the seasonal cycle of $\delta^{18}O$-CO_2 resembles that of GPP isoforcing (+3‰ case in Figure 5.1). A new modeling experiment is planned in which I will couple a more comprehensive isotopic ecosystem model, ISOLSM [*Riley et al.*, 2002] with atmospheric transport from the TransCom3 [*Gurney et al.*, 2002] pulse tracer experiment to investigate temperature effects on the seasonal cycle of $\delta^{18}O$-CO_2 further. A key feature of the coupled model is that it will allow for feedbacks on Δ_A from changes in $\delta_a^{CO_2}$ caused by warmer temperatures and more enriched source water.

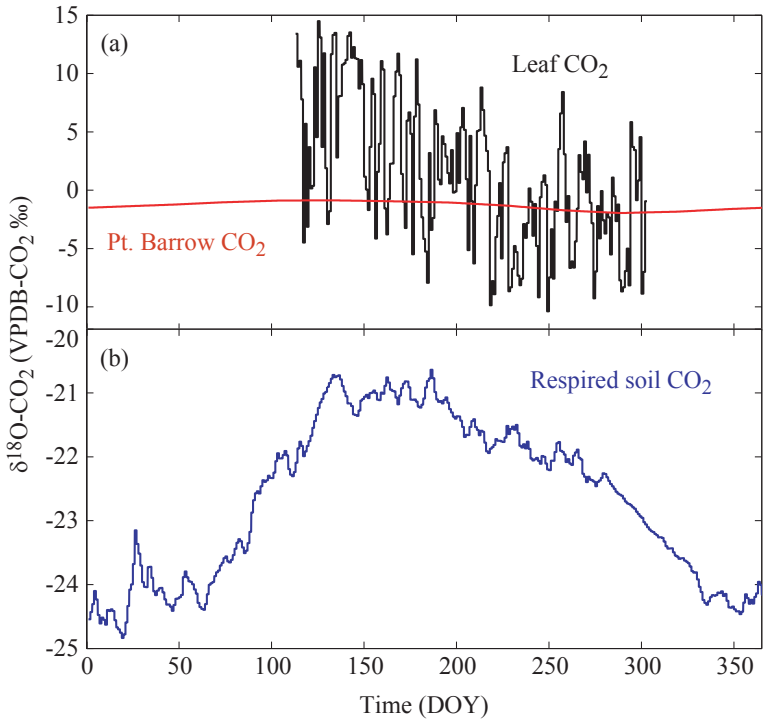

Figure 5.3 (a) δ^{18}O-CO_2 measured in the atmosphere at Pt. Barrow, Alaska (NOAA/CMDL) compared to modeled δ^{18}O of CO_2 diffusing out of leaves (proportional to GPP isoforcing) and (b) δ^{18}O of CO_2 diffusing out of the soil at the 15-year forest modeled in Chapter 3.

5.4 Advantages of δ^{18}O-CO_2

The temperature-induced changes in the δ^{18}O of precipitation could make the seasonal cycle of high-latitude δ^{18}O-CO_2 a useful Arctic thermometer. One might suggest that instrumental temperature records and the Global Network of Isotopes in Precipitation (GNIP) are more direct ways to measure temperature and δ^{18}O changes at high latitudes. However, each network is limited in spatial coverage and remote regions of the north are considerably under sampled. The high frequency of temporal and spatial variability makes accurate high-latitude means difficult to construct.

There have been some recent measurements of the $\delta^{18}O$ of woody plant biomass, reflective of the $\delta^{18}O$ of plant source water and local precipitation, that show conflicting trends over the last century. We know that temperatures have increased over this period [*Chapman and Walsh*, 1993; *Hansen et al.*, 1999] and expect that the $\delta^{18}O$ of precipitation has increased as well. *Welker et al.* [2005] showed increasing $\delta^{18}O$ of an Arctic shrub (*Cassiope tetragona*) on Ellesmere Island, Canada since the 1930's, on the order of 10‰, correlated with changes in the phase of the North Atlantic Oscillation which controls air temperature and moisture source regions. Contrary to that study, *Saurer et al.* [2002] showed a spatial pattern of changes in $\delta^{18}O$ of Eurasian Arctic trees (*Larix*, *Picea*, and *Pinus*) between the periods 1861–1890 and 1961–1990. Most changes over this period were negative (decreasing $\delta^{18}O$ with current warmer temperatures on the order of -0.2 to -0.4‰), although, there were a few regions of 0.2‰ increase in $\delta^{18}O$ of wood. They explained these results (the opposite of the temperature controlled trends) by an increase in the relative amount of winter precipitation over this time period.

Some of the difference between these two proxy records could be due to spatial variability in precipitation trends or the different time intervals studied. Another potential explanation could be differences in seasonal plant source water use. Measurements of seasonal stem water of *Larix* trees and *Betula* shrubs in the same forest near Cherskii, Siberia showed that they each utilized different water sources over the course of the growing season (Figure 5.4). *Betula* and *Larix* stem $\delta^{18}O$ were similar in the spring; however, as the growing season progressed, *Betula* used a water source that was enriched in $\delta^{18}O$, whereas the *Larix* source water was much more negative.

Sugimoto et al. [2002] also showed that during dry summers, particularly the late-summer months, *Larix* are capable of drawing from very negative $\delta^{18}O$ waters, presumably at the freeze/thaw soil active layer boundary (or permafrost melt). These studies show the potential for very large changes in the $\delta^{18}O$ of plant source water and complications in comparing $\delta^{18}O$ biomass proxies of precipitation.

The seasonal cycle of $\delta^{18}O$-CO_2 integrates signatures of soil and plant water across boreal and Arctic terrestrial ecosystems. For this reason, monitoring changes in the $\delta^{18}O$ of precipitation and plant water use as temperatures increase may be effectively done by closely observing the seasonal cycle of $\delta^{18}O$-CO_2.

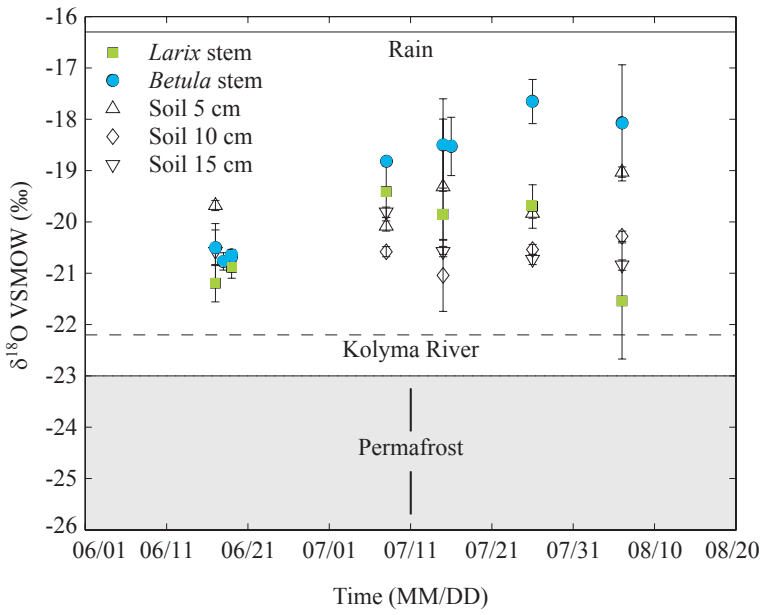

Figure 5.4 Time series of stem waters from Siberia during the 2003 growing season. *Betula* and *Larix* stem water were similar in June, but diverged as the growing season progressed. The shallower rooted *Betula* stem water $\delta^{18}O$ approached the mean summer rain water $\delta^{18}O$ towards the end of the growing season, and deeper rooted *Larix* stem water became very negative, indicating an increased contribution of snowmelt or permafrost melt.

5.5 References

ACIA (2004), *Impacts of a Warming Arctic: Arctic Climate Impact Assessment*, Cambridge University Press, http://www.acia.uaf.edu.

Aristarain, A. J., J. Jouzel, and M. Pourchet (1986), Past Antarctic Peninsula climate (1850 - 1980) from an ice core isotope record, *Climate Change*, *8*, 69-89.

Chapman, W. L., and J. E. Walsh (1993), Recent variations of sea ice and air-temperature in high-latitudes, *Bulletin of the American Meteorological Society*, *74*, 1, 33-47.

Dansgaard, W. (1964), Stable isotopes in precipitation, *Tellus*, *16*, 4, 436-468.

Epstein, S., and C. J. Yapp (1976), Climatic implications of D-H ratio of hydrogen in C-H groups in tree cellulose, *Earth and Planetary Science Letters*, *30*, 2, 252-261.

Gurney, K. R., et al. (2002), Towards robust regional estimates of CO_2 sources and sinks using atmospheric transport models, *Nature*, *415*, 6872, 626-630.

Hansen, J., R. Ruedy, J. Glascoe, and M. Sato (1999), GISS analysis of surface temperature change, *J. Geophys. Res.*, 104, D24, 30,997-31,002.

Hoffmann, G., J. Jouzel, and V. Masson (2000), Stable water isotopes in atmospheric general circulation models, *Hydrol. Process.*, *14*, 8, 1385-1406.

Jouzel, J., C. Lorius, J. R. Petit, C. Genthon, N. I. Barkov, V. M. Kotlyakov, and V. M. Petrov (1987), Vostok ice core - A continuous isotope temperature record over the last climatic cycle (160,000 years), *Nature*, *329*, 6138, 403-408.

Keeling, C. D., J. F. S. Chin, and T. P. Whorf (1996), Increased activity of northern vegetation inferred from atmospheric CO_2 measurements, *Nature*, *382*, 6587, 146-149.

Libby, L. M., and L. J. Pandolfi (1974), Temperature-dependence of isotope ratios in tree rings, *Proc. Natl. Acad. Sci. U. S. A.*, *71*, 6, 2482-2486.

Peterson, B. J., R. M. Holmes, J. W. McClelland, C. J. Vorosmarty, R. B. Lammers, A. I. Shiklomanov, I. A. Shiklomanov, and S. Rahmstorf (2002), Increasing river discharge to the Arctic Ocean, *Science*, *298*, 5601, 2171-2173.

Peylin, P., P. Ciais, A. S. Denning, P. P. Tans, J. A. Berry, and J. W. C. White (1999), A 3-dimensional study of delta O-18 in atmospheric CO_2: contribution of different land ecosystems, *Tellus, Ser. B*, *51*, 3, 642-667.

Riley, W. J., C. J. Still, M. S. Torn, and J. A. Berry (2002), A mechanistic model of (H_2O)-O-18 and (COO)-O-18 fluxes between ecosystems and the atmosphere: Model description and sensitivity analyses, *Glob. Biogeochem. Cycle*, *16, 4*, 1095, doi:10.1029/2002GB001878.

Saurer, M., F. Schweingruber, E. A. Vaganov, S. G. Shiyatov, and R. Siegwolf (2002), Spatial and temporal oxygen isotope trends at the northern tree-line in Eurasia, *Geophys. Res. Lett.*, *29*, 9, doi:10.1029/2001GL013739.

Sugimoto, A., N. Yanagisawa, D. Naito, N. Fujita, and T. C. Maximov (2002), Importance of permafrost as a source of water for plants in east Siberian taiga, *Ecol. Res.*, *17*, 4, 493-503.

Welker, J. M., S. Rayback, and G. H. R. Henry (2005), Arctic and North Atlantic Oscillation phase changes are recorded in the isotopes (delta O-18 and delta C-13) of *Cassiope tetragona* plants, *Global Change Biol.*, *11*, 7, 997-1002.

Yurtsever, Y., and J. R. Gat (1981), Atmospheric waters, in *Stable isotope hydrology: Deuterium and oxygen-18 in the water cycle*, pp. 103-141, International Atomic Energy Agency.